NANOSCALE COMMUNICATIONS BASED ON FÖRSTER RESONANCE ENERGY TRANSFER (FRET)

by

Murat Kuşcu

A Thesis Submitted to the
Graduate School of Engineering
in Partial Fulfillment of the Requirements for
the Degree of

Master of Science

in

Electrical and Electronics Engineering

Koç University

September, 2013

Koç University

Graduate School of Sciences and Engineering

This is to certify that I have examined this copy of a master's thesis by

Murat Kuşcu

and have found that it is complete and satisfactory in all respects,
and that any and all revisions required by the final
examining committee have been made.

Committee Members:

Prof. Dr. Özgür B. Akan (Advisor)

Prof. Dr. A. Murat Tekalp

Assoc. Prof. Dr. Alper Kiraz

Date: _____

To my parents,

Fikriye Kuşcu and Süreyya Kuşcu.

ABSTRACT

Nanoscale communication is a novel and quite interdisciplinary research area which aims to design and develop communication networks among nano-size machines to extend their limited capabilities for groundbreaking biomedical, industrial and environmental applications. In this thesis, we propose and investigate a novel nanoscale wireless communication method based on a physically realizable phenomenon, Förster Resonance Energy Transfer (FRET) which is observed among fluorescent molecules such as semiconductor nanoparticles and organic dyes. Based on the well-established theory of FRET, we first information theoretically model FRET-based point-to-point communication channel between a single pair of fluorophore-based nanomachines with single-exciton transmission scheme. Furthermore, we analyze the performance of FRET-based point-to-point and broadcast nanoscale communications with multi-exciton transmission scheme performing realistic Monte Carlo simulations. We also propose a long range nanoscale communication channel based on multi-step FRET. We develop electrically and chemically controllable information routing techniques that are applicable to FRET-based nanonetworks. Moreover, we analyze FRET-based mobile molecular nanonetworks deriving analytical models for FRET-based mobile ad hoc molecular nanonetworks (FRET-MAMNET) and FRET-based mobile molecular sensor/actor nanonetworks (FRET-MSAN). Lastly, we perform an experiment in which we achieve to transfer data with the transmission rates of 50, 150 and 250 kbps through the mixture of Fluorescein and Rhodamine B as the donor/acceptor pair. This experiment is one of the first physical realizations of communications at nanoscale.

ÖZETÇE

Nano-haberleşme nano boyutlu makineler arasında haberleşme ağları geliştirerek nano-makinelerin kısıtlı yeteneklerini yenilikçi uygulamalarda faydalanılmak üzere geliştirmeyi amaçlayan yeni ve disiplinlerarası bir araştırma alanıdır. Bu tezde, yarıiletken nano-tanecikler ve organik boyalar gibi floresan moleküller arasında gözlemlenen ve fiziksel olarak gerçeklenebilen bir fenomen olan Förster Rezonans Enerji Transferi'ne (FRET) dayalı nano boyutlu kablosuz haberleşme metotu önerilmiş ve incelenmiştir. Öncelikle, FRET teorisi temel alınarak, floresan özellikli iki nano-makine arasındaki tekli eksiton iletimine dayalı FRET tabanlı noktadan noktaya haberleşme kanalı bilgi kuramsal olarak modellenmiştir. Buna ilaveten, çoklu eksiton iletimine dayalı FRET tabanlı nano boyutlarda noktadan noktaya ve yayım haberleşmesinin performansı gerçekçi Monte Carlo simülasyonları ile analiz edilmiştir. Bu tezde ayrıca, çok basamaklı FRET tabanlı uzun mesafeli bir nano-haberleşme kanalı da önerilmiştir. FRET tabanlı haberleşme ağları için elektriksel ve kimyasal olarak uzaktan kontrol edilebilen iki ayrı sinyal yönlendirme mekanizması tasarlanmıştır. Ayrıca, FRET tabanlı mobil tasarsız moleküler nano-ağlar ve mobil moleküler sensör/aktör nano-ağları için analitik modeller geliştirilmiştir. Son olarak, Fluorescein ve Rhodamine B organik boya molekülleri arasında FRET ile deneysel olarak bigi aktarımı gerçekleştirilmiştir. Bu deney, nano boyutlarda bilgi aktarımının fiziksel olarak gerçekleştirilebildiği öncü çalışmalardan biri olmuştur.

ACKNOWLEDGMENTS

First, I would like to give particular thanks to Dr. Özgür B. Akan for the enthusiastic supervision in all steps of the development of this work. He shared his knowledge and experience with me. I achieved more than I ever dreamed of in two years by his precious guiding and help.

My cordial thanks also extend to Dr. Murat Tekalp and Dr. Alper Kiraz for taking part in my thesis committee, for critical reading of this thesis and for their valuable suggestions and comments.

I would also like to thank Dr. Alper Kiraz for his invaluable contributions to this thesis by providing me the opportunity to experimentally validate my research in the Nano-Optics Research Laboratory (NRL) and for his insightful discussions. I am also grateful to Adnan Kurt, Selçuk Çakmak and the members of NRL for their support during the experiment.

I would like to express my gratitude to the members of the Next-generation and Wireless Communications Laboratory (NWCL) for their contributions to my personal and academic life in terms of friendship, advice and collaboration. I would also like to thank to Dr. Burhan Gülbahar, Dr. Barış Atakan, and Ahmet O. Biçen, the former members of the group, for sharing their valuable experience and knowledge with me.

I must also express my profound gratitude to my beloved friends Pelin, Samet(s), Uğur, Eda, Ege and Masal. I am deeply thankful to them for their invaluable support they have given me wherever they are and whenever I need.

I also gratefully acknowledge the support of Scientific and Technological Research Council of Turkey (TÜBİTAK) and Koç University.

Lastly, I am very grateful to my family for their unconditional support throughout this period. If it were not for their support and dedication to my education, I would never have made it as far as I have.

TABLE OF CONTENTS

LIST OF TABLES

LIST OF FIGURES

NOMENCLATURE

FRET	Förster (or Fluorescence) Resonance Energy Transfer
FRET-MAMNET	FRET-Based Mobile Ad Hoc Molecular Nanonetwork
FRET-MSAN	FRET-Based Mobile Molecular Sensor/Actor Nanonetwork
QD	Quantum Dot
PDT	Photodynamic Therapy
IS	Information Source
TN	Transmitter Nanomachine
RN	Receiver Nanomachine
HN	Relay Nanomachine
RtN	Router Nanomachine
OOK	ON/OFF Keying
ISI	Inter-Symbol Interference
QCSE	Quantum Confined Stark Effect
ECFP	Enhanced Cyan Fluorescent Protein
EYFP	Enhanced Yellow Fluorescent Protein
DAQ	Data Acquisition Card
EOM	Electro-Optic Modulator

Chapter 1

INTRODUCTION

Nanoscale communication is a novel research area aiming to develop communication networks among nano-size machines to extend their capabilities for groundbreaking applications. Traditional communication techniques are not applicable at nanoscale due to size and energy restrictions of nanomachines and relatively tough ambient conditions. Therefore, the literature about nanoscale communications mostly focus on developing bio-inspired communication techniques such as molecular communications.

In this thesis, we propose and investigate a radically different molecular communication method based on a quantum-mechanical phenomenon, Förster Resonance Energy Transfer (FRET) which is observed among fluorescent molecules like organic dyes and semiconductor nanoparticles. Low dependence on the environmental factors, controllability of its fundamental parameters, and relatively wide transfer range make FRET a promising candidate to be used for high-rate nanoscale communications.

Based on the well-established theory of FRET, we informational theoretically model FRET-based point-to-point communication channel between a single pair of fluorophore-based nanomachines with single-exciton transmission scheme and relate the communication performance with environmental and intrinsic parameters. We perform realistic Monte Carlo simulations to analyze the FRET-based point-to-point and broadcast nanoscale communications with multi-exciton transmission scheme. We also propose another nanoscale communication channel with higher communication coverage based on multi-step FRET. We develop electrically and chemically controllable information routing techniques that are applicable to FRET-based nanonetworks. We also investigate FRET-based mobile molecular nanonetworks, and derive analytical models of FRET-based mobile ad hoc molecular nanonetworks (FRET-MAMNET) and FRET-based mobile molecular sensor/actor nanonetworks (FRET-MSAN). We finally conduct an experiment in which we realize a nanocommunication system

based on FRET.

1.1 Nanoscale Communications

Recent developments in nanotechnology have enabled manufacturing of low-power and low-cost molecular-size machines, i.e., nanomachines, with the most basic sensing, actuating and computing capabilities by the manipulation of molecules at individual level. The limited coverage and functionalities of nanomachines can be improved significantly with the development of intra- and inter-communication systems for these tiny machines. A group of nanomachines cooperatively exchanging some sort of information or command is envisioned as *nanonetwork*.

The coordination of nanomachines with various capabilities in nanonetworks is envisaged to enable many cutting-edge applications in medical, industrial and military fields. The medical applications that nanonetworks are promising include immune system support, bio-hybrid implants to be used especially in restoration of central nervous system, in-body health monitoring with cellular precision, efficient drug delivery systems, and genetic engineering. Food and water quality control, battlefield monitoring, as well as nuclear defence can be given as the possible industrial and military applications of nanonetworks [1].

Many research efforts have been directed toward the development of a communication system between nanomachines. While some of the studies concentrate on the adaptation of traditional communication systems to nanoscale, e.g., electromagnetic, acoustic communications, some of them are inspired by nature and imitate the biological communication systems for their models. Electromagnetic communication for nanomachines is based on encoding the information by modulating electromagnetic waves in the THz band [2]. In acoustic communication, the information is encoded into acoustic energy [28]. The majority of the efforts have been devoted to the molecular communications [8]. Molecular communication has been emerged as the most promising method to realize the communication between future nanomachines, especially, biological nanomachines. Many of the molecular communication methods proposed so far are inspired from the existing in-body systems. In molecular communication, the information is basically encoded into the concentration, availability, or constituents of the molecules. Examples of biologically inspired molecular communication methods include the systems based on calcium signaling, gap

junction channels [59], pollens and spores [30], molecular motors and microtubules [9], as well as pheromones.

A major drawback of the proposed molecular communication methods is the requirement of mimicking the cellular communication components, i.e., it necessitates complex cell-like nanomachines with advanced capabilities such as releasing molecules at the desired concentration and receiving through receptors. Furthermore, since the proposed methods are mainly based on the diffusion of molecules through propagation medium, the communication is very slow compared to the traditional communication systems.

In this thesis, we propose a radically different molecular communication solution based on FRET that can provide very high-rate and reliable communication even between the simplest, single molecular functional units.

1.2 Förster Resonance Energy Transfer (FRET)

Förster Resonance Energy Transfer (FRET) is a non-radiative energy transfer process mostly observed among fluorescent molecules, i.e., fluorophores, such as organic dyes, fluorescent proteins, chemiluminescent substrates, fluorescent polymers, as well as semiconductor nanoparticles, e.g., Quantum Dots (QDs), Carbon Nanotubes (CNTs), which have spectral similarities, and are located in a close proximity such as 0-10 nm [51]. Acceptor molecule does not have to be fluorescent to be involved in the transfer process. When both donor and acceptor molecules are fluorescent, the phenomenon is also named Fluorescence Resonance Energy Transfer.

FRET is a quantum mechanical phenomenon based on the long range dipole-dipole interaction of an excited donor fluorophore with a suitable ground-state acceptor fluorophore in its close proximity. It does not require a collision of the fluorophores, and the transfer process does not produce heat.

FRET is widely exploited in studies of biotechnological research including fluorescence microscopy, molecular biology and optical imaging [23]-[39]. The phenomenon yields a significant amount of structural and spatial information about the donor and acceptor pair by means of optical signals with nanoscale resolution, therefore, many methods based on FRET have been developed and used in these areas. For example, using its strong dependence on distance, FRET is exploited as a spectroscopic ruler [74] while determining the

intramolecular and intermolecular distances and monitoring the conformational changes of proteins [37]. Several chemical and biological nano-sensors based on FRET, some of which utilize DNA as the scaffold for fluorophores, have been developed [56], [73], [81]. Furthermore in nanomedicine, exploiting FRET, QDs have been employed as the photosensitizing agents for photodynamic therapy (PDT) in cancer treatment [71], [22]. Moreover, the quantum coherence behavior of FRET in short distances has been widely studied showing the potential usage of FRET for future quantum computer designs [72]. Despite an extensive literature about the phenomenon, FRET is investigated from the communication theoretical perspective for the first time in this thesis.

1.3 Research Objectives and Solutions

The objectives of our research and the solution approaches are explained in this section.

1.3.1 FRET-Based Point-to-Point Nanoscale Communication Channel with Single Exciton Transmission

Realizing communication among nanomachines extends their limited capabilities for groundbreaking applications. Among the numerous solutions proposed for communication at nanoscale, molecular communication has attracted the most attention because of its biocompatibility. However, the complex nature of the molecular processes like transmission and reception required for molecular communication makes it infeasible at the current stage of nanotechnology. Besides, the slowness of information transmission processes limits its applications. To overcome this limitations, in this chapter, we propose to exploit a well-known phenomenon, Förster Resonance Energy Transfer, as a radically different molecular communication method.

We aim to model FRET-based nanocommunication channel between a donor fluorophore as the transmitter nanomachine (TN) and an acceptor fluorophore as the receiver nanomachine (RN). A single exciton, i.e., excited state of a participating molecule, is considered to be the information carrier. Assuming that a remote optical information source is available to excite the donor fluorophore, i.e., TN, and employing binary ON/OFF Keying (OOK) modulation scheme, we first investigate the probability of successful transmission of information from TN to RN. We mostly benefit from the rate equations given by Theodor Förster

in his seminal work [29]. We also investigate the information transmission through a long-range sequential FRET-based channel that includes a relay nanomachine (HN) between TN and RN. We information theoretically analyze the proposed communication channels, and derive analytical expressions for the mutual information between TN and RN, and channel capacity. The dependence of the channel capacity on the fundamental parameters of FRET, e.g., intermolecular distance, spectral similarity, molecular orientations, and the refractive index of the medium, is demonstrated through numerical simulations. The results of the simulations show that high capacity nanoscale communication is possible with FRET by selecting the appropriate values for the controllable system parameters.

1.3.2 FRET-Based Point-to-Point and Broadcast Nanoscale Communication Channels with Multi-Exciton Transmission

FRET-based nanocommunication can be very unreliable when the intermolecular distance is much greater than the Förster radius of the employed molecules [45], or there are more than one RN in the proximity of TN. To solve this unreliability problem, we propose to encode single bit information into multiple excitons by the excitation of TN with longer stimulations coming from the information source.

Based on the facts that an excited fluorophore cannot be re-excited until it relaxes to the ground state, and the excited state lifetime is a random variable, during the long stimulation, the generation of excitons on the donor fluorophore occurs at random times. Also, for the different excitations of donor during a single stimulation, the system parameters, e.g., the availability of the acceptors and the relative orientation of the nanomachines, can change significantly. The high degree of randomness of the transmission process makes it impossible to derive analytical expressions for the performance parameters like channel capacity. Therefore, we simulate the transmission of information through the point-to-point and broadcast communication channels with realistic Monte Carlo algorithms to obtain successful transmission probabilities of information for different values of system parameters. We also investigate Inter-Symbol Interference (ISI) for different lengths of stimulation signal, and derive the maximum reliable communication rates.

1.3.3 Information Routing in FRET-Based Nanonetworks

Design of nanonetworks composed of a large number of nanomachines with different sensing, actuating and computing capabilities requires to investigate the feasible methods for controlling the route of the information flow. The reliable routing of information coming from an information source to the target nanomachine or cluster of nanomachines is crucial for the proper operation of nanonetworks. In this chapter, we propose two different routing methods, electrical and chemical routing, applicable to the FRET-based nanonetworks.

We first propose and investigate an electrically controllable information routing method exploiting the Quantum Confined Stark Effect (QCSE) observed among fluorescent semiconductor nanoparticles. QCSE defines the Stark Shift that occurs in the emission spectra of semiconductor nanoparticles with the application of an external electrical field. Shift in the emission spectrum of a donor molecule changes the extent of spectral overlap between the donor's emission and the nearby acceptors' absorption spectra. Considering a deployment of two receiver nanomachines with different spectral characteristics (RN_1 and RN_2) near a transmitter nanomachine (or router nanomachine) (RtN), the FRET-based communication channels between RtN-RN_1 and RtN-RN_2 can be switched on and off according to the amount of electrical field applied to RtN.

The second information routing method proposed in this chapter is based on the nanoscale shuttle-like movement of [2]rotaxane macrocycle between two nodes with acid/base treatment. This chemical routing exploits the strong dependence of FRET probability on the intermolecular distances.

Transmission of information from RtN to RNs for different states of RtN is simulated using the Monte Carlo algorithms developed for the FRET-based broadcast communication. We show that information flow can be efficiently directed in an FRET-based nanonetwork by either external control, i.e., electric field, or depending on the environmental conditions, i.e., acid/base condition.

1.3.4 Multi-Step FRET-Based Long-Range Nanoscale Communication Channel

The low communication range is the main limitation of FRET-based nanoscale communication method. Although the multi-exciton scheme leverages the reliable communication range up to $5 \times R_0$, it is still much lower than the typical range of diffusion-based molecular

communication methods. To further improve the spatial range and the achievable transmission rate of the communication, in this chapter, we propose a novel method for FRET communication based on multi-step FRET employing identical relay fluorophores between TN and RN, and utilizing multi-exciton transmission scheme.

We investigate two deployment scenarios for the relay fluorophores: ordered relays in a host material with prescribed locations, and disordered, i.e., randomly deployed, relays in a three dimensional aqueous medium. The channel with ordered relays is considered for immobile nanomachines communicating through a wire-like channel that can find practicality for several on-chip applications. The channel with randomly deployed relays is considered for mobile nanomachines that can constitute mobile ad-hoc nanonetworks and nanosensor networks. We simulate the communication through the proposed channels following a realistic algorithm based on the competitive behavior of the multiple excitons and concerning many sources of randomness intrinsic to the phenomenon. Following a Monte Carlo approach, we evaluate the performance of the channels by means of information theoretical capacity and interference probability between successive transmissions, then we derive the maximum achievable data transmission rates over these channels. We infer from the results that using the channels with both ordered and disordered relays, two nanomachines can communicate at a rate up to tens of Mbps through distances over tens of nanometers. To the best of our knowledge, the achievable rates with multi-step FRET-based communication over this range of distances are significantly higher than that can be achieved by any biologically inspired communication method proposed so far.

1.3.5 FRET-Based Mobile Molecular Nanonetworks

In the previous chapters, we model FRET-based communication channels with different configurations assuming that the communicating nanomachines are immobile during the communication. However, most of the applications, especially in-body applications, that nanonetworks promise require for nanomachines to be mobile. Therefore, in this chapter, we focus on network of *mobile* nanomachines communicating through FRET.

We introduce two novel mobile molecular nanonetworks: *FRET-based mobile molecular sensor/actor nanonetwork (FRET-MSAN)* which is a distributed system of mobile fluorophores acting as sensor or actor node; and *FRET-based mobile ad hoc molecular nanonet-*

work (FRET-MAMNET) which consists of fluorophore-based nanotransmitter, nanoreceivers and nanorelays. We model the single message propagation exploiting the SIR model of epidemics. We derive closed form expressions for the probability of the actor nodes to detect a message generated on the sensor nodes in FRET-MSAN, and for the average detection time of the transmitted message by the nanoreceivers in FRET-MAMNET. We numerically evaluate the performance of these networks in terms of reliability and transmission delay for varying number of nanonodes and varying size of nanomachines, as well as, for several FRET-related parameters.

1.3.6 Experiment

The literature about nanocommunications is mostly focused on the theoretical development of nanocommunication techniques and communication theoretical modeling of nanocommunication networks, and lacks of empirical studies that validate the feasibility of the proposed nanocommunication methods.

In this chapter, we carry out an experiment to realize a nanocommunication system based on FRET. Using a common fluorescent dye pair of Fluorescein and Rhodamine B as the donor and the acceptor, respectively, we design a multi source multicast communication network, and transmit a pseudorandom binary digital information through this network at different rates. We investigate the performance of the communication system by means of eye diagrams and calculating the error rates for transmission rates of 50, 150 and 250 kbps.

The results of the experiment reveal that information can be transmitted reliably using FRET with the information transmission rates up to 150 kbps. At these rates, the bit error rate is calculated as less than 10^{-4}. However, the received signal is significantly distorted above 150 kbps. At the transmission rate of 250 kbps, we observe the bit error rate as higher than 10^{-2}.

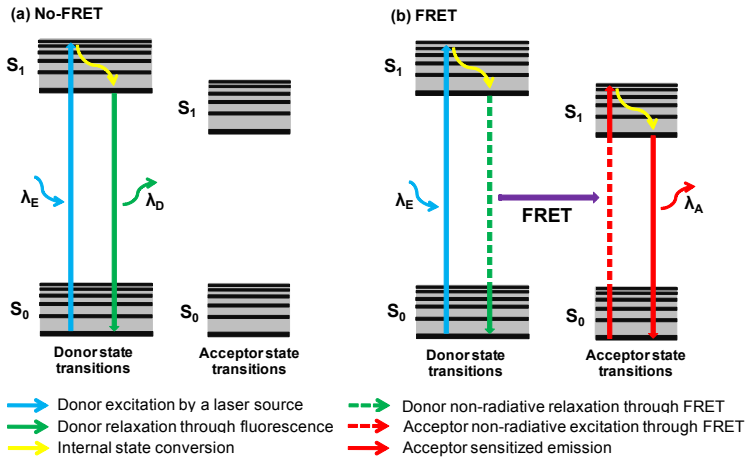

Figure 2.1: Jablonski diagram demonstrating state transitions of donor and acceptor for fluorescence and FRET cases.

Chapter 2

THEORY OF FÖRSTER RESONANCE ENERGY TRANSFER

The theory of FRET between immobile fluorophores is established in 1948 by Theodor Förster's seminal work [29]. The governing equations are then validated experimentally in late 1970s [74].

There are two types of possible relaxation pathways for an excited donor fluorophore: radiative and nonradiative relaxation. Radiative relaxation occurs through fluorescence. Nonradiative relaxation can be through collisional quenching or FRET. Collisional quenching is rarely observed, and mostly fluorescence and FRET are the main processes that compete with each other for the relaxation of the donor. If there is not a suitable acceptor in the proximity of the excited donor, it relaxes through fluorescence, i.e., by emitting a photon, as shown in Fig. 2.1(a). In case there is a suitable energy acceptor, FRET can occur, and the excited donor can transfer its excitation, i.e., exciton, to the nearby acceptor molecule and sensitize it as in Fig. 2.1(b). If the sensitized acceptor is fluorescent, it releases a photon with a wavelength belonging to its emission spectrum. The photon released

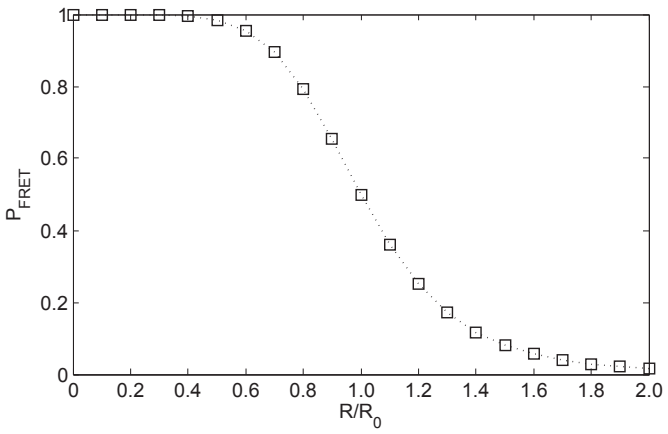

Figure 2.2: Probability of FRET with varying intermolecular distance.

from the sensitized acceptor generally has a lower energy than the photons released through fluorescence of the donor molecule.

The occurrence of FRET depends on mainly three conditions: *i*) an excited fluorophore must be in close proximity (0-10 nm) with at least one ground-state acceptor; *ii*) the emission spectrum of the donor and the absorption spectrum of the acceptor must overlap; and *iii*) the relative orientation of dipole moments of the donor and the acceptor fluorophores must not be orthogonal. When these conditions are satisfied, FRET competes with fluorescence process. The probability of FRET for an excited donor fluorophore can be given in terms of process rates as the following

$$P_{FRET} = \frac{k_T}{k_R + k_T} \tag{2.1}$$

where k_R and k_T are the fluorescence and FRET rates, respectively. k_R is the reciprocal of the mean of excited state lifetime of the donor τ_D in the absence of a nearby acceptor, i.e., $1/\mu_{\tau_D}$. τ_D denotes the time that the excited donor molecule stays in the excited state before relaxing through fluorescence, and it is a random variable. The probability distribution of τ_D can be approximated generally as a single exponential based on the fluorescence lifetime measurements [51]. The mean lifetime is shortened when there exists different pathways for the donor to relax including FRET. In the case that there exists an acceptor in the proximity of the donor, i.e., FRET is a possible relaxation pathway for the donor, the mean

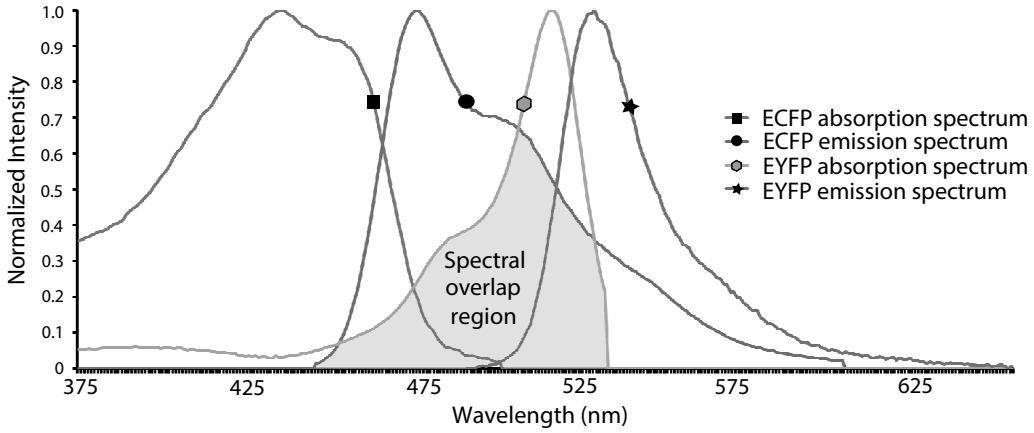

Figure 2.3: Absorption and emission spectra of Enhanced Cyan Fluorescent Protein (ECFP) as the donor fluorophore and Enhanced Yellow Fluorescent Protein (EYFP) as the acceptor fluorophore, and the spectral overlap of ECFP emission and EYFP absorption [22].

of the donor lifetime τ_{DA} is given as

$$\mu_{\tau_{DA}} = \frac{1}{k_R + k_T} \tag{2.2}$$

τ_{DA} is also an exponential random variable [51]. FRET rate k_T is given in terms of fluorescence rate as the following

$$k_T = k_R(\frac{R_0}{R})^6 \tag{2.3}$$

where R_0 is the Förster radius denoting the distance between the molecules when P_{FRET} is 0.5, and R defines the intermolecular distance between the transition dipole centers of the molecules. The strong dependence of probability of FRET on the intermolecular distance is demonstrated in Fig. 2.2.

R_0 relates the FRET rate with environmental and intrinsic parameters and can be expressed by

$$R_0^6 = 8.8 \times 10^{22} \kappa^2 n^{-4} Q_D \int_0^\infty F_D(\lambda)\epsilon_A(\lambda)\lambda^4 \mathrm{d}\lambda \tag{2.4}$$

where the κ^2 is the relative orientation factor, Q_D is the quantum yield of the donor and n is the refractive index of the medium. The integral part of (2.4) denotes the degree of the overlap of the emission band of the donor and the absorption band of the acceptor and is denoted by $J(\lambda)$,

$$J(\lambda) = \int_0^\infty f_D(\lambda)\epsilon_A(\lambda)\lambda^4 \mathrm{d}\lambda \tag{2.5}$$

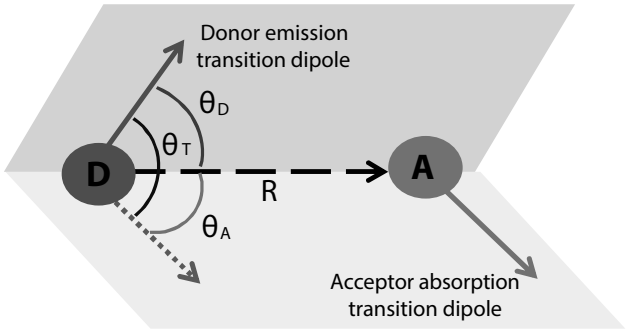

Figure 2.4: Critical angles of relative orientation between donor and acceptor fluorophores.

where $f_D(\lambda)$ is the normalized fluorescence emission intensity and $\epsilon_A(\lambda)$ is the acceptor molar absorptivity. The spectral overlap of a common FRET pair, Enhanced Cyan Fluorescent Protein (ECFP) - Enhanced Yellow Fluorescent Protein (EYFP), is demonstrated in Fig. 2.3.

The orientation factor (κ^2) can be given as follows

$$\kappa^2 = (\cos\theta_T - 3\cos\theta_D \cos\theta_A)^2 \tag{2.6}$$

where θ_T, θ_D and θ_A are the angles determined by the emission and absorption transition dipoles of the fluorophores [51] as shown in Fig. 2.4. Assuming isotropic and unrestricted distributions for all three angles, the distribution of κ^2 can be given as follows [9]

$$p_{\kappa^2}(\kappa^2) = \begin{cases} \frac{1}{2\sqrt{3\kappa^2}} \ln(2+\sqrt{3}) & 0 \le \kappa^2 \le 1 \\ \frac{1}{2\sqrt{3\kappa^2}} \ln(\frac{2+\sqrt{3}}{\sqrt{\kappa^2}+\sqrt{\kappa^2-1}}) & 1 \le \kappa^2 \le 4 \end{cases} \tag{2.7}$$

In most FRET studies, κ^2 is taken as its mean value which is 2/3 assuming isotropically free molecules.

In the case of mobile fluorophores, the situation is radically different in the sense that during the excited state lifetime of the donor, the intermolecular distances and the relative orientation of the dipole moments of fluorophores are not constant. Furthermore, the excited donor fluorophore can get in close proximity with a varying number of acceptors if the donor lifetime or the diffusion coefficient of the fluorophores is sufficiently long. Considering that the excitons randomly walk in a random lattice consisting of diffusing fluorophores, giving a closed form expression for the transfer rate requires some assumptions. Stryer et al.

postulated the governing rate equations for the energy transfer from a single excited donor to a single ground-state acceptor in a three dimensional environment assuming that the fluorophores are in the rapid-diffusion limit [76]:

$$k_{rd} = \frac{4\pi k_0 R_{0,d-a}^6}{3V a_{d-a}^{-3}} \tag{2.8}$$

where $R_{0,d-a}$ is the Förster radius between the donor and the acceptor, and V is the volume of the three dimensional medium. a_{d-a} is the possible closest distance between the centers of the donor and the acceptor. When there are more than one acceptor molecules, the total FRET rate between the donor and the acceptors becomes

$$k_t = k_{rd} N_a \tag{2.9}$$

where N_a is the number of available, i.e., ground-state, acceptor molecules in the environment. The rapid-diffusion criterion is given as

$$\frac{D\tau_0}{s^2} \gg 1 \tag{2.10}$$

where D is the sum of diffusion coefficients of the donor and the acceptor, τ_0 is the natural excited state lifetime of the donor, i.e., $\tau_0 = 1/k_0$, and s is the mean intermolecular distance between donor-acceptor fluorophores [76], [41].

The rapid diffusion limit can be achieved by using fluorophores with moderate diffusion coefficients and long lifetimes such as $1 - 2\ \mu s$ [41]. Stryer et al. showed that the transfer rate and efficiency of the energy transfer are greatly enhanced when molecules are diffusing in the rapid diffusion limit [76].

Chapter 3

FRET-BASED POINT-TO-POINT NANOSCALE COMMUNICATION CHANNEL WITH SINGLE EXCITON TRANSMISSION

In this chapter, a novel and physically realizable nanoscale communication paradigm is introduced based on a well-known phenomenon, Förster Resonance Energy Transfer (FRET) for the first time in the literature. As reviewed in Chapter 2, FRET is a non-radiative energy transfer process between fluorescent molecules based on the dipole-dipole interactions of molecules. Energy is transferred rapidly from a donor to an acceptor molecule in a close proximity such as 0 to 10 nm without radiation of a photon. Low dependency on the environmental factors, controllability of its parameters and relatively wide transfer range make FRET a promising candidate to be used for a high rate nanoscale communication channel. In this chapter, the simplest form of the FRET-based molecular communication channel comprising a single transmitter-receiver nanomachine pair and an extended version of this channel with a relay nanomachine for long range applications are modeled considering nanomachines as nanoscale electromechanical devices with basic sensing, computing and actuating capabilities. Furthermore, using the information theoretical approach, the capacities of these communication channels are investigated and the dependency of the capacity on some environmental and intrinsic parameters is analyzed. It is shown that the capacity can be increased by appropriately selecting the donor-acceptor pair, the medium, the intermolecular distance and the orientation of the molecules.

3.1 Introduction

Nanoscale communication is a novel and quite interdisciplinary research area. In recent years, several potential approaches have been proposed in order to achieve communication in the nanoscale such as electromagnetic, acoustic or molecular [1], [60]. Here, we introduce a novel and radically different method for the communication in the nanoscale by exploiting a well-known, physical controllable phenomenon, Förster (or Fluorescence) Resonance Energy

Transfer (FRET).

In this chapter, for the first time in the literature, FRET has been approached from the communication perspective and introduced as a novel molecular communication paradigm. There are many biologically inspired and theoretically modeled molecular communication techniques in the literature including the communication models devised based on intercellular calcium signaling [58], pheromones [30], flagellated bacteria and catalytic nanomotors [31], carbon nanotubes [7], pollen and spores [30], as well as morphogenesis [54] in order to encode, transfer and decode information. FRET-based communication method is based on a physically existing phenomenon and unlike the other techniques it provides significantly higher capacity communication. The excited state energy of molecules that conveys the information is transferred in the nanosecond range so that FRET-based communication is incomparably faster than the already proposed nanoscale communication techniques. Furthermore, high-level controllability of almost all of the system parameters makes FRET-based channel more reliable. The abundance of both theoretical and practical studies about FRET in the literature and availability of its experimental setups provide the opportunity of making improvements validating theoretical model based on experiments. Hence, unlike most of the existing approaches in the literature, we introduce an already analyzed and experimented, therefore, a physically realizable, and hence, clearly realistic solution to the problem of nanoscale communication.

In this chapter, we also enhance the FRET-based communication channel in order to realize nanoscale communication over distances longer than 10 nm with the integration of a relay node between transmitter and receiver. In this extended version of the model, excited energy of the donor is transferred first to the fluorophore on the relay nanomachine, afterwards the excited relay fluorophore transfers its energy to the acceptor fluorophore on the receiver nanomachine via FRET. This sequential energy transfer (also called multi-step FRET in the literature) is achieved experimentally in some studies related to fluorescence spectroscopy such as [36], [79] locating several numbers of fluorophores in a linear order over several distances. Such enhancement is significant because it shows the potential of the FRET based nanoscale communication in the sense that it can be extended further being a solution for long range nanoscale communication and similar network schemes such as multiple-access or broadcast.

The remainder of this chapter is organized as follows. In Section 3.2, we model the FRET-based communication channel with a single donor-acceptor pair. In section 3.3, the extended version of the channel with an addition of a relay node is modeled to realize a longer range communication based on FRET. An information theoretical analysis of FRET-based channel is performed in Section 3.4 in order to determine the closed-form expression for the capacity of the channel. In Section 3.5, we analyze the dependence of the channel capacity on some environmental and intrinsic factors and demonstrate a selection strategy for these parameters to achieve higher communication capacity. Besides, we investigate the dependence of the capacity of the channel with a relay node on internodal distances.

3.2 Channel Model

We constructed our communication model with a single donor fluorescence molecule (D) bound to a transmitter nanomachine (TN), and a single acceptor fluorescence molecule (A) bound to a receiver nanomachine (RN), at fixed locations separated by a reasonable distance R in an aqueous medium considering FRET as the communication channel with the system exciton, i.e., the combined state of electron and hole, being a carrier as shown in Fig. 3.1, where θ_T is the angle between the emission transition dipole of donor and the absorption transition dipole of the acceptor, θ_D and θ_A are the angles between these dipoles and vector joining the donor and the acceptor, respectively. The arrow between (D) and (A) shows the FRET direction. Other arrows show the transition dipoles of (D) and (A) as well as the direction of incoming photon with a wavelength of λ_i. Assuming the molecules are properly selected, i.e., they have sufficient spectral overlap ($J(\lambda)$), in the case of a donor excitation, FRET occurs with probability of P_{FRET}.

When a laser source excites the donor at a proper wavelength, basically there are two ways of relaxation for the donor, the first one is through radiative emission, i.e., fluorescence and the second one is through FRET disregarding the other low-probability non-radiative relaxation pathways such as dissipation as heat or collision with another molecule, i.e., collisional quenching as well as intersystem crossing to an excited triplet state which can actually result in phosphorescence.

In FRET spectroscopy, the FRET efficiency is determined by continuously exciting the donor and calculating the proportion of the number of FRET relaxations to the number

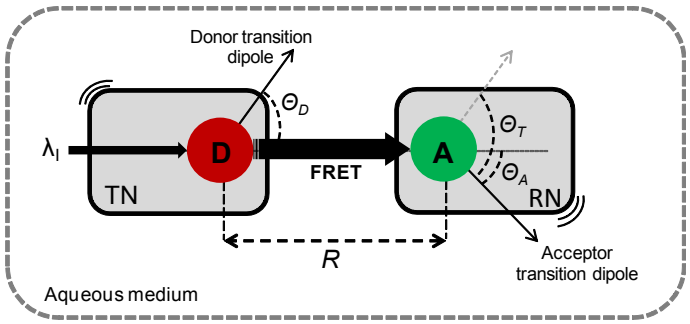

Figure 3.1: Point-to-point FRET-based molecular communication channel model with single TN and RN communicating via FRET.

of total relaxation processes in a specified time interval [16]. The efficiency of the energy transfer as a function of intermolecular distance and Förster radius, R_0 is formulated as

$$E(R) = \frac{R_0^6}{R_0^6 + R^6} \tag{3.1}$$

where R is the distance between the donor and the acceptor molecules [51]. For a single cycle of excitation and relaxation of the donor, the FRET efficiency can be considered as the probability of the excited donor to relax through resonance energy transfer. Thus, using (3.1), for a single exciton, the probability of FRET as a function of intermolecular distance can be given by

$$P_{FRET}(R) = E(R) = \frac{R_0^6}{R_0^6 + R^6} \tag{3.2}$$

where R_0 is the Förster radius and it is calculated according to (2.4). In [63], in a medium of water with a refractive index of 1.3342 at 25 °C, assuming rapid randomization of relative orientation of molecules, i.e., $\kappa^2 = 2/3$, for a pair consisting of ECFP (Enhanced Cyan Fluorescent Protein) as donor and EYFP (Enhanced Yellow Fluorescent Protein) as acceptor, the Förster radius is calculated as 4.92 nm. Both ECFP and EYFP are the variants of Green Fluorescent Protein (GFP) and widely used in various fluorescence spectroscopy applications for their similar spectral characteristics, photostability, high extinction coefficients and high quantum yields [67]. At the same time, the pair ECFP-EYFP is a good candidate for communication purposes due to the relatively large value of R_0.

In FRET-based communication model, donor excitation is realized by a pulsed laser source which has a waveshape approximated in Fig. 3.2. The duration of pulses can be selected very short compared to the lifetimes of the fluorophores used in the model because

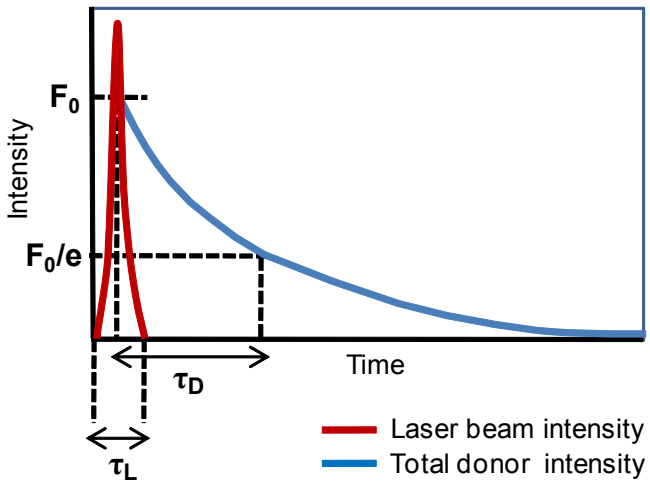

Figure 3.2: Approximated laser pulse shape and lifetime determination.

of energy saving concern. Lasers with femtosecond-width pulses are already commercially available. The laser source could be considered as the main information source of the communication system and is not considered to be a part of TN at present due to energy and size limitations. Vast number of photons released by the laser with wavelengths near to the excitation maximum of the donor, guarantee the donor excitation in femtoseconds duration, since the absorption probability of the donor is almost 1 for that wavelengths. Therefore, in the subsequent probability calculations, the probability of donor excitation at any instant of laser pulse duration is assumed to be 1.

Excited state lifetime is determined by measuring and recording the fluorescence times of many fluorophores of the same kind after an excitation by a very small duration pulsed laser and calculating the mean of these records as shown in Fig. 3.2. Therefore, it is very possible for the employed donor and acceptor flurophores not to have the anticipated lifetimes. In addition, the lifetime of the same fluorophore is not always constant. The lifetime of a fluorophore is a critical parameter in determination of the laser excitation period (T_H) in the sense that an excited fluorophore cannot be re-excited until it relaxes to the ground state [14]. For example, the donor molecule cannot transfer the excited state energy to the acceptor through FRET if the acceptor is still in its excited state as a result of the preceding FRET process. Therefore, we consider the worst -with the longest duration- case while determining T_H.

In the model, we implemented On-Off Keying Modulation with two bits available as in the traditional digital communications. The excitation of the donor by the information source at the beginning of a time interval (T_H) corresponds to bit 1, and no-excitation at the beginning of a time interval corresponds to bit 0. The RN is assumed to have the ability of checking whether the acceptor is excited through FRET or not during the corresponding time interval. If it is excited through FRET, it decides that the TN transmitted bit 1, otherwise it decides that the TN transmitted bit 0. With further investigations on nanoscale system design, such RN designs can be potentially realizable. At current FRET studies, acceptor fluorescence is observed with a system comprising a Photomultiplier Tube (PMT) and a Near-field Scanning Optical Microscope (NSOM) in order to detect whether or not FRET occurs [24]. This mechanism is considered to be used as the ultimate destination of information in the future studies aiming to validate the FRET-based communication channel experimentally.

In Fig. 3.3, conceptually we demonstrate the different cases for data transmission. For the case in Fig. 3.3-a, a laser directed to the donor molecule releases a pulse which has a duration of τ_L. The wavelength of photons released by laser is near to the excitation maximum of the donor in order to guarantee the donor excitation. During τ_L, donor absorbs a photon and becomes excited at any instant. In the excited state, after an average time τ_{DA}, i.e., the lifetime of donor in the case of FRET, donor succeeds in transferring the excited energy to the acceptor molecule through FRET with the probability of $P_{FRET}(R)$. Therefore, acceptor molecule in RN also becomes excited through FRET. The time required for FRET to be completed is the reciprocal of FRET rate, i.e., $\tau_{FRET}(R) = 1/k_T(R) = \tau_D(R/R_0)^6$. Acceptor molecule stays in excited state for an average time of τ_A and then it relaxes by emitting a photon which has a Stokes shifted wavelength, i.e., greater wavelength and lower energy. RN detects the excited state of acceptor in the time interval $0 - T_H$ and decides bit 1. In the figure, excitation and fluorescence durations are neglected since they are too small compared to the lifetimes and FRET duration which are approximated according to the measured values for previously mentioned fluorescent protein pair ECFP-EYCP. The measured lifetimes are 2.68 ns for the donor ECFP and 2.88 ns for the acceptor EYFP [66].

In Fig. 3.3-b, again the donor is excited to transmit bit 1, however, this time donor

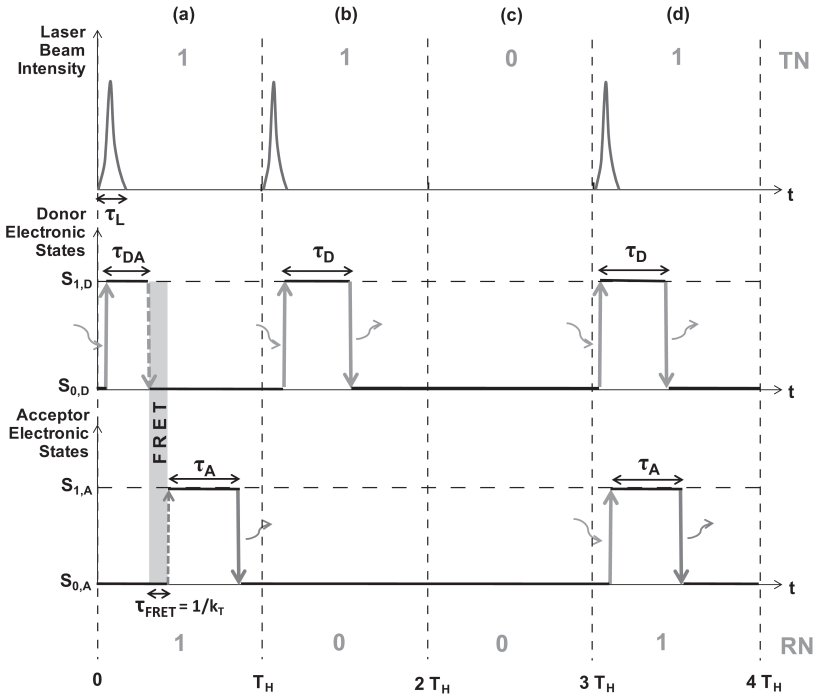

Figure 3.3: Example data stream demonstrating pulsed laser beam intensity, donor state transitions and acceptor state transitions for different cases. (a) FRET case; bit 1 is transmitted by TN, bit 1 is detected by RN. (b) No-FRET case; bit 1 is transmitted, bit 0 is detected. (c) No-excitation case; bit 0 is transmitted, bit 0 is detected. (d) Direct excitation case; bit 1 is transmitted, bit 1 is detected.

fails to deliver its excited energy to the acceptor molecule of RN with the probability of $1 - P_{FRET}(R)$ in the time interval $T_H - 2\ T_H$. Therefore, RN cannot detect an excited state during this time interval and decides bit 0. The probability of failure for this case can be minimized by adjusting the intermolecular distance to the values smaller than R_0.

In Fig. 3.3-c, the laser source does not release pulse in order for TN to transmit bit 0, therefore, the donor is not excited in the time interval $2\ T_H - 3\ T_H$. As a result, the acceptor also is not excited and RN decides the correct bit, i.e., bit 0.

In Fig. 3.3-d, the laser source excites both the donor and the acceptor directly. This undesired situation is known as direct excitation and can be very problematic for FRET applications in fluorescence microscopy. Direct excitation occurs when donor is excited by a laser source at a wavelength that belongs to excitation spectrum of both donor and acceptor. Although direct excitation can be minimized by using a laser with a small excitation volume

and appropriately directing the laser source to the donor molecule in TN, it is seen in Fig. 3.3-d that direct excitation does not result in any confusion for RN to detect the correct bit.

The case in Fig. 3.3-a can be extended to the worst -with the longest duration- case for data transmission to determine minimum excitation period, i.e., T_{H-min}. Since the fluorophores with lifetimes longer than the determined average lifetime constitute a small portion of the entire as seen in Fig. 3.2, in order to ease the calculation, we assume that the maximum values of lifetimes are the same as the specified mean values, i.e., $\tau_{D-max} = \tau_D$ and $\tau_{A-max} = \tau_A$ as well as $\tau_{DA-max} = \tau_{DA}$. Assuming that the donor excitation occurs with the absorption of the last photon released by laser source and neglecting the relatively small excitation time of the donor and disregarding direct excitation, in order to prevent intersymbol interference, the minimum value of the excitation period T_H is given as

$$T_{H-min} = \tau_L + \tau_{DA} + \tau_{FRET} + \tau_A \tag{3.3}$$

T_H must be reasonably greater than the minimum value considering the weakness of the assumptions made.

3.3 Relay Channel

In the literature, there are several studies that achieve multi-step FRET for transmission of excited energy over distances longer than 10 nm [36], [79]. Furthermore, in one of the related works, multi-step FRET is proposed for design of a photonic wire [77]. Multi-step FRET is realized by employing relay molecules between donor and acceptor. These relay nodes act like both donor and acceptor at the same time, i.e., they transfer the energy absorbed via FRET to the next ground-state molecule in close proximity through FRET. A long-range version of FRET-based communication comprising sequential FRET channels can be realized using multi-step method.

In Fig. 3.4, the simplest form of multi-step FRET-based communication model with one transmitter nanomachine (TN) with a donor fluorophore (D), one receiver nanomachine (RN) with an acceptor fluorophore (A) and one relay nanomachine (HN) with a relay fluorophore (R) is demonstrated. The arrows between (D), (R) and (A) show the FRET direction. Other arrow shows the direction of incoming photon with a wavelength of λ_i.

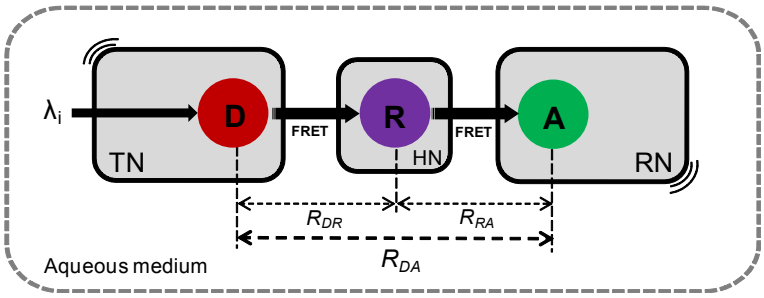

Figure 3.4: Long-range FRET-based communication model with multi-step FRET.

The nanomachines are located linearly to improve the energy transfer range, therefore, the intermolecular distance between the donor fluorophore on TN and the acceptor fluorophore on RN, i.e., R_{DA} is given by

$$R_{DA} = R_{DR} + R_{RA} \tag{3.4}$$

where R_{DR} is the distance between the donor fluorophore on TN and the relay fluorophore on HN and R_{RA} is the distance between the relay fluorophore on HN and the acceptor fluorophore on RN.

The overlap between the emission spectrum of donor fluorophore and the absorption spectrum of the relay fluorophore as well as the overlap between the emission spectrum of relay fluorophore and the absorption spectrum of the acceptor fluorophore must be significantly large to allow multi-step FRET to occur between these molecules. The probability of direct FRET between TN and RN is ignored assuming R_{DA} is significantly greater than $R_{0,DA}$, i.e., the Förster distance of donor-acceptor pair. As a consequence, the direct communication between TN and RN is assumed to be disabled. Therefore, the multi-step channel is considered as a series of two independent channels. Therefore, the overall transfer efficiency between the excited donor and the ground state acceptor via multi-step FRET, i.e., E_{DA} is given by

$$E_{DA} = E_{DR} \times E_{RA} \tag{3.5}$$

where E_{DR} is the FRET efficiency between the excited donor fluorophore and the ground-state relay fluorophore and E_{RA} is the FRET efficiency between the excited relay fluorophore and the ground-state acceptor fluorophore [79]. Using (3.1), (3.2) and (3.5), the probability of FRET between the donor and the acceptor for a single exciton in terms of R_{DR} and R_{RA}

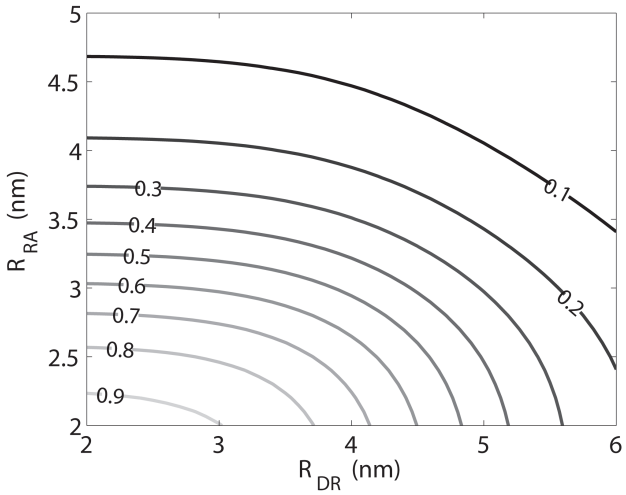

Figure 3.5: $P_{FRET,DA}$ with varying R_{DR} and R_{RA} for ECFP(D)-EYFP(R)-EGFP(A) arrangement.

is given by

$$P_{FRET,DA}(R_{DR}, R_{RA}) = \frac{R_{0,DR}^6}{R_{0,DR}^6 + R_{DR}^6} \times \frac{R_{0,RA}^6}{R_{0,RA}^6 + R_{RA}^6} \tag{3.6}$$

where $R_{0,DR}$ is the Förster distance of donor-relay pair and $R_{0,RA}$ is the Förster distance of relay-acceptor pair. As it is seen in (3.6), if $R_{0,DR}$ and $R_{0,RA}$ are not equal, $P_{FRET,DA}$ is not directly related to $R_{0,DA}$ as in the case of single pair FRET-based communication.

In order to demonstrate the dependence of $P_{FRET,DA}$ on R_{DR} and R_{RA}, we theoretically construct a multi-step communication model using the previously mentioned fluorescent proteins in linear arrangement and in a medium of water at 25 °C assuming rapid randomization of relative orientation of molecules. We select ECFP as the donor, EYFP as the relay and EGFP (Enhanced Green Fluorescent Protein) as the acceptor molecule. The Förster distances between these molecules under given constraints are measured in [63] as $R_{0,ECFP-EYFP} = 4.92\ nm$ and $R_{0,EYFP-EGFP} = 3.25\ nm$. The dependence is shown in Fig. 3.5. As it is seen, in order to optimize this two-step channel for high FRET efficiency and long communication range, it would be a wise decision to set R_{DR} greater than R_{RA}, because $R_{0,DR}$ is greater than $R_{0,RA}$.

The idea of multi-step (or multi-channel) can be applied to realize longer communication with more than one relay in the same manner. For example, in the experimental study [36], a relatively high FRET efficiency of $\sim$ 68% is achieved with five flurophores over

a distance of $\sim$ 13 nm. We believe, with the discoveries of high efficiency FRET pairs and further improvements on locating and orienting techniques of fluorophores, nanoscale communication can be realized over longer internodal distances with less relay nodes by using multi-step FRET technique and the advantages of this communication paradigm over wiring the nanomachines together such as mobility and minimizing energy cost and budget become more clear.

3.4 Information Theoretical Analysis

The FRET Channel is modeled similar to Z-channel with On-Off Keying (OOK) Modulation as in Fig. 3.6 assuming the excitation period i.e., T_H, is large enough to prevent ISI. Every

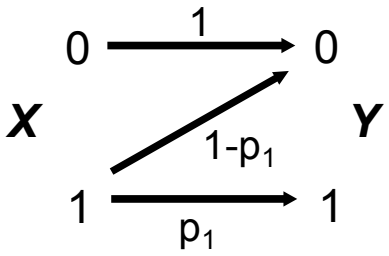

Figure 3.6: Z channel transition diagram with the transition probabilities.

time when the laser excites the donor at the beginning of the interval T_H, i.e., it intends to transmit bit 1 with probability P_F, the probability of FRET occurrence during that interval determines the success of transmission of bit 1. Thus, using (3.2), TN achieves to deliver bit 1 with probability of p_1 given in terms of intermolecular distance R as follows

$$p_1[R] = \frac{R_0^6}{R_0^6 + R^6} \tag{3.7}$$

Therefore, the probability of failure of transmitting bit 1 when the donor is excited is $(1 - p_1[R])$.

When the donor is not excited at the beginning of an interval, the probability of FRET abstinence during that interval gives the success probability of bit 0. The only noise source for that transmission might be an external laser source exciting the acceptor molecule and causes the acceptor to fluorescence randomly. In our model with one information source, assuming there is no noise factor that affects the channel and the receiver is reasonable.

Hence, the successful transmission probability of bit 0 is unity, i.e., $p_0 = 1$. Therefore, in this case, the failure probability of transmitting bit 0 becomes $(1 - p_0) = 0$.

Although we disregard the external noise factors, the channel acts like a noisy channel since the probability of FRET occurrence is intrinsically not equal to 1. According to the transmission probabilities, the transition matrix of the Z-channel considering X as the transmitted bit by TN, and Y as the received bit by RN is given as

$$P(Y|X) = \begin{bmatrix} \Big(1 - P_F\Big)p_0 & \Big(1 - P_F\Big)\Big(1 - p_0\Big) \\ P_F\Big(1 - p_1[R]\Big) & P_F\ p_1[R] \end{bmatrix}$$

The simplified form of the transition matrix for $p_0 = 1$ can be given by

$$P(Y|X) = \begin{bmatrix} \Big(1 - P_F\Big) & 0 \\ P_F\Big(\frac{R^6}{R_0^6+R^6}\Big) & P_F\Big(\frac{R_0^6}{R_0^6+R^6}\Big) \end{bmatrix}$$

Consequently, the mutual information *I(X;Y)* between X and Y can be inferred from the transition matrix as

$$I(X;Y) = H(P_F\ p_1[R]) - P_F\ H(1 - p_1[R]), \tag{3.8}$$

where *H(.)* denotes the binary entropy. Therefore, the capacity of the FRET channel, C_F, can be given by maximizing the mutual information as follows

$$C_F = \max\left[I(X;Y)\right] \tag{3.9}$$

It is possible to increase the channel capacity that varies in accordance with some external and intrinsic parameters by selecting appropriate excitation probabilities, i.e., P_F.

3.5 Numerical Analysis

In this section, we present the numerical analysis performed over the mutual information expression given in (3.8) to show how the FRET-based communication capacity varies according to some environmental parameters and some intrinsic parameters that are specific to the employed FRET pair. The aim of this analysis is to determine the appropriate configuration of FRET-based communication parameters, which can achieve high communication capacity according to changing environmental parameters. We perform the numerical analysis using MATLAB. The simulation parameters can be seen in Table 3.1.

Table 3.1: Simulation Parameters

Donor - Acceptor pair	EBFP - DsRed ECFP - EYFP EGFP - EYFP ECFP - EYFP - EGFP (relayed case)
Intermolecular distance (R)	$(3-6)\ nm$
Refractive index (n)	1 (vacuum) 1.3342 (water at 25 °C) 1.5185 (silicon oil at 25 °C)
Orientation factor (κ^2)	2/3 (rapid randomization) 4 (parallel dipole moments)

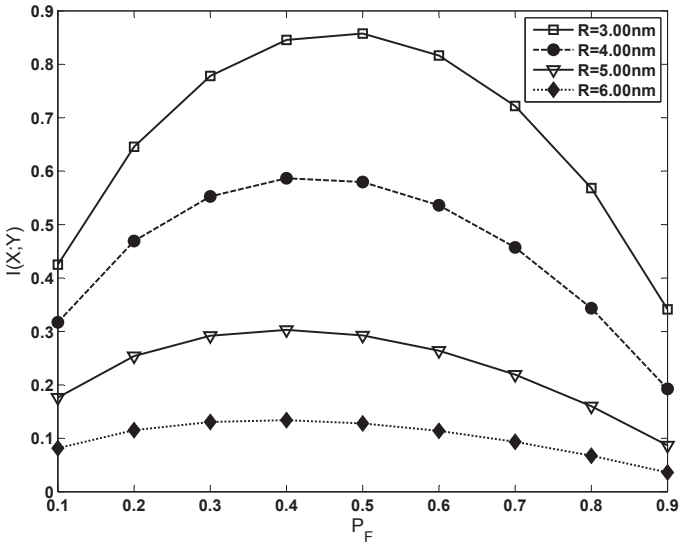

Figure 3.7: $I(X;Y)$ in bits with varying P_F for different R.

3.5.1 Effect of Intermolecular Distance

For the first analysis, we investigate the effect of the intermolecular distance (R) on the capacity of FRET-based communication channel. The analysis is carried out with single donor and single acceptor configuration using ECFP-EYFP as the FRET pair assembled on the nanomachines assuming rapid randomization of the relative orientation of the molecules as well as the nanomachines in a medium of water at 25 °C.

Selecting the medium and orientation parameters as specified before, the Förster radius

for ECFP - EYFP pair is calculated as $R_0 = 4.92\ nm$ [63]. In Fig. 3.7, mutual information ($I(X;Y)$) given in (3.8) is shown with varying excitation probability of the donor (P_F) for different R. For R values higher than the R_0, the probability of FRET in the case of donor excitation, i.e., p_1, significantly decreases. As a result, the transmission of bit 1 can be erroneous when the distance between TN and RN is large. Therefore, the capacity decreases for higher R. On the other hand, when R is less than R_0, p_1 increases. Therefore, the capacity increases with decreasing internodal distance. Consequently, it is necessary to select appropriate R and P_F according to the assembled donor - acceptor pair to achieve higher communication capacity. The capacity is maximized for $R = 3\ nm$ by $P_F = 0.474$. We find $C_{max} = 0.86\ bit$. Hence, we can communicate more information by using input symbol 0 more frequently than 1 with intermolecular distance of 3 nm.

3.5.2 Effect of Medium

In this analysis, we investigate the channel capacity for different media. The analysis is carried out with single ECFP-EYFP pair as the donor and the acceptor assembled on TN and RN, respectively. The nanomachines are located in different mediums and separated by a distance of $4nm$ assuming rapid randomization of relative orientation of the molecules and nanomachines.

For ECFP - EYFP pair, the Förster radius calculated in [63] assuming the medium as water at 25 °C changes in accordance with the medium. In Fig. 3.8, mutual information $I(X;Y)$ given in (3.8) is shown for varying excitation probability of the donor (P_F) for different media and different refractive indices. As the refractive index of the medium decreases, the Förster radius given in (2.4) increases. Therefore, the probability of FRET, i.e., successful transmission probability of bit 1 for the pre-specified intermolecular distance increases. As a consequence, the capacity of the channel increases with decreasing refractive index of medium. The capacity is maximized for vacuum by $P_F = 0.43$. We find $C_{max} = 0.57\ bit$.

3.5.3 Effect of Relative Orientation Factor

Here, we investigate the effect of relative orientation factor (κ^2) on the channel capacity using ECFP - EYFP as the donor - acceptor pair assembled on the nanomachines. The

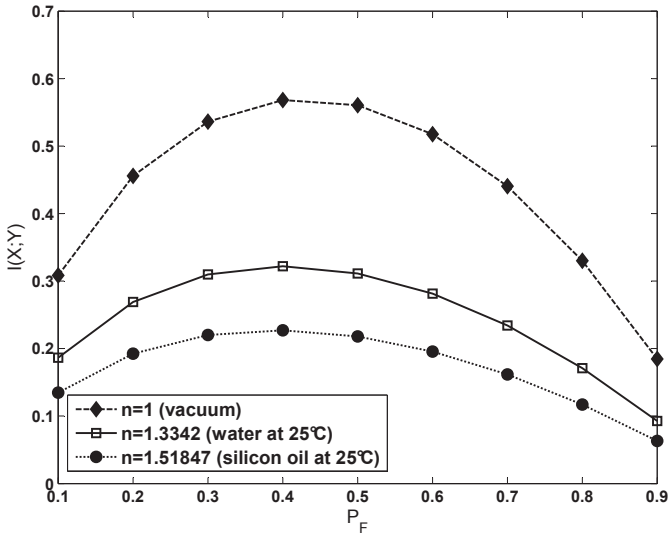

Figure 3.8: $I(X;Y)$ in bits with varying P_F for different n.

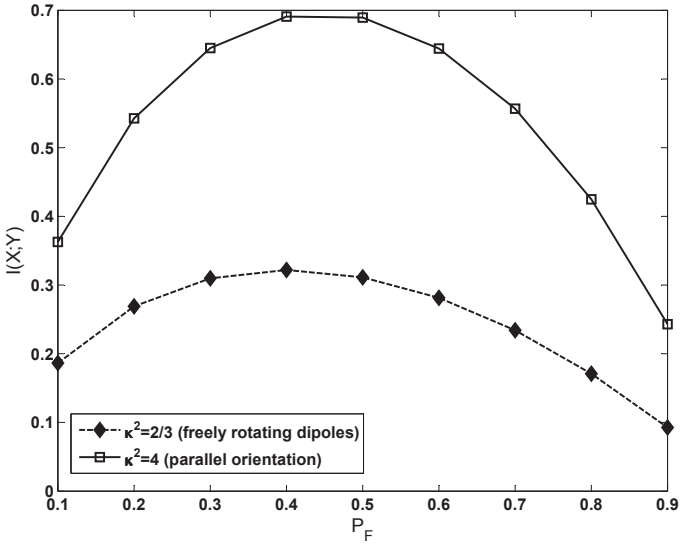

Figure 3.9: $I(X;Y)$ in bits with varying P_F for different κ^2.

nanomachines are located in a medium of water at 25 °C and separated by a distance of 4 nm.

Relative orientation factor is a measure of the relative orientation of the donor emission dipole moment and the acceptor absorption dipole moment. Determining the exact orientations of donor and acceptor molecules is impossible at this point. However, many of the

studies in the literature about FRET assume rapid randomization of the relative orientation of the dipole moments. The orientation factor is 2/3 in the case of rapid randomization. In addition, we investigate the mutual information when the orientation of the dipole moments of the molecules are parallel. In this case, the orientation factor reaches its maximum value, i.e., $\kappa^2 = 4$. The result of the analysis seen in Fig. 3.9 reveals that the parallel orientation can significantly increase the capacity of FRET-based channel compared to rapid randomization. When further advances in the nanotechnology make it possible to control the orientation of molecules, orienting the dipole moments of the donor and the acceptor molecules in parallel will be a wise strategy to achieve higher communication capacities. For parallel orientation, the capacity is $P_F = 0.47$. We find $C_{max} = 0.70$ *bit*.

3.5.4 Capacity Analysis for Different FRET Pairs

In this analysis, we investigate the FRET-based molecular communication capacity for various donor - acceptor pairs with different spectral properties, assembled on TN and RN respectively. The nanomachines are located in a medium of water at 25 °C and separated by a distance of 4 *nm*. The molecules that constitute the FRET pairs are selected among the variants of Green Fluorescent Protein (GFP). The selected donor - acceptor pairs are commonly used in FRET studies and there is a wide variety of studies about GFP variants in the literature.

There is a direct relationship between the spectral overlap of molecules and R_0 as well as FRET efficiency, i.e., the transmission probability of bit 1 (p_1). As the overlap of the spectra increases, R_0 as well as p_1 increases. The emission and absorption spectra of the selected donor - acceptor pairs are demonstrated in Fig. 3.10. For the pair of Enhanced Blue Fluorescent Protein (EBFP) and Red Fluorescent Protein (DsRed), the spectral overlap is the minimum among the other selected pairs. Therefore, R_0 for EBFP and DsRed is the minimum and calculated as 3.17 *nm* [63]. Conversely, the overlap between the emission spectrum of Enhanced Green Fluorescent Protein (EGFP) and the absorption spectrum of EYFP is the maximum among the others. As a result, R_0 for EGFP - EYFP pair is the maximum and calculated as 5.64 *nm* [63]. For the remaining FRET pair ECFP - EYFP, R_0 is previously given as 4.92 *nm* [63].

Fig. 3.11 demonstrates the mutual information, $I(X;Y)$, given in (3.8) for varying exci-

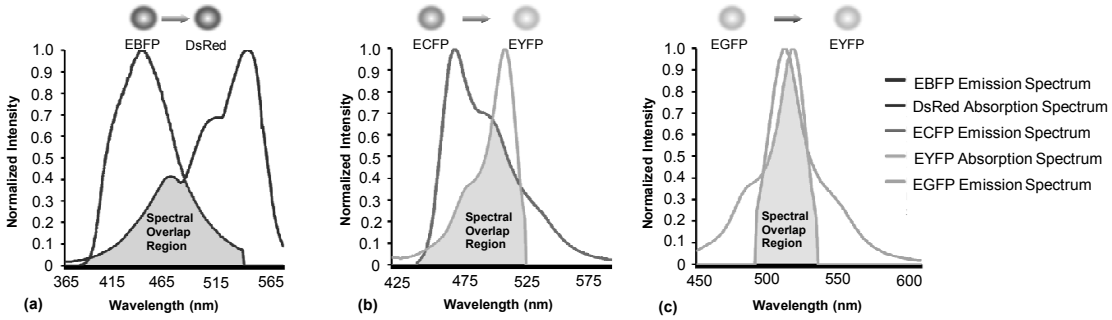

Figure 3.10: Overlapping spectra for various fluorescent protein pairs [55]. a) Emission spectrum of EBFP and absorption spectrum of DsRed. b) Emission spectrum of ECFP and absorption spectrum of EYFP. c) Emission spectrum of EGFP and absorption spectrum of EYFP.

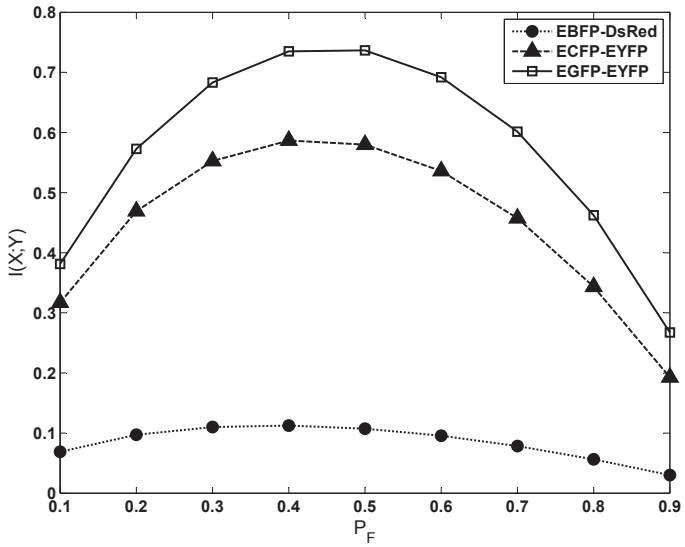

Figure 3.11: $I(X;Y)$ in bits with varying P_F for various donor - acceptor pairs.

tation probability of the donor (P_F) for donor - acceptor pairs. As expected, the capacity is higher for the pair EGFP - EYFP because of the higher transmission probability of bit 1 (p_1) as the consequence of higher spectral overlap. As the spectral overlap decreases, the capacity also decreases. Therefore, for the pair EBFP - DsRed, the capacity is the minimum among the others. The selection of the donor and acceptor pair with larger spectral overlap is the key strategy in order to achieve higher communication capacity. The capacity is maximized for EGFP - EYFP by $P_F = 0.45$. We find $C_{max} = 0.74\ bit$. Hence, we can

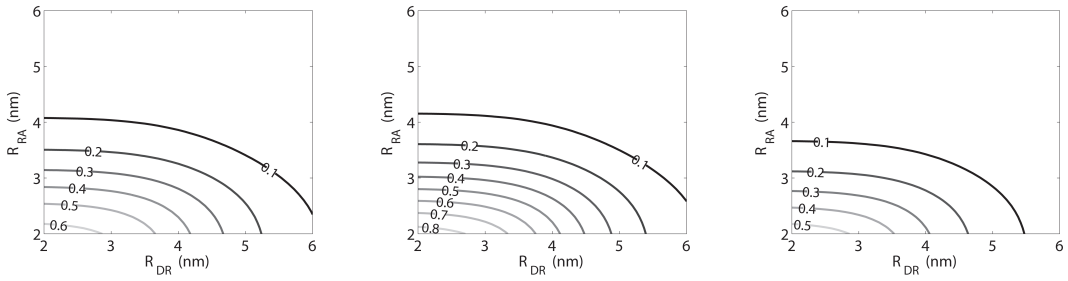

(a) $P_F = 0.2$ (b) $P_F = 0.5$ (c) $P_F = 0.8$

Figure 3.12: $I(X;Y)$ in bits for several P_F with varying R_{DR} and R_{RA} for ECFP(D)-EYFP(R)-EGFP(A) configuration.

communicate more information by using input symbol 0 more frequently than 1 for EGFP - EYFP pair.

3.5.5 Capacity Analysis for Long-range FRET-based Communication Channel with Multi-step FRET

Here, we analyze the multi-step FRET-based communication channel information theoretically for the simplest form with only one relay in a similar manner with the single-pair analyses. The main difference of the multi-step case is the determination of p_1. Assuming that a proper selection for excitation period (T_H) is made, neglecting direct excitation and using the fact that $p_1 = P_{FRET}$, p_1, i.e., the probability of successful transmission of bit 1 between TN and RN for the linear two-step donor-relay-acceptor arrangement can be expressed as the same as the right-hand side of (3.6) in terms of the intermolecular distances.

With the same assumption for T_H, the probability of success in transmission of bit 0 between TN and RN ($p_{0,DA}$) is 1, i.e., the same as in the case of the single-pair FRET-based communication. With these transmission probabilities, we conclude that the multi-step channel also shows the Z-channel characteristics demonstrated in Fig. 3.2.

For a linear arrangement of the previously mentioned triplet ECFP-EYFP-EGFP on TN, HN and RN respectively which are located in a medium of water at 25 °C and assuming rapid randomization of relative orientation of the molecules on the nanomachines, i.e., $\kappa^2 = 2/3$, the dependence of mutual information ($I(X;Y)$) on R_{DR} and R_{RA} is analyzed using (3.8)

and the results are demonstrated in Fig. 3.12.

As it is seen in Fig. 3.12, the dependence of the reliability of the channel on internodal distances is in parallel with the results obtained for efficiency dependence in Fig. 3.5. Particularly, we conclude that using bit 0 more frequently than bit 1, i.e., decreasing P_F, results in an increase in the mutual information and the capacity for the same arrangement.

Chapter 4

FRET-BASED POINT-TO-POINT AND BROADCAST NANOSCALE COMMUNICATION CHANNELS WITH MULTI-EXCITON TRANSMISSION

Nanoscale communication based on Förster Resonance Energy Transfer (FRET) enables nanoscale single molecular devices to communicate with each other utilizing excitons generated on fluorescent molecules as information carriers. Based on the point-to-point single-exciton FRET-based nanocommunication model, we investigate the multiple-exciton case for point-to-point and broadcast communications following an information theoretical approach and conducting simulations through Monte Carlo approach. We demonstrate that the multi-exciton transmission significantly improves the channel reliability and the range of the communication up to tens of nanometers for immobile nanonodes providing high data transmission rates. Furthermore, our analyses indicate that multi-exciton transmission enables the broadcasting of information from a transmitter nanonode to many receiver nanonodes pointing out the potential of FRET-based communication to extend over nanonetworks. The high transmission rates obtained by multi-exciton scheme for point-to-point and broadcast communications make FRET-based communication promising for future molecular computers.

4.1 Introduction

Nanonetworks allow nanomachines to cooperatively exchange information to achieve more complex tasks ranging from nuclear defense to in-body drug delivery and disease treatments [1], [3]. The exchanged information among nanomachines might be an output of a sensing process or a logic operation, as well as a control signal sent by a remote information source that intends to control the operation of nanomachines. Modeling the potential information sharing mechanisms among nanomachines are crucial for the design of fully functional nanomachines with networking capabilities. Several approaches have been proposed in order

to achieve communication at nanoscale such as electromagnetic, acoustic, nanomechanical or molecular, some of which are inspired by nature [30], [2]. In addition to the existing techniques, in this thesis, we propose and investigate a novel and radically different nanoscale molecular communication method exploiting FRET.

In this chapter of the thesis, based on the channel model given in 3, we investigate the feasibility and performance of FRET-based broadcast communication channel between one TN and many RNs from the network perspective. Furthermore, we propose encoding information into multiple excitons, instead of single-excitons, in order to improve the reliability of the communication. We analyze the performance of FRET-based point-to-point and broadcast communication channels with multi-exciton transmission. Performance evaluations of the communication channels are carried out through simulations with Monte Carlo algorithms based on the competitive behavior of multiple excitons.

The remainder of this chapter is organized as follows. In Section 4.2, we briefly present the basics of the proposed multi-exciton transmission scheme. In Sections 4.3 and 4.4, we information theoretically model FRET-based point-to-point and broadcast communication channels with multi-exciton transmission. In Section 4.5, we evaluate the performance of the proposed communication schemes in terms of information theoretical capacity.

4.2 Multi-Exciton Transmission Scheme

FRET-based communication can be very unreliable if the internodal distance is greater than the Förster radius of the molecules [45], or there are more than one RN communicating with TN. In order to reduce the error probability, one might come up with the idea of transmitting the signal many times through the channel. However, without a feedback mechanism, i.e., without the knowledge of the TN about the success of the transmission, this method has to be applied for each transmission with the number of repetitions determined prior to communication. For the case of single TN - single RN communication with fixed repetitions, the bit interval required for negligible ISI is multiplied with the number of repetitions, N:

$$T_{b,repeat-min} = N \times T_{b,min} = N \times (\tau_{DA,max} + \tau_{A,max}) \tag{4.1}$$

Assuming, R, n, and κ^2 are constant for each transmission, the transmission probability of bit-1 becomes

$$p_1 = 1 - (1 - P_{FRET})^N \tag{4.2}$$

p_0 is again equal to 1 for repeated transmission. As can be seen intuitively, this transmission scheme significantly reduces the error probability of bit-1. Therefore, the capacity is expected to increase with increasing N. However, high bit duration T_b required for negligible ISI significantly reduces the transmission rate.

Since the excited state lifetimes of the molecules are random variables with exponential distributions, it is very possible for an exciton to be removed from the system in a duration smaller than $T_{b,min}$. This makes it inefficient for IS to send fixed period pulses to TN. An alternative way to reduce the error probability of transmission with relatively small bit intervals is to increase the pulse duration sent by IS into nanoseconds range and allow many excitations to be generated on TN in one pulse duration with a probabilistic manner. In this scheme, for the representation of bit-1, IS continuously sends photons or electrons to TN in a pulse duration. TN is expected to be excited by the first photon or electron coming from IS. After a duration of τ_{DA}, TN relaxes through FRET or fluorescence. If τ_{DA} is smaller than the pulse duration, then TN is excited again as soon as it relaxes, and this continues until the pulse duration ends. In other words, multiple excitons are transmitted during a pulse duration to represent bit-1.

In the following sections, multi-exciton transmission scheme is applied to FRET-based point-to-point and broadcast channels, and transmission probabilities, channel capacities and ISI characteristics are investigated through Monte Carlo simulations.

4.3 FRET-Based Point-to-Point Communication with Multi-Exciton Transmission

In this section, we revisit our point-to-point communication channel model in order to investigate the communication performance of the channel with multi-exciton transmission scheme. Here, IS sends an optical or electrical pulse with T_{pulse} duration to TN in the beginning of a T_b-duration time slot to make it transmit bit-1. In order for TN to transmit bit-0, IS does not send any pulse during the time interval T_b. In one slot time interval, i.e., bit interval, TN can be excited and relaxed through FRET or fluorescence many times. When

RN is excited through FRET, bit-1 is detected by RN, and then the transferred exciton is removed from the system after a random occupation time, τ_A, which is also an exponential random variable with mean μ_{τ_A}. Once RN detects bit-1, it neglects other excitations until the current bit interval ends. If RN is not excited in a bit duration, it decides that bit-0 is sent.

Assuming that there is no other excitation source except IS, the successful transmission probability of bit-0, i.e., p_0, equals to 1. The transmission probability of bit-1 can be written as

$$p_1 = 1 - \prod_{i=1}^{N}(1 - P_{FRET,i}) \tag{4.3}$$

where N is a random variable which defines the number of excitons generated by the pulse with duration T_{pulse}. Note that in this scheme, TN is always in the excited state during T_{pulse}, such that, when it is relaxed through fluorescence or FRET, it is immediately excited by another photon or electron coming from IS. Therefore, the generation time of the i^{th} exciton on the donor is expressed by

$$T_{g,i} = \sum_{l=1}^{i-1} \tau_{DA,l} \tag{4.4}$$

where $\tau_{DA,i}$ denotes the excited state lifetime of the donor for the ith exciton, i.e., the occupation time of the ith exciton on the donor. $\tau_{DA,i}$ is an exponential random variable with a mean that depends on the state of the acceptor at time $T_{g,i}$. The acceptor can be in the excited state at time $T_{g,i}$ due to the transfer of a preceding exciton. Therefore, $\mu_{\tau_{DA,i}}$ can be expressed as

$$\mu_{\tau_{DA,i}} = \begin{cases} \frac{1}{k_R} & \text{if A is excited at } T_{g,i} \\ \frac{1}{k_R + k_{T,i}} & \text{if A is available at } T_{g,i} \end{cases} \tag{4.5}$$

where $k_{T,i}$ is the FRET rate for the ith exciton that can be given as follows

$$k_{T,i} = k_R \left(\frac{R_{0,i}}{R}\right)^6 \tag{4.6}$$

where $R_{0,i} = (8.8 \times 10^{22} \kappa_i^2 n^{-4} J(\lambda))^{1/6}$. $R_{0,i}$ depends on the random variable κ_i^2 which defines the relative orientation of the fluorophores during the generation and relaxation of the ith exciton. Assuming the molecules are isotropically free, κ_1^2, ..., κ_N^2 are independent and identically distributed (i.i.d.) random variables with the probability distribution defined in (2.7).

Accordingly, the ith exciton on the donor fluoresces or is transferred to the acceptor through FRET at time $T_{r,i} = T_{g,i} + \tau_{DA,i}$. If the exciton is transferred to the acceptor at $T_{r,i}$, it occupies the acceptor until the acceptor fluoresces at time $T_{r,i} + \tau_{A,i}$. Note that the emission spectrum of the acceptor and the absorption spectrum of donor are assumed to be non-overlapping, therefore, fluorescence is the only way for the excited acceptor to relax. $\tau_{A,i}$ denotes the occupation time of the ith exciton on the acceptor, and it is an exponential random variable with mean μ_{τ_A}. The exciton i, stays in the system for $\tau_{DA,i}$, if it results in fluorescence of the donor; and for $\tau_{DA,i} + \tau_{A,i}$, if it results in fluorescence of the acceptor.

The FRET probability for the ith exciton, i.e., $P_{FRET,i}$, is a random variable that depends on the state of the acceptor at time $T_{r,i}$:

$$P_{FRET,i} = \begin{cases} 0 & \text{if A is excited at } T_{r,i} \\ \frac{k_{T,i}}{k_R + k_{T,i}} & \text{if A is available at } T_{r,i} \end{cases} \tag{4.7}$$

The randomness of $P_{FRET,i}$ as well as p_1 is originated from the random nature of relative orientations and the occupation times. Due to high degree of stochasticity, we simulate the transmission of bit-1 following a Monte Carlo approach in order to obtain numerical expressions for p_1 as well as ISI probability for different system parameters. Using the obtained values, we analyze the channel capacity and achievable rates in Section V-A.

4.4 FRET-Based Broadcast Communication with Multi-Exciton Transmission

FRET occurs when the transition dipole moments of two fluorophores come into resonance. Therefore, FRET is a pairwise energy transfer, such that it is not possible for an excited donor molecule to transfer its excited energy to more than one acceptors at the same time. However, if the donor is excited and relaxed continuously for a sufficiently large time interval, as in the case of multi-exciton transmission, it is possible that each of the acceptor molecules is excited through FRET by different excitons.

FRET-based broadcast communication can be realized with one TN surrounded by many RNs in a close proximity as seen in Fig. 4.1. TN sends the same binary information come from IS to each of RNs. The information theoretical capacity of this broadcast communication channel is limited by the performance of the worst point-to-point channel in the network. If we assume that RNs are located by the same distance from TN, the broadcast

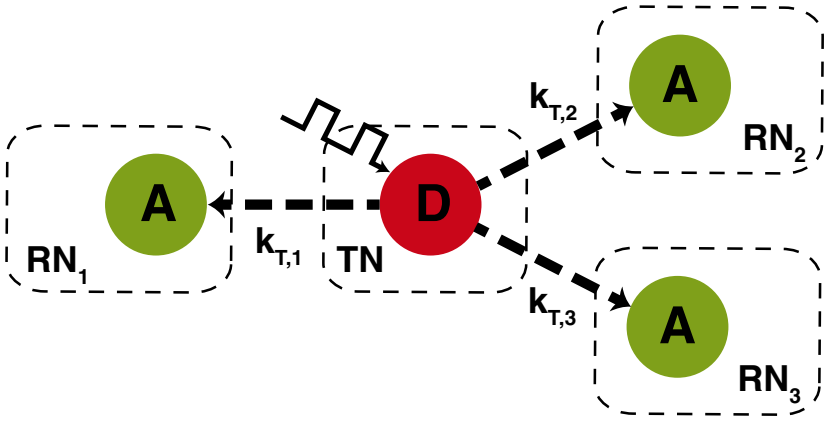

Figure 4.1: Demonstration of FRET-based broadcast communication with a single TN communicating with three RNs in close proximity

channel capacity equals to the capacity of one of the TN-RN point-to-point channels. Therefore, we investigate the binary transmission probabilities through single TN-RN channel in the broadcast network to determine the overall broadcast channel capacity.

Assuming that TN communicates with k number of RNs, the successful transmission probability of bit-1 to the jth RN, $p_{1,j}$, is the probability that jth RN gets excited via FRET in a bit interval T_b, when TN is continuously excited by IS in a time duration of T_{pulse}. Note that $T_{pulse} \leq T_b$, and T_{pulse} begins at the beginning of T_b. Assuming that the length of T_b guarantees the no-ISI condition, $p_{1,j}$ can be given as

$$p_{1,j} = 1 - \prod_{i=1}^{N} (1 - P_{FRET,j,i}) \tag{4.8}$$

$p_{0,j}$, i.e., the non-excitation probability of the jth RN during T_b, when IS sends no pulse, is 1 assuming that there is no other excitation source. Here, $P_{FRET,j,i}$ is a random variable that represents the probability of FRET between TN and the jth RN for the ith exciton. N is a random variable indicating the number of the excitons generated by one pulse. Note that the donor is always in the excited state, and the generation time of the ith exciton is given as in (4.4). $\tau_{DA,i}$, i.e., the occupation time of the exciton i on the donor, is an exponential random variable and its mean can be expressed as

$$\mu_{\tau_{DA,i}} = (k_R + \sum_{j=1}^{k} k_{T,j,i} \mathbf{1}_{g,j,i})^{-1} \tag{4.9}$$

where $k_{T,j,i}$ is a random variable which defines the FRET rate between TN and the jth RN for the ith exciton, and $\mathbf{1}_{g,j,i}$ is the indicator function defined on the set of the acceptor molecules. $\mathbf{1}_{g,j,i} = 1$, if the jth acceptor A_j is available at time $T_{g,i}$, and $\mathbf{1}_{g,j,i} = 0$, if A_j is in the excited state at time $T_{g,i}$. $k_{T,j,i}$ in terms of the orientation parameter can be expressed by

$$k_{T,j,i} = 8.8 \times 10^{22} \kappa_{j,i}^2 n^{-4} J_j(\lambda) \frac{k_R}{R_j^6} \tag{4.10}$$

where R_j is the distance between the centers of the transition dipole moments of TN and the jth RN. $J_j(\lambda)$ is the degree of the overlap between the emission spectrum of the donor and the absorption spectrum of A_j. R_j and $J_j(\lambda)$, as well as n, are assumed to be constant during the communication. $\kappa_{j,i}$ is the relative orientation factor of the donor and A_j during the generation and relaxation of the exciton i. For isotropically free molecules, $\kappa_{j,1}^2$, ..., $\kappa_{j,N}^2$, as well as $\kappa_{1,i}^2$, ..., $\kappa_{k,i}^2$ are i.i.d. random variables with the probability distribution defined in (2.7).

At time $T_{g,i} + \tau_{DA,i}$, the exciton i is either removed from the system by the fluorescence of TN, or is transferred to one of the RNs. The probability of the transfer for the ith exciton to A_j in terms of process rates is given as

$$P_{FRET,j,i} = \frac{k_{T,j,i} \mathbf{1}_{r,j,i}}{k_R + \sum_{l=1}^{k} k_{T,l,i} \mathbf{1}_{r,l,i}} \tag{4.11}$$

where $\mathbf{1}_{r,j,i} = 1$ when A_j is available at time $T_{r,i}$, and $\mathbf{1}_{r,j,i} = 0$ when A_j is excited at time $T_{r,i}$.

The transmission of bit-1 is simulated for FRET-based broadcast communications with different system parameters following a Monte Carlo approach. We numerically obtain $p_{1,j}$, and then, investigate the broadcast channel capacity and ISI probability in Section V-B.

4.5 Information Theoretical Analysis

In this section, we investigate the performance of FRET-based point-to-point and broadcast communications in terms of information theoretical capacity and ISI probability for varying system parameters.

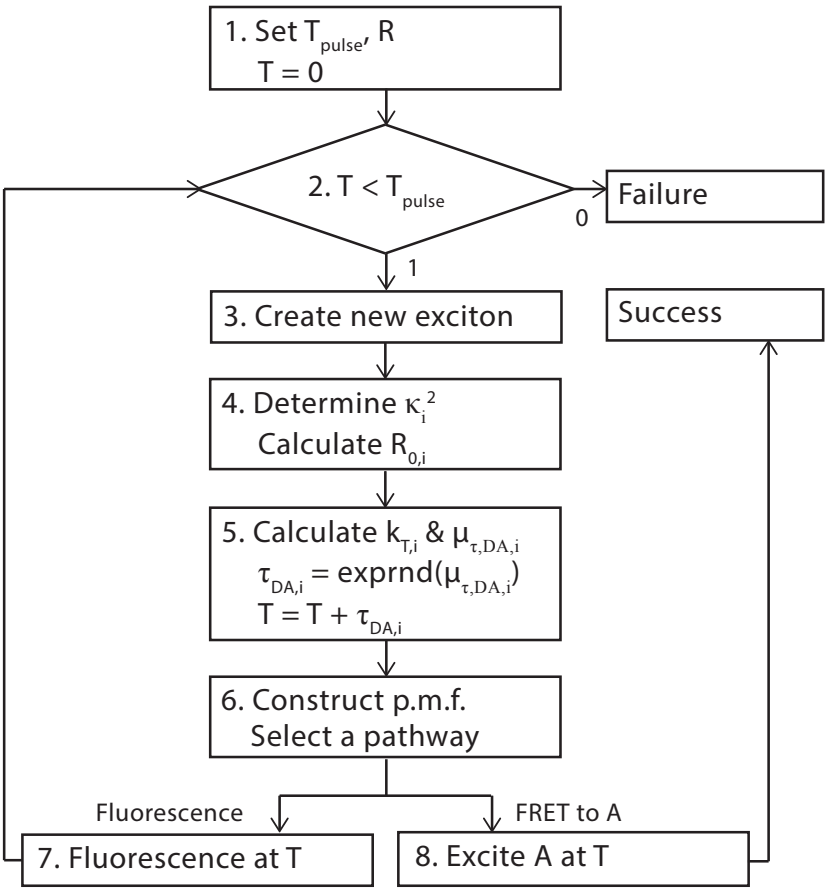

Figure 4.2: Monte Carlo algorithm for the simulation of the transmission of bit-1 through the point-to-point communication channel.

4.5.1 Analysis of FRET-Based Point-to-Point Communications with Multi-Exciton Transmission

The degree of randomness over the transmission probability of bit-1 makes it hard to find an analytical expression for the information theoretical capacity of the channel. Therefore, we simulate the channel model for the transmission of bit-1 following a Monte Carlo approach.

Simulation Algorithm

Fig. 4.2 demonstrates the algorithm used in the simulations operating through the following steps:

1. The pulse length T_{pulse} and the internodal distance R between TN and RN are set. The simulation time T is set to its initial value 0.

2. The algorithm checks whether simulation time reaches at T_{pulse}.

3. If T_{pulse} is not reached, a new exciton is generated on donor, i.e., TN, with the index i at time $T = T_{g,i}$. If $T > T_{pulse}$, then the simulation ends with the failure of the transmission of bit-1.

4. For the time that the new exciton is created, the relative orientation of the isotropically free molecules is determined randomly according to the distribution (2.7). The Förster radius $R_{0,i}$ between the donor and the acceptor for the ith exciton is calculated accordingly.

5. FRET rate $k_{T,i}$ is determined using $R_{0,i}$. The algorithm checks the availability of the acceptor at $T = T_{g,i}$, and calculates mean lifetime μ_τ accordingly. The lifetime τ_{DA} is determined randomly from the exponential distribution with mean μ_τ. The simulation time T is proceeded as τ_{DA}, i.e., $T = T_{r,i}$, since it is not possible for another exciton to be generated until the donor relaxes.

6. At time $T = T_{r,i}$, the algorithm checks the availability of the acceptor, and calculates $P_{FRET,i}$ using the relation (4.7). A probability mass function (p.m.f.) for the possible pathways is constructed. The pathway that will be followed by the exciton i is selected randomly according to the constructed p.m.f.

7. In the case that the exciton undergoes fluorescence, the donor is relaxed through fluorescence at $T = T_{r,i}$, and the exciton i is removed from the system. The simulation continues at Step 2.

8. In the case that the exciton is transferred to RN through FRET, the donor is relaxed, and the acceptor is excited at time $T = T_{r,i}$. Therefore, the simulation ends with the successful transmission of bit-1.

The simulation is carried out for two hypothetical molecules with the typical parameters; $\tau_D = 2$ ns, $\tau_A = 2$ ns and $R_0 = 5$ nm for the mean orientation factor [51], and with varying T_{pulse} and R. p_1 is calculated as the number of the successful transmissions divided by the total number of the simulation runs. Note that the simulation is repeated until p_1 converges to a finite value.

Channel Capacity

The channel capacity C is derived information theoretically from the obtained value of p_1, given that $p_0 = 1$ in all of the cases. Since the transmission of bit-0 is always successful and the transmission of bit-1 is problematic, the channel information theoretically shows Z-channel characteristics [19]. The channel capacity of Z-channel for each parameter is derived as the maximum mutual information between input and output alphabets over all input distributions. By omitting the calculations, the results are demonstrated in Fig. 4.3. As expected, the capacity significantly decreases with increasing R after a critical distance due to the sixth power dependence of the P_{FRET} on R. For low values of T_{pulse}, the critical distance is approximately equal to R_0. However, as T_{pulse} increases, the number of excitons employed in the transmission of bit-1 increases, therefore, the capacity is considerably improved over internodal distances larger than R_0.

ISI and Achievable Rates

If the bit period T_b is not set carefully, the resultant communication might be ambiguous, such that, the excitons created during T_b might arrive the RN at a time greater than T_b, i.e., in the next bit interval. Since the governing time parameters are exponential random variables, it is not possible to completely remove ISI, however, the ISI probability might be reduced to negligible values by setting T_b over some threshold value. In order to determine the ISI probabilities for varying T_b, we observe the maximum removal times of the excitons that reaches to RN conducting the Monte Carlo simulations and recording the time data for the last-arrive excitons. The histograms of the obtained data are demonstrated in Fig. 4.4 for four different typical combinations of T_{pulse} and R with Gaussian fits. According to the data, we conclude that, for the same R, varying T_{pulse} only changes the mean of the distribution of the removal times in proportion, and the variance of the removal times is not affected

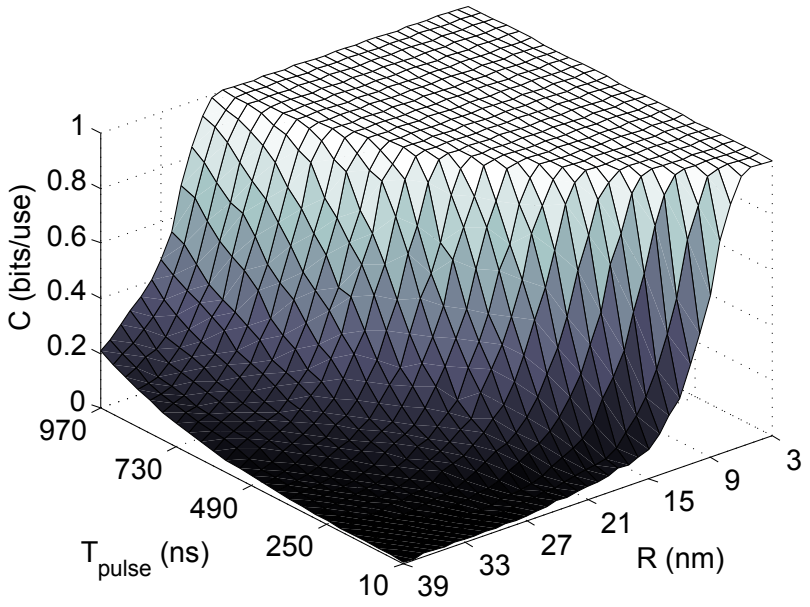

Figure 4.3: Channel capacity with varying T_{pulse} and R.

considerably. However, for constant T_{pulse}, varying R results in a significant variation of the distribution of the removal times. This is due the fact that the variation in T_{pulse} has no effect on the excited state lifetimes of the employed molecules, i.e., the occupation times of the excitons on the molecules, however, the variation in R alters the process rates significantly, and finally results in the variation of the time parameters. Therefore, ISI probabilities are analyzed for a constant T_{pulse} and varying R. Setting $T_{pulse} = 10$ ns and $T_b = T_{pulse} + T_{off}$, the resultant ISI probabilities for varying R are demonstrated in Fig. 4.5. ISI considerably decreases with increasing R for different values of T_{off}, and setting T_b as greater than $T_{pulse} + 20$ ns results in negligible ISI for all R values.

The upper bound for reliable communication rate can be expressed by $R_{max} = C/T_b$. Neglecting ISI by setting $T_{off} = 20$ ns, the achievable rate for different pulse lengths over varying internodal distances is shown in Fig. 4.6. We conclude that nanomachines can reliably communicate at a rate up to 33 Mbps over 5-nm distance, and at a rate up to 300 kbps over 35-nm distance. Note that, for short-range communication, using shorter pulses results in higher data rates, however, over longer distances, we can get higher data rates with long-width pulses. With these results, we can certainly conclude that FRET-based

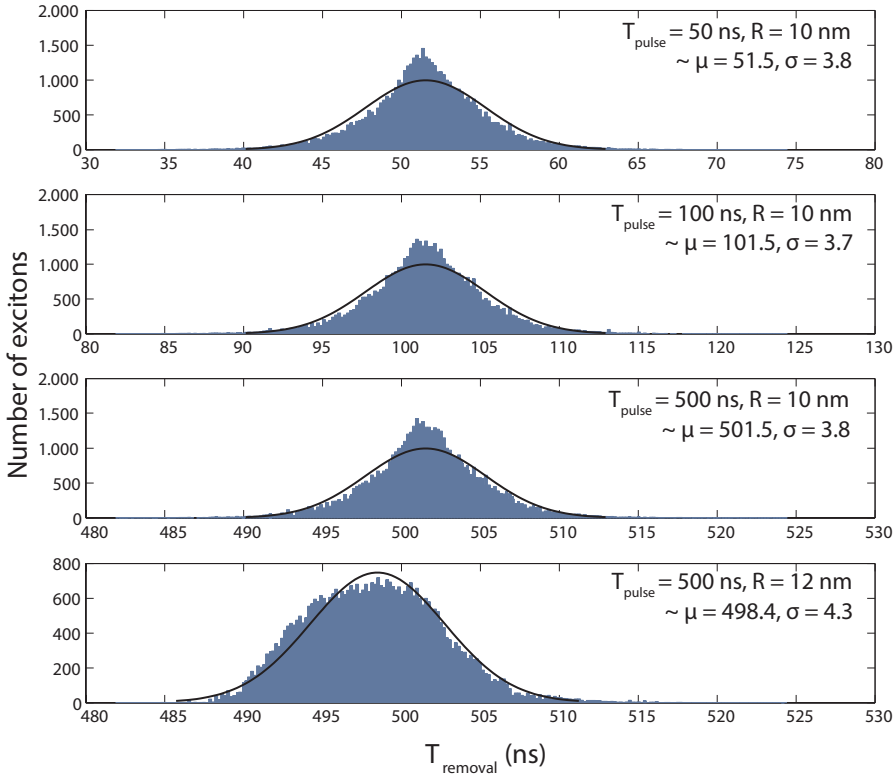

Figure 4.4: Distribution of removal times with Gaussian fit for different T_{pulse} and R.

communication strongly outperforms other molecular communication methods by means of communication rate.

4.5.2 Analysis of FRET-Based Broadcast Communications with Multi-Exciton Transmission

In this section, we analyze the information theoretical capacity and investigate the ISI problem for FRET-based broadcast communication channel of which principles are expressed in Section III-B. The transmission of bit-1 from TN to the mth RN out of k RNs through the broadcast channel is simulated using the algorithm described in Fig. 4.7. The transmission probability of bit-1 between TN and the mth RN, i.e., $p_{1,m}$, is obtained following a Monte Carlo approach. The algorithm used for broadcast communication differs from the single pair communication algorithm basically in Step 9 and Step 10, such that the simulation does not end in success until the mth RN is excited. If jth RN with $j \neq m$ is excited,

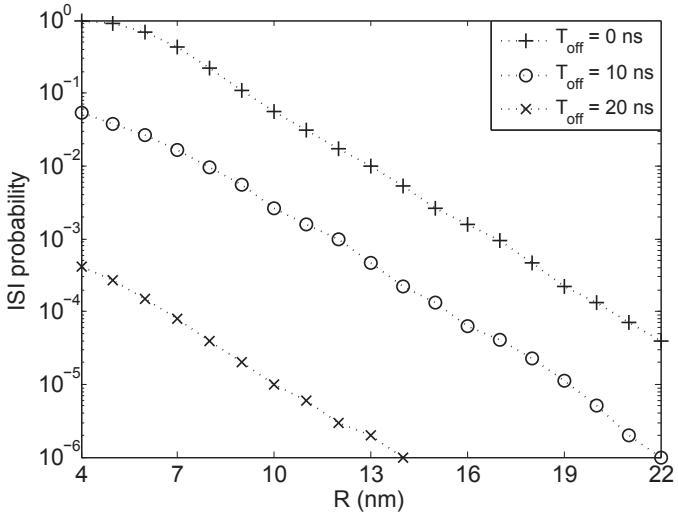

Figure 4.5: ISI probability for several T_{off} with varying R.

the simulation continues with Step 10, where the ith exciton on the jth RN is removed by fluorescence after a random occupation time.

In the simulations, we assume all of the RNs have the same optical characteristics and are at the same distance R from TN. We employ the same hypothetical molecules as in Section III-A, with the typical values of the intrinsic parameters, such that, $\tau_D = 2$ ns, $\tau_A = 2$ ns and $R_0 = 5$ nm for the mean relative orientation [51]. $p_{1,m}$ is calculated as the proportion of the number of successful transmissions of bit-1 from TN to the mth RN over the total number of simulation runs, and the simulation is repeated until $p_{1,m}$ converges. The information theoretical capacity of the resultant Z-channel is determined as the maximum mutual information between the input and output alphabets over all input distributions [19]. The derived capacity of the channel between TN and mth RN gives the capacity of the overall broadcast communication channel.

Channel Capacity

The obtained capacity values for typical k, R and T_{pulse} combinations are plotted in Fig. 4.8. A remarkable result of the analysis is that the critical distance where the capacity begins to significantly decrease does not alter notably with varying number of RNs if T_{pulse} is set sufficiently large. Therefore, the capacity of point-to-point communication channel can be

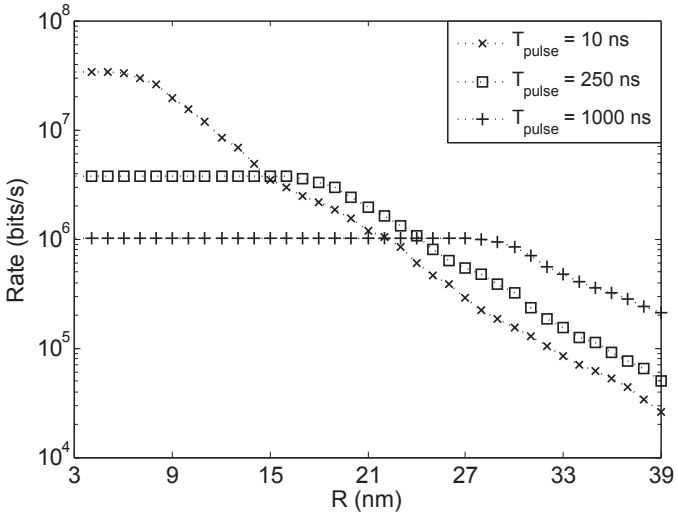

Figure 4.6: Achievable rates for several T_{pulse} with varying R.

achieved in a broadcast network with appropriately selected pulse lengths. However, for low values of T_{pulse}, addition of extra RNs into the network reduces the capacity for the same internodal distances, since the number of excitons generated with a short pulse might not be sufficient to excite all of RNs. Furthermore, we observe that the slope of the capacity decrease for distances greater than the critical distance is sharpened as k increases. This is because as the number of RNs increases, the FRET processes that contribute to the relaxation of the donor increases. As a result, the sixth power dependence of many FRET processes combine improving the distance effect on the capacity expression.

ISI and Achievable Rates

The ISI probability is analyzed using the last exciton removal times on the acceptor, and we conclude that the distribution of the removal times does not alter notably for varying T_{pulse}, however, the variation of R significantly effects the characteristics of the distribution as in the case of point-to-point communications. By setting $T_{pulse} = 10$ ns and $T_b = T_{pulse} + T_{off}$, the result of the analysis is plotted for different combinations of k, R and T_{off} in Fig. 4.9. As is seen, the ISI probability decreases with increasing R and the increasing number of RNs. Setting the offset time as $T_{off} = 20$ ns results in a negligible probability of ISI as in the point-to-point communications. Therefore, the achievable rates for broadcast

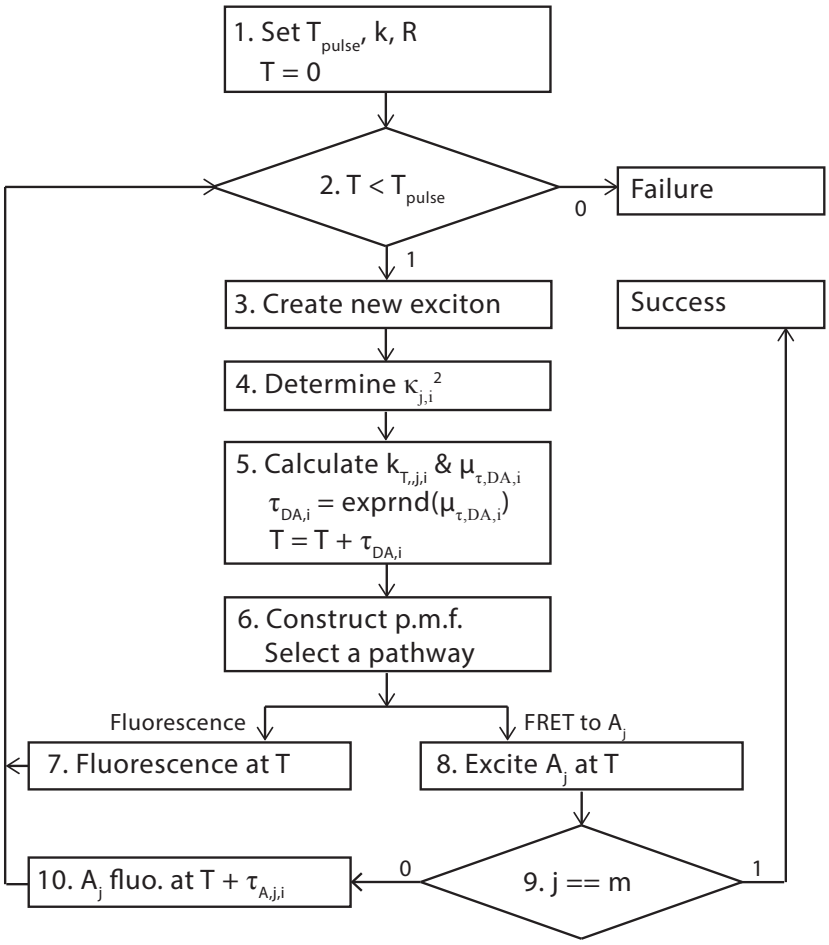

Figure 4.7: Monte Carlo algorithm for the simulation of the transmission of bit-1 through the broadcast communication channel.

communication are approximately the same as that of the point-to-point communication with sufficiently large T_{pulse}.

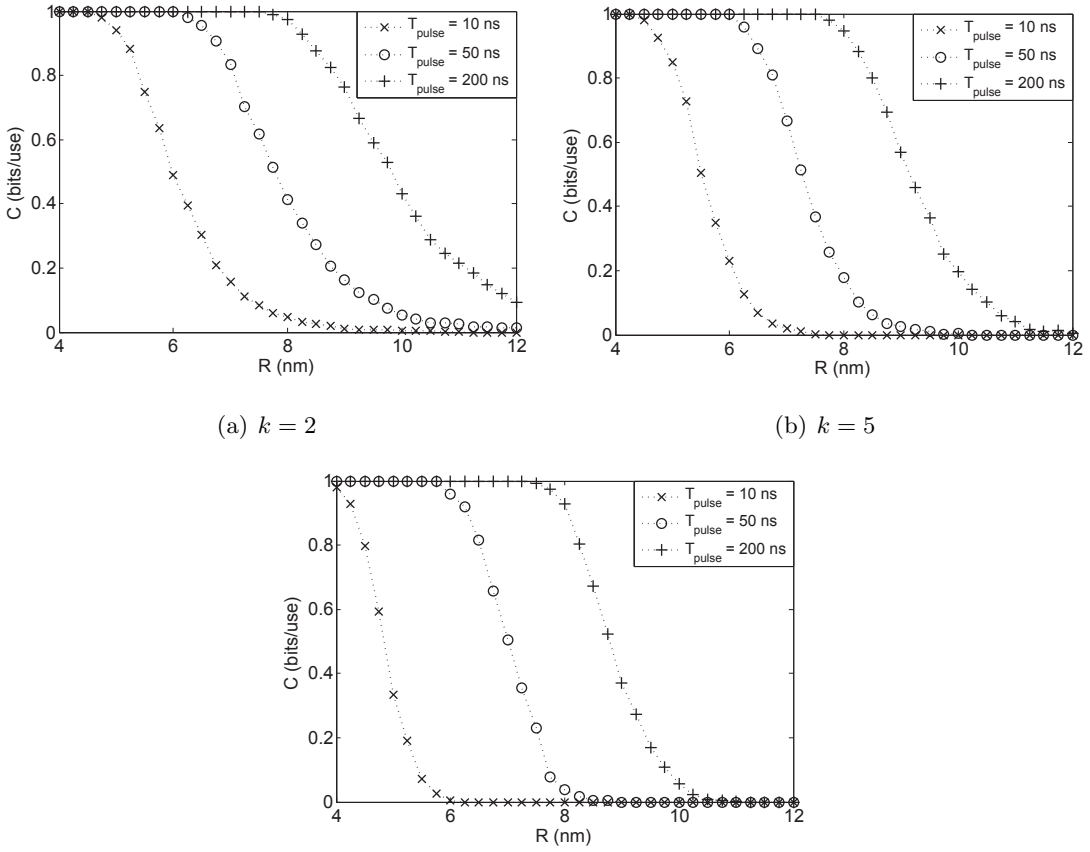

(a) $k = 2$

(b) $k = 5$

(c) $k = 10$

Figure 4.8: Broadcast channel capacity for several k with varying T_{pulse} and R.

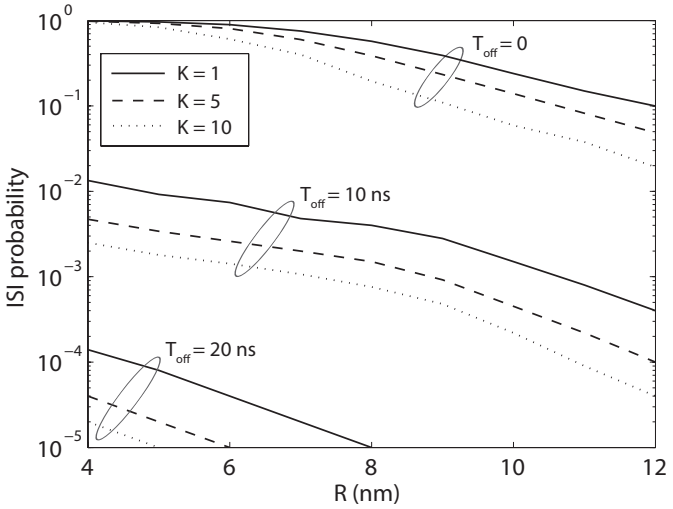

Figure 4.9: ISI probability of broadcast communication for different k and T_{off} with varying R.

Chapter 5

INFORMATION ROUTING IN FRET-BASED NANONETWORKS

5.1 Introduction

The ability of controlling the route of the information flow in a nanonetwork comprising many nanonodes with various sensing, computing and actuating capabilities brings the advantage of making the nanonodes cooperatively perform several complex tasks. In this chapter, we propose electrically and chemically active routing mechanisms to control the information flow in an FRET-based nanonetwork exploiting the remarkable dependence of FRET on spectral and spatial parameters of fluorophores.

5.2 Electrical Routing

Semiconductor nanoparticles are extensively used in fluorescence-based applications owing to their exceptional properties which are mainly originated from the effect of quantum confinement, such as size-dependent tunable emission, high quantum yield and broad absorption spectrum as well as narrowband emission [4]. Another distinctive property of semiconductor nanoparticles is Quantum Confined Stark Effect (QCSE) that defines the Stark Shift in the emission spectrum of the particle with varying internal or external electric field [70]-[42]. QCSE brings another dimension to the spectral tunability of the emission allowing post-synthesis tuning of the optical characteristics.

In a quantitative sense, the shift of a semiconductor nanoparticle in terms of electric field is approximated as a sum of linear and quadratic functions [26] as

$$\Delta E = \mu\xi + \frac{1}{2}\alpha\xi^2 + \dots \tag{5.1}$$

where ΔE is the shift in the energy spectrum; μ is the projection of excited-state dipole; α is the polarizability along the electric field, and ξ is the magnitude of the applied electric field.

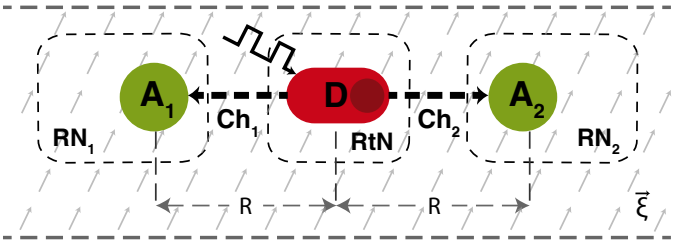

Figure 5.1: Demonstration of electrically controllable routing of the communication between a single RtN and two RNs.

The tunability of the emission with an electric field is exploited as a control mechanism over the FRET efficiency in [13]. Becker *et al.* investigate the FRET between CdSe/CdS Quantum Rods (QR) and Cy5 derivative dye molecules exposed to an external electric field, and the switch behavior of the mechanism over FRET is experimentally demonstrated obtaining a typical 10 nm wavelength shift [13]. The idea is based on tuning the degree of the spectral overlap between donor CdSe/CdS and acceptor Cy5 by altering the magnitude of the applied electric field. As the electric field increases, the emission spectrum of CdSe/CdS is red-shifted, however, the absorption spectrum of the dye molecule is not affected by the electric field. Thus, the overlap either increases or decreases depending on the relative positions of the emission and absorption spectra of CdSe/CdS and Cy5, respectively. As a result, efficiency is tuned with electric field.

In this section, we further develop the idea introduced in [13] by approaching from the communication perspective and exploiting QCSE in order to enable a nanoscale communication network which is capable of altering its state depending on the magnitude of the applied electric field. Using a semiconductor nanoparticle as a network node brings the selective routing capability to the node such that it becomes able to route the incoming information packets from IS or a preceding node, through one of the FRET channels making the selection according to the magnitude of the applied electric field. Employing this type of routing mechanism brings the advantage of directing the information flow at nanoscale by controlling it at macroscale.

In the considered scenario, a single quantum rod CdSe/CdS as the Router Nanonode (RtN) is the first destination of the information coming from an IS. Two spectrally distinct acceptors as RNs with different absorption characteristics are located in the opposite sides

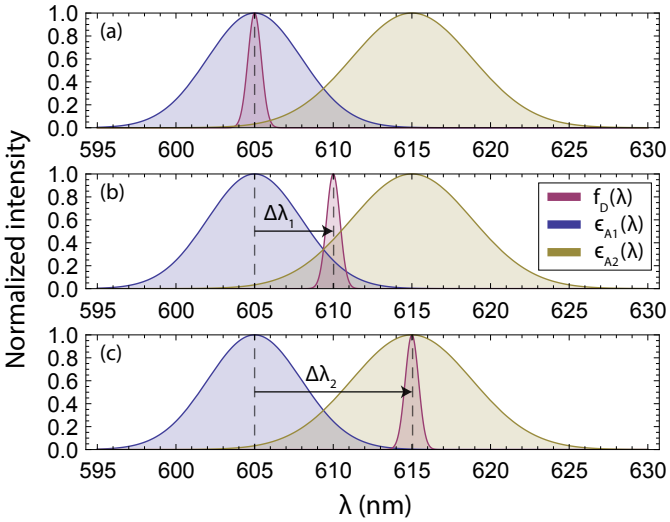

Figure 5.2: Approximated emission spectrum of single CdSe/CdS and absorption spectra of the hypothetical dye molecules at different spectral shifts (a) $\Delta\lambda_0 = 0$, (b) $\Delta\lambda_1 = 5$ nm, (c) $\Delta\lambda_2 = 10$ nm.

of RtN with a distance R to RtN as demonstrated in Fig. 5.1.

In order to investigate the performance of the routing mechanism in terms of communication capacity, we approximate the normalized emission of the router CdSe/CdS, i.e., $f_D(\lambda)$, and the absorption spectra of the RN dye molecules, i.e., $\epsilon_{A_1}(\lambda)$ and $\epsilon_{A_2}(\lambda)$, as Gaussian distributions given as

$$f(\lambda) = exp\left(k(\lambda - \lambda_c)^2\right) \tag{5.2}$$

where λ_c is the center wavelength at which emission or absorption is maximum, and k is the fitting parameter which gives the measure of the spectral broadening about the mean wavelength, i.e., linewidth of the spectrum. For a single CdSe/CdS, λ_c is 605 nm under zero electric field condition and it is shifted in the red direction with the application of an electric field, thus, $\lambda_{c,CdSe/CdS}$ is equal to $605 + \Delta\lambda$ nm, where $\Delta\lambda$ is the amount of the spectral shift in nanometers. k is set according to the spectral linewidth 1.6 nm of CdSe/CdS at 50 K [13]. The absorption spectra of dye molecules A_1 and A_2 are designed hypothetically with $\lambda_{c,A_1} = 605$ nm, $\lambda_{c,A_2} = 645$ nm and linewidths equal to 7 nm and 9 nm, respectively.

The approximated emission spectrum of CdSe/CdS and the absorption spectra of hypo-

thetical dye molecules for different spectral shifts are demonstrated in Fig. 5.2. Under zero electric field condition, the spectral shift of CdSe/CdS is also zero and A_1 and CdSe/CdS have a significant spectral overlap, however, the overlap of A_2 and CdSe/CdS is negligible. As the spectral shift increases with increasing electric field, the spectral overlap of CdSe/CdS and A_1 decreases with increasing spectral shift; conversely, the spectral overlap of CdSe/CdS and A_2 increases. The Förster radius is related to the spectral overlap as follows

$$R_0^6 \propto \int_0^\infty F_D(\lambda)\epsilon_A(\lambda)\lambda^4 \mathrm{d}\lambda \tag{5.3}$$

As a consequence, p_1 and spectral overlap vary proportionally. We analyze the resultant deviation of the capacity for each channel with varying spectral shift in Section V-C.

5.3 Chemical Routing

Mimicking the macroscopic machine-like actuating capabilities on the molecular scale is of great interest for nanotechnology. For this aim several artificial molecular machines inspired by the nature, e.g., charge separation in photosynthesis or muscle movement, have been designed [10], [11], [12], [17]. Mechanically interlocked molecules providing controllable and reversible motion can be considered as the most simplest molecular machines with the electrochemically or photochemically active components that undergo basic translational or rotational movements [34]-[65]. Here, we focus on a specific kind of synthetic interlocked molecules, namely [2]rotaxane, that can be employed for selective routing of information in an FRET-based communication network.

[2]rotaxane is an interlocked supramolecule consisting of a macrocyclic ring trapped onto a dumbbell component containing two separate recognition sites and two stopper molecules at the both end of the dumbbell as seen in Fig. 5.3. The ring undergoes a reversible translational movement between two recognition sites on the dumbbell axes when [2]rotaxane is induced by a chemical or optical signal [65], [6]. Therefore, the ring acts as a bistable molecular shuttle between two stations. There are several studies which combine the ring displacement in [2]rotaxane and the strong distance dependence of FRET in order to develop a mechanical switch that outputs an optical signal. Some of the studies concerning FRET and [2]rotaxane follow a way through replacing the [2]rotaxane components with photoactive molecules [52], [78], and some of them covalently binding the fluorophores onto

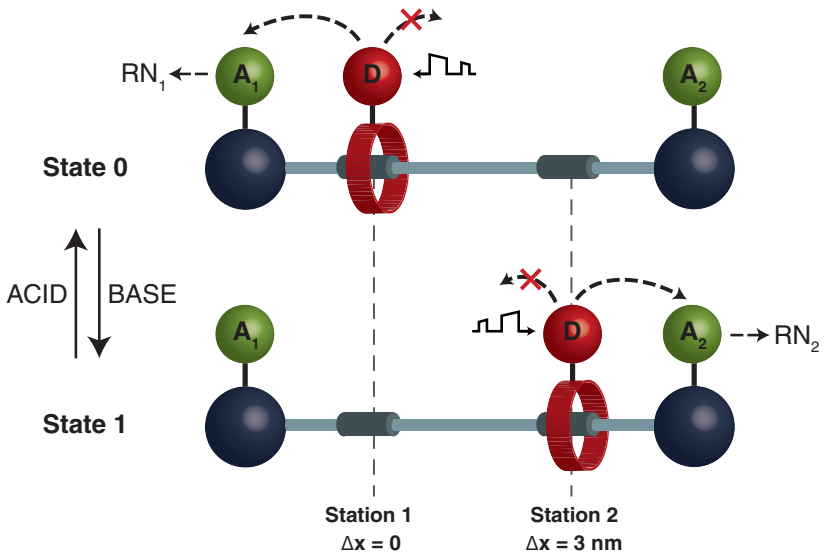

Figure 5.3: Demonstration of chemically controllable routing.

the ring and stopper components [62]. In both ways, the fluorescence intensity of the donor molecule located at the end of the axis is altered when the ring acting as acceptor or bearing an acceptor molecule is moving through the axis.

In our proposed model, two acceptor fluorophores of the same kind as the receiver nanonodes are immobilized through covalent binding on the stoppers of a chemically active [2]rotaxane, and a donor fluorophore as the routing node, i.e., RtN, is covalently bound to the macrocycle DB24C6 [6] as demonstrated in Fig. 5.3. The length of the [2]rotaxane axis is assumed to be 5 nm. The recognition sites consist of dialkylammonium center and 4,4'-bipyridinium unit as in the configuration proposed in [6]. The recognition sites are assumed to be located at 1 nm inside from the stopper molecules. The center of the transition dipole moments of the donor and acceptor molecules are assumed to be aligned linearly on a second axis parallel to the [2]rotaxane axis. The donor molecule on the ring is the first destination of the information coming from IS. In the stable case, i.e., state 0, the macrocycle with the donor molecule is expected to be located around the dialkylammonium center because of the strong hydrogen bonding interactions between the cycle and the center. Upon the protonation, the macrocycle moves from the ammonium station to the bipyridinium station and is located around it, therefore, the whole system goes into state 1 [6]. The reversible displacement of the macrocycle is based on an electrochemical stimuli such as acid/base

treatment [6]. We do not go into detail about the chemical reactions, but analyze the effect of the ring displacement on the communication capacity of the channels established among three nodes located on the [2]rotaxane system in order to demonstrate the routing capability in Section V-D.

5.4 Information Theoretical Analysis

In this section, we investigate the performance of FRET-based point-to-point and broadcast communications in terms of information theoretical capacity and ISI probability for varying system parameters. Furthermore, we simulate the electrical and chemical routing scenarios, and derive the channel capacity for each state of the routers in order to evaluate the performance of each routing scheme.

5.4.1 Analysis of Electrical Routing in FRET-Based Communication

The performance of the electrical routing scheme for the nanonetwork demonstrated in Fig. 5.1 is analyzed information theoretically in terms of communication capacity. We assume that bit-1 is represented with a pulse of duration T_{pulse}, and bit-0 is represented as silence during a time slot of duration T_b which is assumed to be long enough to overcome ISI. The distance of RtN to both RNs is set to R_{0,DA_1} which is the Förster radius of CdSe/CdS-A_1 pair when the electric field is zero. The molecules on the nanomachines are assumed to be isotropically free, therefore orientation factor κ^2 has the probability distribution defined in (2.7) independently for each exciton. The configuration is similar to that of the broadcast communication investigated in Section III-B except that R_0 changes also with varying spectral shift. The transmission probability of bit-1 through the individual channels, i.e., channel RtN-RN_1 and RtN-RN_2, for varying spectral shift is obtained using the broadcast simulation algorithm described in Fig. 4.7 and following a Monte Carlo approach. The varying channel capacity is then derived using the obtained value of p_1 for both channels.

The resultant capacity for different pulse lengths and varying level of wavelength shift is plotted in Fig. 5.4. As is seen for each value of T_{pulse}, RtN-RN_1 channel capacity is maximum under zero electric field condition and decreases to negligible values with increasing shift; conversely, RtN-RN_2 channel capacity is negligible at zero electric field, however, it increases to its maximum as shift increases to 10 nm. Therefore, around the zero electric field, the

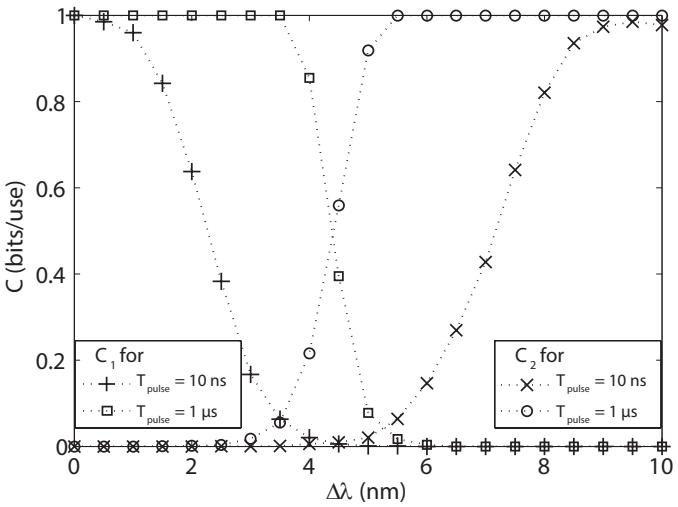

Figure 5.4: Channel capacity of individual channels, i.e., C_1 and C_2 for varying spectral shift $\Delta\lambda$.

information is transmitted only to RN_1; conversely, RtN transmits only to RN_2, when the shift is around 10 nm. Additionally, we conclude that increasing T_{pulse} decreases the wavelength shift required for full switching between two channels, therefore, larger T_{pulse} provides faster routing performance.

5.4.2 Analysis of Chemical Routing in FRET-Based Communication

In order to investigate the performance of the chemical routing method proposed in Section IV-B, we analyze the deviation of the communication capacity of the channels RtN-RN_1 and RtN-RN_2 with varying position of the ring. The transition probability of bit-1 through the individual communication channels is simulated using the broadcast simulation algorithm described in Fig. 4.7. Here, we assume the transition dipole moments of the molecules are in-line with the secondary axis, the relative orientation factor is deterministic with $\kappa^2 = 4$. The Förster radius of the donor-acceptor pairs R_0 is assumed to be 2 nm for in-line orientation and constant during the transmission of the information bits. Although the relative orientation factor is maximized, R_0 is taken as relatively small in order to show that one can pick the donor and acceptor pair from a large set of fluorophores which are not required to have significant spectral similarity [51]. Bit-1 is represented with a T_{pulse}-duration optical pulse coming from IS at the beginning of a time slot with duration T_b that

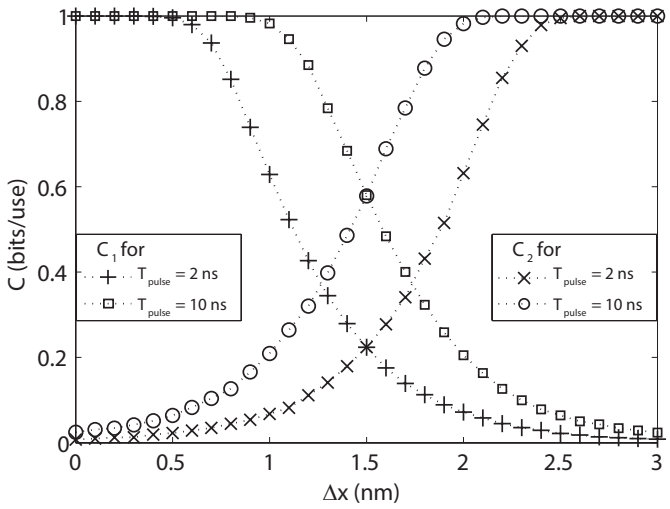

Figure 5.5: Channel capacities of individual channels, i.e., C_1 and C_2, with varying displacement of macrocycle.

is assumed to be enough for avoiding ISI, and bit-0 is represented as silence during the time slot. We assume that the effective volume of the laser beam uniformly covers the whole trajectory traveled by the donor molecule, such that, the donor is excited with the same probability at each point that it is located. Following the assumptions, the transmission probabilities of bit-1, i.e., p_1, for the individual channels are calculated as the number of successful transmissions divided by the total number of simulations.

Using the obtained p_1 values, and given $p_0 = 1$, the information theoretical capacities of the individual channels are calculated for different locations of the donor, i.e., the ring. The results are plotted for two different T_{pulse} values in Fig. 5.5. As is seen in the figure, when the ring is at its initial position, i.e., $\Delta x = 0$, RtN transmits the incoming information only to RN_1 with the capacity $C_1 = 1$ bit/use. At this position, the channel RtN-RN_2 is in the closed state with $C_2 = 0$, such that, RN_2 cannot receive any information from RtN. As with the protonation, the macrocycle slightly moves in the direction of station 2, and C_2 increases while C_1 decreases with about sixth degree dependence on the displacement. If the communication is established when the displacement of the macrocycle is around 1.5 nm, both channels are in the transition states, and RtN broadcasts the incoming information to both of the RNs in a relatively unreliable manner. When the macrocycle reaches at the station 2, the channel 2 enters into open state with the communication capacity $C_2 = 1$

bits/use, while channel 1 becomes closed. Note that for different T_{pulse}, the displacement required for the transition between two states of the channels does not change significantly, however, the capacity of the broadcast communication in the transition state, i.e., when Δx is around 1.5 nm, increases notably for large pulse lengths.

Chapter 6

MULTI-STEP FRET-BASED LONG-RANGE NANOSCALE COMMUNICATION CHANNEL

In this chapter, we propose a novel nanoscale communication method based on multi-step FRET using identical fluorophores as relay nodes between communicating nanomachines, and utilizing multi-exciton transmission scheme in order to improve the limited range of the communication and achievable transmission rate over the nanoscale channel. We investigate two communication scenarios: immobile nanomachines communicating through a channel in a host material with linearly located relay nodes, and mobile nanomachines communicating through a channel in a three dimensional aqueous environment with randomly deployed relay nodes. We simulate the communication over these channels with realistic algorithms considering the high degree of randomness intrinsic to FRET phenomenon. Using the simulation results and following a Monte Carlo approach, we evaluate the performance of the channels by means of information theoretical capacity and interference probability. We show that multi-step FRET-based communication significantly outperforms the other biologically inspired nanocommunication techniques proposed so far in terms of maximum achievable data transmission rates. The results underline the compatibility and practicality of the FRET-based communication for several applications ranging from molecular computers to nanosensor networks.

6.1 Introduction

In Chapter 3, we have modeled the FRET-based nanocommunication channel between a single Transmitter-Receiver Nanomachine (TN-RN) pair and analyzed its information theoretical capacity. In that chapter, utilizing binary On-Off Keying (OOK) modulation, the information is encoded into two bits: bit-1 and bit-0. Bit-1 is represented by the transfer of a single exciton from the excited donor on TN to the ground-state acceptor on RN that is in the close proximity of TN, and bit-0 is represented as silence during a bit interval.

In the same chapter, we also investigate the effects of some environmental and intrinsic parameters of fluorophores on the channel capacity, and underline the strong dependence of the capacity on the distance between TN and RN. This dependence strongly reduces the reliability of the communication for internodal distances over 10 nm, and thus confines its practicality to very limited applications.

In this chapter, we propose a novel method for FRET communication based on multi-step FRET employing identical relay fluorophores between TN and RN, and utilizing multi-exciton transmission scheme in order to improve the spatial range and the achievable transmission rate of the communication. We investigate two deployment scenarios for the relay fluorophores: ordered relays in a host material with prescribed locations, and disordered, i.e., randomly deployed, relays in a three dimensional aqueous medium. The channel with ordered relays is considered for immobile nanomachines communicating through a wire-like channel that can find practicality for several on-chip applications. The channel with randomly deployed relays is considered for mobile nanomachines that can constitute mobile ad-hoc nanonetworks and nanosensor networks. We simulate the communication through the proposed channels following a realistic algorithm based on the competitive behavior of the multiple excitons and concerning many sources of randomness intrinsic to the phenomenon. Following a Monte Carlo approach, we evaluate the performance of the channels by means of information theoretical capacity and interference probability between successive transmissions, then we derive the maximum achievable data transmission rates over these channels. We infer from the results that using the channels with both ordered and disordered relays, two nanomachines can communicate at a rate up to tens of Mbps through distances over tens of nanometers. To the best of our knowledge, the achievable rates with multi-step FRET-based communication over this range of distances are significantly higher than that can be achieved by any biologically inspired communication method proposed so far.

The remainder of this chapter is organized as follows. In Section 6.2, we explain the basic principles of multi-step FRET-based nanocommunications and excitonic processes. In Sections 6.3 and 6.4, we model the point-to-point multi-step FRET-based communication channels with ordered and randomly deployed relay fluorophores. The proposed channels are information theoretically analyzed, and the achievable rates are derived in Section 6.5.

In Section 6.6, we discuss the networking capabilities of multi-step FRET-based nanocommunications.

6.2 Principles of Multi-Step FRET-Based Communications

Multi-step FRET defines the sequential transfer of excitons, i.e., excited state of fluorophores, through more than one fluorophore. The excitons generated on the donor and transferred to the acceptor molecule might be transferred to another fluorophore that is spectrally similar and spatially proximal to the acceptor. Multi-step FRET has been studied extensively in order to improve the spatial range of FRET over 10 nm [35]. Based on the multi-step FRET, we modeled a communication channel for a TN-RN pair with a single additional relay node (HN) located in the middle of them comprising a fluorophore which is spectrally similar to both the donor on TN and the acceptor on RN in Chapter 3. In that basic model, the nodes are located in a linear arrangement, and utilizing ON-OFF Keying (OOK) modulation IS sends a picosecond-duration pulse to TN in order to represent bit-1. We have shown that the channels TN-HN and HN-RN are independent with the proper selection of the bit interval T_b. Therefore, the overall transition probabilities between TN and RN are just the multiplication of the transition probabilities of each of the channel that participates in the communication.

Here, we extend our basic model employing more than one identical fluorophore as the relay nodes between TN and RN, and utilizing multi-exciton transmission with ns-duration pulses.

6.2.1 Communication System Model

The multi-step FRET-based nanoscale communication system is composed of four main parts similar to traditional communication systems: an Information Source (IS), a transmitter nanomachine, a communication channel, and a receiver nanomachine:

- ***Information Source:*** The main information source of the system can be an external excitation source such as commercial laser that aims to remotely control the operation of a nanonetwork by sending optical pulses to TN. It might also be an electrical source that is embedded onto TN in the case semiconductor nanomaterials are used on TN

as donor molecules. Utilizing OOK modulation, the information is encoded into two bits: bit-1 and bit-0. We assume that IS sends optical or electrical excitation pulses to TN with T_{pulse}-duration at the beginning of a bit interval T_b in order to represent bit-1, and keeps TN silent during T_b to represent bit-0.

- ***Transmitter Nanomachine:*** The transmitter with molecular sizes includes a donor molecule that receives the excitation pulses sent from IS and generates excitons to the system. The emission spectrum of the donor molecule is assumed to overlap with the absorption spectra of the channel molecules, i.e, relay fluorophores, and the donor is assumed to be in close proximity of the relays, such that, the transfer of the generated excitons from the donor to the relay fluorophores is possible. On the contrary, we neglect the back transfer of the excitons from the relay fluorophores to the donor assuming the emission spectra of the relays and the absorption spectrum of the donor do not overlap.

- ***Communication Channel:*** For the communication channel, we investigate two basic cases. For the first case, the relay fluorophores are located on prescribed locations with prescribed orientations throughout a zeolite L backbone. The communication between TN and RN located on the different ends of zeolite L is realized through the wire-like structure with sequential energy transfers. In the second case, the relay fluorophores are randomly located and oriented in a three dimensional virtual lattice over aqueous medium and assumed to undergo random movements following Brownian statistics. In both cases, the excitons are transferred between the identical relay fluorophores via homoFRET. The underlying mechanism of homoFRET is the same as the one of FRET, except that it occurs between identical molecules, therefore, it requires that the emission and absorption spectra of the employed molecules must have a significant overlap.

- ***Receiver Nanomachine:*** The receiver includes an acceptor fluorophore that is the final destination of the excitons. The absorption spectrum of the acceptor and the emission spectra of the relays are assumed to overlap. However, the emission spectrum of the acceptor and the absorption spectra of the relays do not overlap in order to

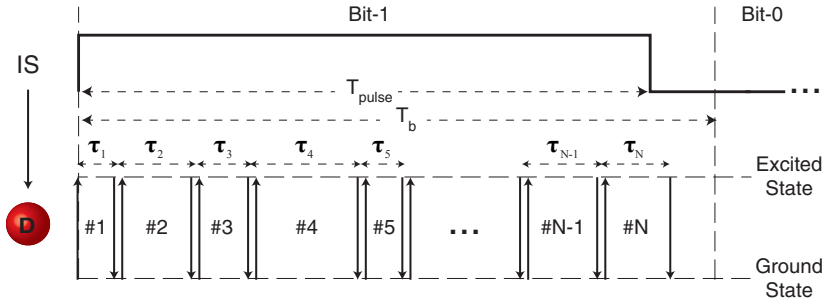

Figure 6.1: Representation of bit-1 and bit-0 by IS, and sequential generation of N excitons on Donor (D) with random inter-generation times.

avoid back transfer from the acceptor to the relays. The receiver is assumed to be synchronized with TN and continuously senses the state of the acceptor. We assume that the detection is realized by an external or internal photon detector. When the acceptor is excited via FRET during T_b, it releases a photon that is detected by the photon detector, and RN decides bit-1. If the photon detector does not detect any photon with a wavelength that is belong to the emission spectrum of the acceptor during the bit interval, RN decides bit-0.

Since we focus on the communication channel characteristics, the design of the transmitter and receiver nanomachines is out of the scope of this thesis.

6.2.2 Principles of Exciton Activity

During the transmission of bit-1, the generated excitons occupy fluorophores for a random time, then they are transferred to another fluorohpore via FRET or removed from the system via fluorescence. These processes are detailed as follows:

- ***Exciton generation:*** When IS sends an excitation pulse to TN, the donor is immediately excited, i.e., it generates an exciton, assuming the absorption coefficient of the donor is 1. Once the exciton is generated, it stays on the donor for a random time, then the donor relaxes through either fluorescence or FRET. In the case of FRET, the generated exciton is transferred to a proximal fluorophore. If T_{pulse} is large enough,

after the first relaxation, the donor is expected to undergo many excitation and relaxation cycles during T_{pulse}, i.e., we expect more than one exciton to be generated by one pulse as demonstrated in Fig. 6.1. However, the number of generated excitons by a single pulse is a random variable, since the inter-generation times, i.e., the occupation times of generated excitons on donor, are random.

- ***Exciton occupation:*** An exciton occupies a fluorophore when it is generated on or transferred to that molecule. An occupied fluorophore is not available for the occupation of another exciton until it relaxes. The interval between the excitation and the relaxation of a fluorophore τ gives the occupation time of that exciton. τ is an exponential random variable with a mean μ_τ which depends on the FRET rate of the donor molecule to the proximal and available, i.e., ground-state, fluorophores, and the intrinsic lifetime of the donor molecule. Assuming there are k fluorophores available for energy transfer in the range of the donor, the mean occupation time of the ith exciton can be expressed in terms of the process rates:

$$\mu_{\tau_i} = (k_R + \sum_{j=1}^{k} k_{T,j,i})^{-1} \tag{6.1}$$

where $k_{T,j,i}$ is the FRET rate between the excited fluorophore and the jth proximal fluorophore for the ith exciton. k_R is the intrinsic fluorescence rate of the excited fluorophore. $k_{T,j,i}$ depends on intrinsic and environmental parameters [51] and can be expressed by:

$$k_{T,j,i} = 8.8 \times 10^{22} \kappa_{j,i}^2 n^{-4} J_j(\lambda) \frac{k_R}{R_{j,i}^6} \tag{6.2}$$

where $\kappa_{j,i}^2$ is the orientation factor which is a measure of the relative orientation of the transition dipole moments of the occupied and the jth proximal fluorophore during the occupation of the ith exciton. J_j is the degree of the spectral overlap between the emission spectrum of the occupied fluorophore and the absorption spectrum of the jth proximal fluorophore. $R_{j,i}$ is the intermolecular distance between the occupied fluorophore and the jth proximal fluorophore for the occupation time of the ith exciton.

- ***Exciton transfer:*** After a random occupation time, the exciton leaves the fluorophore by either fluorescence or FRET to another proximal fluorophore. The exciton

randomly selects the next pathway from a set of possible pathways. Assuming that k proximal fluorophores are available for the energy transfer, the probability of FRET to a specific fluorophore can be expressed by

$$P_{FRET,j,i} = \frac{k_{T,j,i}}{k_R + \sum_{l=1}^{k} k_{T,l,i}} \tag{6.3}$$

- ***Exciton removal:*** An exciton is removed from the system by exciton recombination, i.e., the recombination of electron and hole. The prevalent recombination mechanism among dyes and fluorescent proteins is radiative recombination that results in radiation of a photon. The excitonic energy is converted to a photon with a wavelength dependent on the emission spectrum of the occupied fluorophore. For an exciton that occupies a fluorophore with k available neighbor fluorophores, the probability of fluorescence is given as

$$P_{Fluo,i} = \frac{k_R}{k_R + \sum_{l=1}^{k} k_{T,l,i}} \tag{6.4}$$

The excitons generated on TN are expected to move following random pathways through the relay nodes that surround both TN and RN. The overall movement of the excitons can be described as continuous-time correlated random walk with waiting times. Both the probability mass function (pmf) of the next jump, i.e., transition probabilities, and the waiting times on each node depend on the location, orientation and the availability of the surrounding fluorophores. Therefore, the next jump of an exciton is independent of the previous jumps, however, it depends on the trajectories of other excitons that might simultaneously exist in the channel. The excitons that exist in the channel at the same time compete with each other to occupy the available fluorophores.

6.3 Multi-Step FRET-Based Communication Channel with Ordered Relays

Here, we investigate two FRET-based long-range communication channels with identical relay fluorophores placed in prescribed locations. For the immobility of the fluorophores, we assume a host material zeolite L is employed.

Zeolite L has a porous molecular structure and is composed of strictly parallel channels formed by the combination of these pores in a hexagonal arrangement as demonstrated in Fig. 6.2(a). The free diameter inside the channels is 0.71 nm and the length of the channels

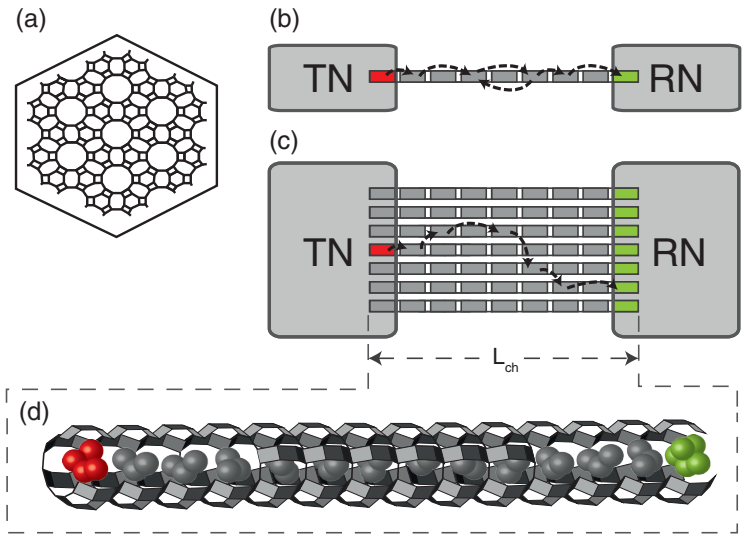

Figure 6.2: (a) Hexagonal structure of zeolite L with seven channels. (b)-(c) 2-dimensional demonstration of multi-step FRET-based communication with relay nodes placed through a single zeolite L channel and seven zeolite L channel. (d) Detailed demonstration of a single zeolite L channel filled up with donor (red), relay (gray) and acceptor (green) fluorophores.

ranges from 30 nm up to 10 μm [15]. Also the center-to-center distance between two parallel channels is 1.84 nm [15]. The dimensions of the channels make it possible to fill these zeolite L channels up with several well-oriented dye molecules. Zeolite L is an advantageous host material for fluorescent dyes because of its negatively charged framework [68]. Unidirectional energy transfer from an energy source to a reaction center through the zeolite L channels filled up with guest molecules, e.g. fluorescent dyes, are extensively studied especially for light harvesting applications, e.g. artificial antenna systems, [15], [64]. In most of the studies, the same kind of dye molecules are employed between two ends of the channels as relay nodes and the excited energy is transferred via homoFRET.

We focus on two basic models. In the first model, the relay fluorophores are placed in a single zeolite L channel, such that they are arranged in a single axis as seen in Fig. 6.2(b). The transition dipole moments of each fluorophore are assumed to be parallel to the common axis. Therefore, the relative orientation factor is maximized, i.e., $\kappa^2 = 4$, which significantly increases the probability of FRET through relay fluorophores. In this communication scheme, TN and RN are assumed to be immobile connected to different ends of the zeolite L channel as in Fig. 6.2(b). The connection can be established mechanically or

covalently through the connector molecules that are employed both on the nanomachines and at the channel ends. We assume the intermolecular distance between the donor and the first relay, as well as between the acceptor and the last relay, is 2 nm which is the spacing between two neighboring pores. We also assume that none of the pores are empty, therefore, the inter-relay distance is also 2 nm. The donor and the acceptor which are the antennas of the nanomachines exchange the excited energy, i.e., excitons, with neighboring relay fluorophores through the FRET mechanism.

For the second model, we utilize seven parallel zeolite L channels in a hexagonal arrangement as the host for fluorophores. A donor molecule is located at one end of the channel in the middle, and seven acceptor molecules are located at the other end of seven channels as shown in Fig. 6.2(c). The rest of the channels are filled up with relay molecules uniformly such that each of the unit cells in the channel is occupied by a relay, theregore, the center-to-center distance between two adjacent fluorophores in the same channel is 2 nm. We assume that the donor molecule can be excited directly by an optical or electrical pulse with the duration in the range of nanoseconds that is sent from an information source that can be external or internally embedded onto TN. The excited donor is relaxed through either fluorescence or FRET to one of the relay molecules in its range with different probabilities. All of the molecules are oriented parallel to the channel axes. Considering the fluorophores located in different parallel channels, the orientation factor for any pair of fluorophores is expressed by $\kappa^2 = (1 - 3\cos^2\theta)^2$, where θ is the angle between the channel axis and the virtual axis that connects the center of both fluorophores [51]. RN is assumed to continuously observe all of the acceptors' states such that if at least one of the acceptors fluoresces in the bit interval, it decides that bit-1 is transmitted.

Since we employ identical relays throughout the channel for both models, it is possible for an exciton occupied on a relay to be transferred in all of the directions: in the direction of the donor end, or the acceptor end. Moreover, for the seven-channel model, excitons can be exchanged between the fluorophores in the different parallel channels of zeolite L. We assume that relay emission band and donor absorption band, as well as, acceptor emission band and relay absorption band do not overlap, therefore, we neglect FRET from a relay to the donor, and from an acceptor to a relay.

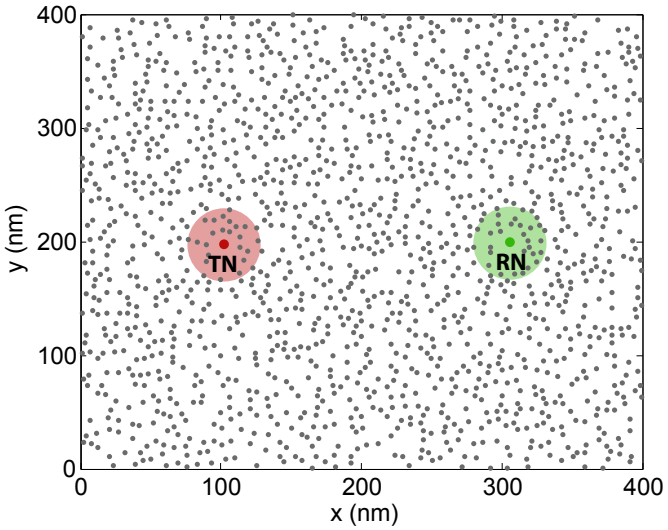

Figure 6.3: Two dimensional demonstration of randomly deployed relays throughout the lattice surrounding TN and RN. The excitons released by TN undergo random jumps through the relay nodes, and some of them reach RN.

6.4 Multi-Step FRET-Based Communication Channel with Disordered Relays

We consider another multi-step FRET based communication case comprising identical fluorophores located randomly in a 3-dimensional aqueous environment as seen in Fig. 6.3. The fluorophores are expected to move uniformly in each direction following Brownian statistics, therefore, at any time instant, the spatial distribution of the fluorophores is assumed to be uniform throughout the environment. Assuming isotropic and unrestricted distributions for all three angles, the individual relay fluorophores freely rotate. Following the assumption, the orientation factor for each pair of the relays is subject to the given probability density function [9]

$$p_{\kappa^2}(\kappa^2) = \begin{cases} \frac{1}{2\sqrt{3\kappa^2}} \ln\left(2+\sqrt{3}\right) & 0 \leq \kappa^2 \leq 1 \\ \frac{1}{2\sqrt{3\kappa^2}} \ln\left(\frac{2+\sqrt{3}}{\sqrt{\kappa^2}+\sqrt{\kappa^2-1}}\right) & 1 \leq \kappa^2 \leq 4 \end{cases} \tag{6.5}$$

The mean of the distribution is 2/3. If the transition dipole moments are parallel to each other, the orientation factor is maximized, i.e., $\kappa^2 = 4$, and in the case of perpendicular orientations, it is minimized, i.e., $\kappa^2 = 0$.

The donor, acceptor and relay fluorophores are considered as spherical molecules with diameter of 1.2 nm. There are just one donor and one acceptor in the considered lattice. The

paper is not concerned with the design of transmitter and receiver nanomachines, therefore, we assume that, a single donor functions as TN which receives the information from a remote IS, and a single acceptor functions as RN which sends the received information to another remote observer through fluorescence. TN and RN are assumed to be mobile with controllable movements, therefore, they are not subject to Brownian statistics.

We assume that there is no collisional quencher which removes the excitons when it collides with an excited fluorophore. Therefore, there are only two processes that an exciton can undergo: fluorescence and FRET to a nearby fluorophore.

If the density of the environment is not too low, an individual fluorophore is expected to have many available fluorophores in its spherical proximity. As a result, the probability of excitons to fluorescence on relay molecules is relatively low for dense environments.

6.5 Information Theoretical Analysis

In this section, we analyze the information theoretical capacity of the aforementioned channels. Additionally, we investigate the interference between successively transmitted bits, and derive the maximum achievable data transmission rates for each channel in the case of OOK modulation.

For each communication system, we utilize the most basic modulation technique: binary OOK modulation with two bits available, bit-1 and bit-0. IS sends a T_{pulse}-duration optical or electrical pulse to TN at the beginning of a T_b-duration time slot in order for TN to transmit bit-1. For bit-0, IS does not send any pulse and keeps TN silent during T_b. Bit-1 is successfully transmitted if the acceptor on RN is excited in the relevant time slot. Bit-0 is transmitted successfully if the acceptor stays in ground-state during T_b.

Assuming there is no excitation-source except from IS, the transmission of bit-0 is always successful, i.e., $p_0 = 1$, if we neglect a probable ISI situation. However, the transmission of bit-1 is ambiguous because of the high degree of randomness and the correlated behavior in the motion of excitons. It is very difficult to derive an analytical solution for the successful transmission probability of bit-1, i.e., p_1. For that reason, we simulate the transmission of bit-1 in Matlab using a common algorithm for all the channel models. Following a Monte Carlo approach, we derive the successful transmission and ISI probabilities for different channel parameters.

Since the transmission of bit-1 is problematic and the transmission of bit-0 is always successful, information theoretically the channels show Z-channel characteristics [19]. Considering an input alphabet $\mathbf{X} = \{0,1\}$ which is transmitted by TN and an output alphabet $\mathbf{Y} = \{0,1\}$ which constitutes the set of received bits, and assuming that IS sends a pulse with probability P_1 and no-pulse with probability $1 - P_1$, the mutual information between the transmitted and received bits is expressed by $I(\mathbf{X};\mathbf{Y}) = H(P_1 \cdot p_1) - P_1 \cdot H(1 - p_1)$. Here, $H(.)$ is the binary entropy function. The capacity of the channel C is the maximum mutual information over all input distribution, i.e., $C = \max_{P_1} I(\mathbf{X};\mathbf{Y})$.

6.5.1 Simulation Algorithm

We conduct simulations for the transmission of bit-1 on each channel based on the algorithm demonstrated in Fig. 6.4. The channel parameters used in the simulations for ordered and disordered cases are given in Table 6.1-6.2. Here, the Förster radius is the intermolecular distance when the FRET probability is 0.5, i.e., when the FRET rate is equal to the fluorescence rate for single pair of fluorophores. It is a measure of the spatial range of FRET, such that, for intermolecular distances greater than $2R_0$, the probability of FRET is negligible because of the sixth power dependence on distance. That is why we set the transfer range of the excitons to $2R_0$. The exciton transfer over distances greater than the transfer range is neglected in the simulations. Depending on the environmental parameters, R_0 ranges from 2 nm to 7 nm for common fluorophores [51].

Table 6.1: Simulation Parameters (Ordered Relays)

Förster radius *(R_0)*	4 nm
Pulse length *(T_{pulse})*	$10, 50, 100, 500$ ns
Channel length *(L_{ch})*	$30 - 134$ nm
Number of zeolite L channels	$1, 7$
Fluorescence rates *(k_D, k_R, k_A)*	5×10^8 1/s
Molecular radius *(r)*	1.2 nm
Transfer range	$2 \times R_0 = 8$ nm

The fluorescence rate is another key parameter for fluorophores. It is the reciprocal of

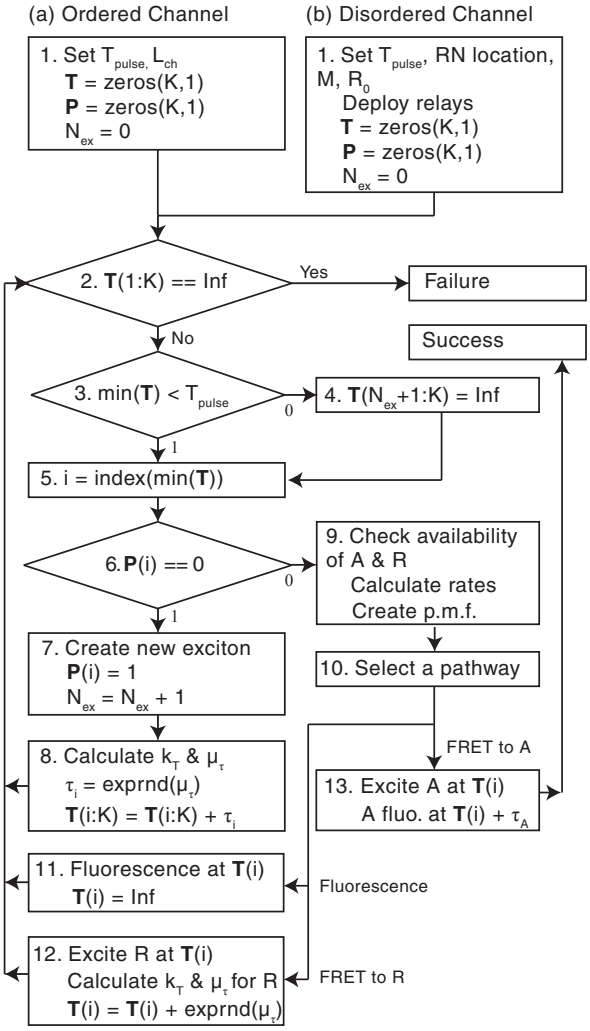

Figure 6.4: Monte Carlo algorithm for the simulation of bit-1 transmission through the channels with (a) ordered and (b) disordered relays.

the mean lifetime of fluorophores when there is no proximal acceptor and quencher. The mean lifetime ranges from picoseconds to tens of nanoseconds for common fluorophores [51]. We use a typical value of 2 ns for fluorescent dyes. Therefore, the fluorescence rate is assumed to be 5×10^8 1/s.

The algorithm used in each channel simulation is based on the competitive behavior of the excitons, and operates through the following steps:

1. The channel parameters are set. A time matrix **T** holding the last active time of each exciton in each row according to the indices of the excitons, and a state matrix

Table 6.2: Simulation Parameters (Disordered Relays)

Förster radius *(R_0)*	$3-7$ nm
Pulse length *(T_{pulse})*	$10, 50, 100, 500$ ns
Lattice size	$400 \times 400 \times 400$ nm
TN location	$(100, 100, 100)$ nm
RN location	$(103, 100, 100) - (301, 100, 100)$ nm
Relay concentration *(M)*	$480, 960, 1920$ mol/m^3
Fluorescence rates *(k_D, k_R, k_A)*	5×10^8 1/s
Molecular radius *(r)*	1.2 nm
Transfer range	$2 \times R_0$

P holding the state of each exciton are generated with K rows. K is set arbitrarily concerning that it has to be greater than the possible number of the excitons created in one transmission cycle. All of the rows of both matrices are set to 0 prior to the transmission. Once the exciton is created with index i on the donor, **P**(**i**) is set to 1. If the ith exciton is removed from the system, **T**(**i**) is set to an infinite value, i.e., **Inf**.

2. The algorithm checks whether all the excitons are removed from the system. If there remains no active exciton, simulation ends with failure, otherwise it continues at Step 3.

3. The algorithm checks whether there is an exciton with the active time is less than T_{pulse}.

4. If the active times of all the excitons become greater than T_{pulse}, it means that the pulse ends, and no more excitons can be generated on the donor. Therefore, all of the inactive excitons are removed from the system by setting the time entries to **Inf**. The simulation continues at Step 5 playing the already-activated excitons.

5. i is set to the index of the exciton with the minimum active time.

6. The algorithm checks whether the ith exciton has been generated before.

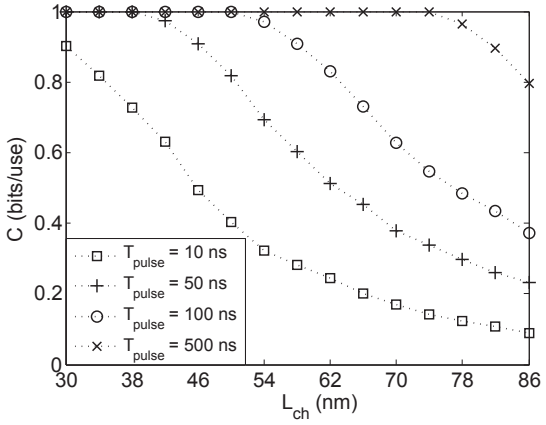

(a) Capacity for different pulse lengths with varying L_{ch}.

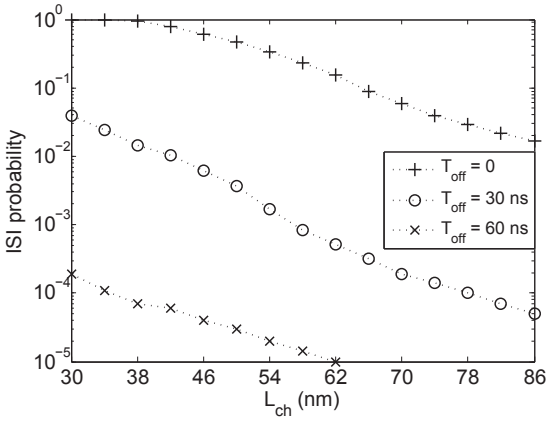

(b) ISI probability for different offset times with varying L_{ch} and $T_{pulse} = 50$ ns.

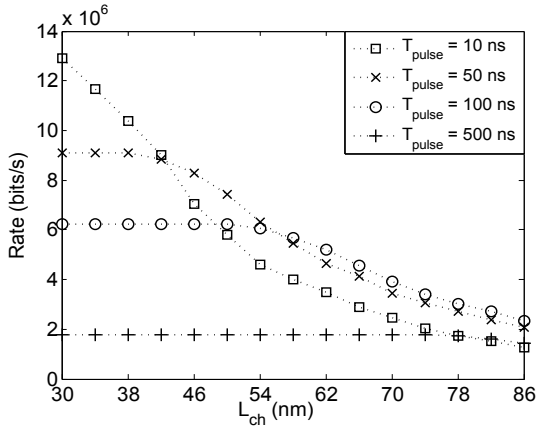

(c) Maximum achievable transmission rates for different pulse lengths with varying L_{ch}.

Figure 6.5: Results of performance analysis for ordered channel with single zeolite L channel.

7. Exciton i is generated, i.e., activated. The number of generated excitons, i.e., N_{ex}, is incremented by 1.

8. The FRET rates k_T between the donor and each relay or acceptor molecules in the range of the donor are calculated considering the intermolecular distance and the relative orientations. μ_τ is calculated using (6.1). The excited state lifetime τ_i is determined randomly from the exponential distribution with mean μ_τ. Exciton i stays at the donor for a time τ_i. The time entries for the exciton i and for the excitons which

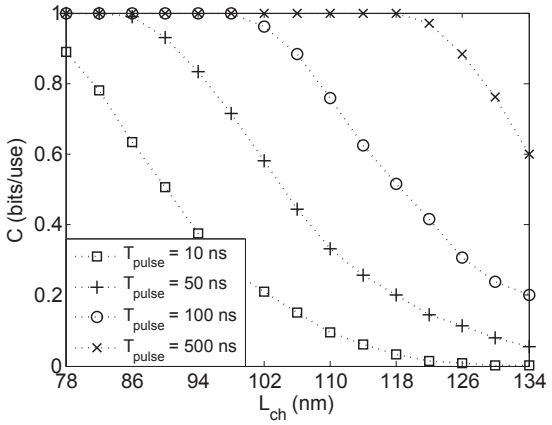

(a) Capacity for different pulse lengths with varying L_{ch}.

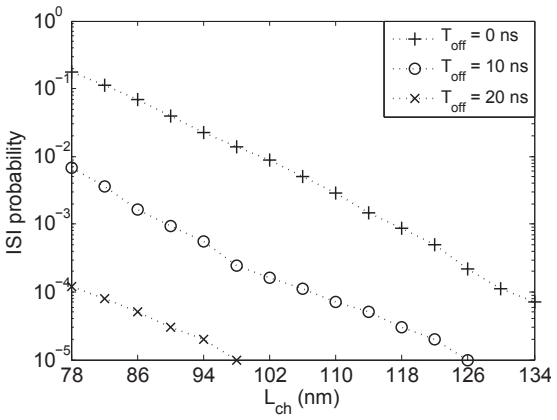

(b) ISI probability for different offset times with varying L_{ch} and $T_{pulse} = 50$ ns.

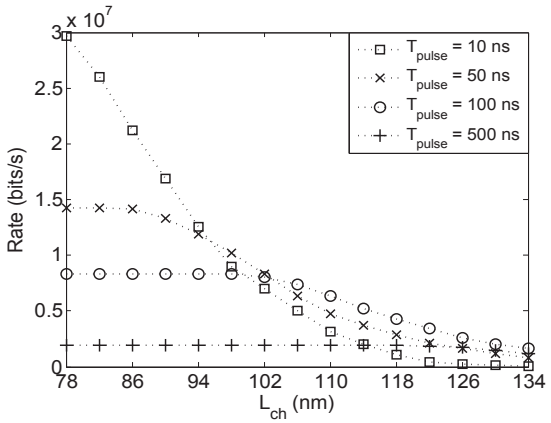

(c) Maximum achievable transmission rates for different pulse lengths with varying L_{ch}.

Figure 6.6: Results of performance analysis for ordered channel with seven zeolite L channels.

have not been generated yet are incremented by τ_i, since the donor is not available until this time for the new excitons to be generated. The simulation continues at Step 2.

9. If the exciton i is already activated, the algorithm checks the available molecules for FRET at time $\mathbf{T}(\mathbf{i})$ and creates p.m.f. for the next pathway calculating the process rates.

10. A new pathway for the exciton i is selected randomly according to the p.m.f.

11. If exciton i results in fluorescence at time $\mathbf{T(i)}$, it is removed from the system by setting $\mathbf{T(i)} = \mathbf{Inf}$. The occupied molecule is relaxed and becomes available for the new excitons. The simulation continues at Step 2.

12. If exciton i occupies a relay molecule through FRET, the process rates are calculated checking the available molecules at time $\mathbf{T(i)}$. μ_τ is calculated accordingly. The exciton i stays at the relay molecule for a time τ_i which is determined randomly from the exponential distribution with mean μ_τ. The simulation continues with Step 2.

13. If exciton i is transferred to an acceptor molecule at time $\mathbf{T(i)}$, receiver detects bit-1 when the acceptor fluoresces at time $\mathbf{T(i)}+\tau_\mathbf{A}$. Since, the only way for the acceptors to relax is to fluorescence, τ_A is determined randomly from the exponential distribution with mean μ_{τ_A} regardless of the available molecules in the range. The simulation ends with the successful transmission of bit-1.

6.5.2 Analysis of Channels with Ordered Relays

The simulation of the transmission of bit-1 for the zeolite L channel models is run many times for different parameters. The success probability of bit-1 transmission p_1 is obtained as the number of successful transmissions divided by the total number of runs. The simulations are repeated until the obtained value of p_1 converges to a finite value, then, the channel capacity is derived information theoretically.

Single Zeolite L Channel Case

Fig. 6.5(a) demonstrates the information theoretical capacity of the communication channel constructed on a single zeolite L channel for different values of T_{pulse} with varying channel length L_{ch}. For the capacity analysis, we assume that the bit interval T_b is sufficiently large to neglect ISI. We investigate the ISI situation in the next analysis. As is seen from Fig. 6.5(a), increasing the pulse length significantly improves the channel capacity, since as we increase T_{pulse}, more excitons are generated and the probability of error for bit-1 transmission decreases. At some critical channel length, the capacity of the channel starts

to decrease. The critical channel length is larger for greater T_{pulse} values. Compared to the single-pair single-exciton FRET-based communication channel [45], the capacity and the range of the communication are significantly improved.

The main reason of InterSymbol Interference (ISI) is the excitons that are generated during a bit interval with duration T_b, and arrive to the receiver at a greater time than T_b. ISI makes ambiguous the detection of bit-0 in the case of a preceding bit-1 transmission. Due to the stochastic behavior of the exciton motion, it is not possible to completely avoid ISI, however, one can set a threshold for the bit interval in order to bring the ISI probability down to negligible values. The time-based characteristics of the channels related to ISI are investigated recording the removal times of the last excitons which are able to reach the receiver. The simulation results show that the variation in T_{pulse} only changes the mean removal time in proportion to T_{pulse}, and has negligible effect on the variance of the distribution. This is due to the fact that only the lastly generated excitons contribute to the late arrivals, therefore, the distribution of last arrival times is independent of the pulse length. Besides, altering the channel length L_{ch} substantially effects both mean and variance of the distribution. Therefore, we conduct ISI probability analysis by setting T_{pulse} to a constant value of 50 ns, and $T_b = T_{pulse} + T_{off}$, and varying L_{ch} and T_{off}. From the results demonstrated in Fig. 6.5(b), we conclude that setting $T_b = T_{pulse} + 60$ ns results in negligible ISI for the typical channel lengths.

The maximum achievable rates are given by $R_a = C/T_b$. Setting $T_{off} = 60$ ns for all T_{pulse} values, R_a with varying channel length is demonstrated in Fig. 6.5(c). We conclude that, two nanomachines can communicate reliably at a rate over 12 Mbps through a distance up to 30 nm, and over 2 Mbps through distances larger than 80 nm.

Seven Zeolite L Channel Case

The analyzes are repeated for the communication channel which includes seven parallel zeolite L channels as the host for fluorophores. The variation of the channel capacity for varying pulse and channel length is shown in Fig. 6.6(a). As seen from the figure, the spatial range of the communication is increased as approximately 40 nm compared to the channel composed of one zeolite L channel, i.e., the same capacity can be obtained at a distance 40 nm larger as compared to the single channel case. One of the reasons of this significant

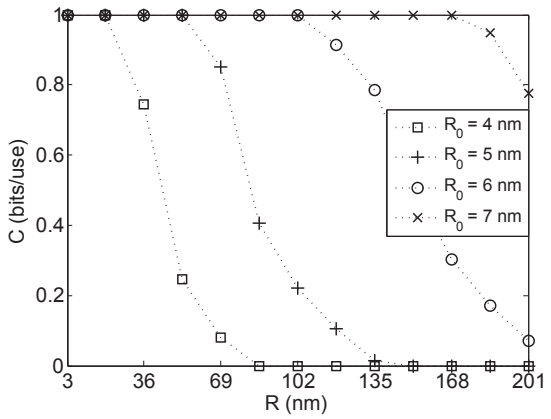

(a) Capacity for $M = 1920$ mol/m^3, $T_{pulse} = 1000$ ns, and varying R_0.

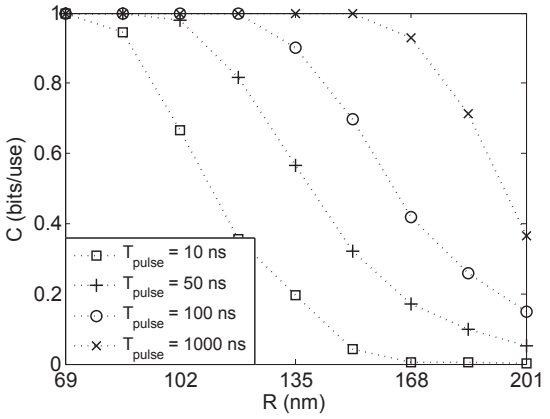

(b) Capacity for $M = 1920$ mol/m^3, $R_0 = 6$ nm, and varying T_{pulse}.

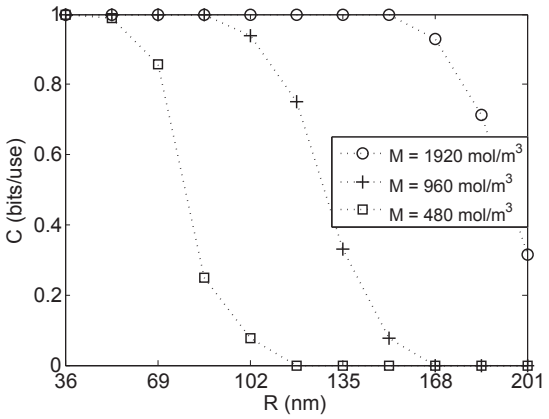

(c) Capacity for $T_{pulse} = 1000$ mol/m^3, $R_0 = 6$ nm, and varying M.

Figure 6.7: Information theoretical capacity of disordered channel for different channel parameters with varying TN-RN distance R.

increase is that seven acceptor fluorophores are employed at RN. Locating more acceptors at RN, we increase the probability of exciton reception. The other reason is the increased number of proximal fluorophores for each fluorophore which reduces the fluorescence, i.e., removal, probability of excitons during the transmission.

The ISI case for seven zeolite L channel is investigated as in the case of one zeolite L channel. Setting $T_b = T_{pulse} + T_{off}$ and $T_{pulse} = 50$ ns, the probability of ISI for varying channel length is plotted in Fig. 6.6(b). Here, we see that as compared to the single channel

case, smaller offset value is sufficient to get negligible ISI. Setting $T_{off} = 20$ ns and neglecting ISI, the achievable rates are derived for different T_{pulse}, and the results are plotted in Fig. 6.6(c). Here, we conclude that with a channel composed of seven zeolite L channels with ordered relays, nanomachines can reliably communicate at a rate up to 30 Mbps over a distance up to 80 nm, and at a rate over 2 Mbps through a distance up to 130 nm. Compared to the single zeolite L channel case, the achievable rates are significantly improved.

6.5.3 Analysis of Channel with Disordered Relays

Here, we investigate the capacity of the disordered channel. The transmission probability of bit-1 is simulated following the algorithm described in Fig. 6.4, and using the parameters given in Table 6.2. The simulations are repeated until p_1 converges to a finite value. Note that, for each run of the simulation, the relay fluorophores are deployed again in random locations following a uniform distribution. In the deployment stage, the algorithm takes the molecular sizes into account, such that, the Euclidean distance between the centers of two fluorophores cannot be smaller than $2r$, i.e., 2.4 nm. Although the relay molecules undergo Brownian motion, the displacement of the molecules during the transfer does not damage the homogeneity of the spatial distribution, since the relays uniformly move in each direction. Additionally, the relative orientation of each pair of fluorophores is randomly selected according to the distribution given in (6.5) for each exciton occupation in order to imitate the isotropic and unrestricted rotations of fluorophores. Using the converged value of p_1, the capacity is derived as the maximum mutual information between the transmitted and received bits over all input distributions.

Setting the molar concentration of relay fluorophores in the environment as 1920 mol/m^3, and using excitation pulses with duration $T_{pulse} = 50$ ns to represent bit-1, the information theoretical capacity of the channel is plotted in Fig. 6.7(a) for different values of Förster distance and varying TN-RN distance R. The results show that R_0 has great effect on the spatial range of the communication, such that, using fluorophores with $R_0 = 7$ nm, TN and RN can communicate reliably over distances larger than 150 nm even with a comparatively low value of T_{pulse}.

The effect of the pulse length on the capacity is demonstrated in Fig. 6.7(b). Here, we set the molar concentration as $M = 1920$ mol/m^3, and use fluorophores with $R_0 = 6$ nm.

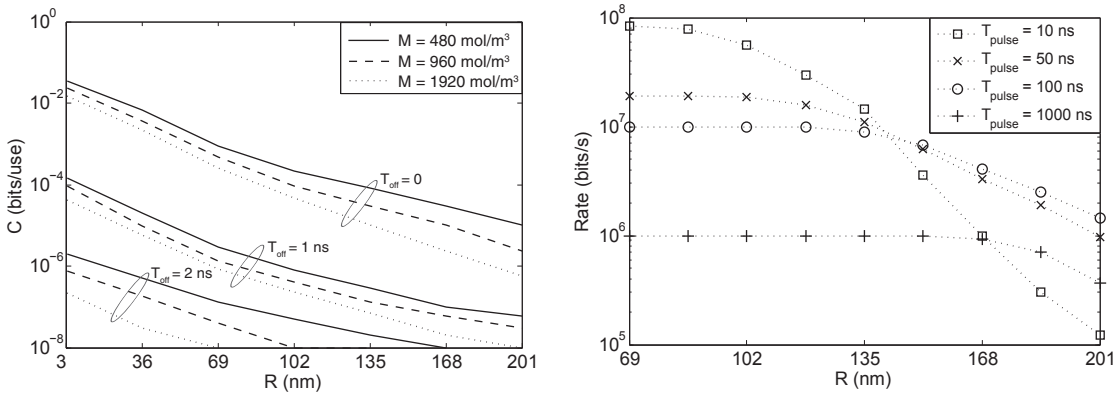

(a) ISI probability for disordered channel with varying T_{off}, M and R.

(b) Maximum achievable rate for disordered channel with varying T_{pulse} and R.

Figure 6.8: Results of ISI and achievable rate analysis for disordered channel.

As expected, increasing the pulse length, the capacity of the channel increases significantly.

Lastly, we investigate the effect of the relay concentration on the channel capacity. In Fig. 6.7(c), the capacity is plotted for three typical concentration values with varying distance between TN and RN. As is seen, increasing the molecular concentration improves the communication range. For relatively denser concentrations, an individual relay fluorophore has many available fluorophores in its proximity. As a result, the removal probability of excitons is comparatively low which increases the probability of exciton transmission from TN to RN for bit-1 case.

We investigate the ISI situation by running the simulation many times, and recording the removal times of excitons that lastly arrive to RN. Setting $T_{pulse} = 10$ ns and $T_b = T_{pulse} + T_{off}$, we plot the ISI probability for different time offsets with varying R and molecular concentration in Fig. 6.8(a). From the results, we conclude that adding a time offset of 2 ns to T_{pulse} reduces the ISI probability to negligible values. The required time offset for negligible ISI is very low compared to that of zeolite L based channels. Since, a relay fluorophore is surrounded by many available fluorophores in brownian channel, the mean occupation time of excitons on relay fluorophores decreases to very low values, e.g., 1-10 ps for very dense environments. As a result, the transit time of excitons from TN to RN is also reduced. The decrease in the ISI probability with increasing molecular concentration also justifies this reasoning.

Setting $T_{off} = 2$ ns and neglecting ISI, in Fig. 6.8(b), we plot the achievable rates with varying R. It is demonstrated that mobile TN and RN can communicate at a rate over 80 Mbps if they are in approximately 70 nm-proximity of each other, and with 200-nm proximity, the reliable communication can be realized at a rate over 1 Mbps.

6.6 FRET-Based Nanonetworks

Here, we discuss the networking capabilities of multi-step FRET-based nanocommunication technique.

Excitons are randomly radiated to a relatively large area through sequential transfers. Therefore, there might be more than one RN in the range of TN, and we expect that all of RNs with the spectrally appropriate acceptor can receive information from TN with a probability of error that is directly dependent on the Euclidian distance between TN and RN. The system is similar to traditional broadcast communication where a transmitter radiates electromagnetic signals in all directions without any knowledge about receivers. In electromagnetic case, receiver antenna has to be tuned to the carrier frequency to receive information from transmitter. Similarly, in FRET-based case, for RN to receive exciton signals, absorption spectrum of RN acceptor must overlap with the emission spectra of relay fluorophores, i.e., carrier fluorophores. Furthermore, the emission spectrum of TN donor must overlap with the absorption spectra of relays for the transfer of excitons into the channel.

Different TN-RN pairs can communicate through the same physical medium if a multiple-access method is utilized. For this aim, wavelength division multiplexing can be applied if another sort of relay fluorophore which spectrally does not overlap with the other relay is available in the medium. Accordingly, different donor and acceptor that overlap with the new relay must be employed on the second TN-RN pair, respectively, so that the second pair can communicate through the new relay fluorophores. The interference between these two channels depends on the separation of the optical spectra of the employed fluorophores. The spectral range of common fluorescent molecules is limited, therefore, in order to employ more channels in the same medium, fluorophores with narrow spectral widths, e.g., fluorescent dyes, must be preferred.

In [46], it is demonstrated that employing a semiconductor donor, e.g., QD or Quantum

Rods (QR), TN can tune the emission spectrum of the donor electrically. Tuning the spectrum of the donor, TN can select the receiver nodes to communicate with if there are more than one sort of relay fluorophores in the channel as in the case of multiple-access.

Chapter 7

FRET-BASED MOBILE MOLECULAR NANONETWORKS

Nanonetworks refer to a group of nano-sized machines with very basic operational capabilities communicating to each other in order to accomplish more complex tasks such as in-body drug delivery, or chemical defense. Realizing reliable and high-rate communication between these nanomachines is a fundamental problem for the practicality of these nanonetworks. Recently, we have proposed a molecular communication method based on *Förster resonance energy transfer (FRET)* which is a nonradiative excited state energy transfer phenomenon observed among fluorescent molecules, i.e., fluorophores. We have modeled the FRET-based communication channel considering the fluorophores as single-molecular immobile nanomachines, and shown its reliability at high rates, and practicality at the current stage of nanotechnology. In this chapter, we focus on network of *mobile* nanomachines communicating through FRET. We introduce two novel mobile molecular nanonetworks: *FRET-based mobile molecular sensor/actor nanonetwork (FRET-MSAN)* which is a distributed system of mobile fluorophores acting as sensor or actor node; and *FRET-based mobile ad hoc molecular nanonetwork (FRET-MAMNET)* which consists of fluorophore-based nanotransmitter, nanoreceivers and nanorelays. We model the single message propagation exploiting the SIR model of epidemics. We derive closed form expressions for the probability of the actor nodes to detect a message generated on the sensor nodes in FRET-MSAN, and for the average detection time of the transmitted message by the nanoreceivers in FRET-MAMNET. We numerically evaluate the performance of these networks in terms of reliability and transmission delay for varying number of nanonodes and varying size of nanomachines, as well as, for several FRET-related parameters.

7.1 Introduction

Based on FRET, we proposed a nanocommunication method between fluorophore-based nanomachines using excitons as information carriers in Chapter 3. Employing a donor fluo-

rophore as the nanotransmitter, and an acceptor fluorophore as the nanoreceiver, and using on-off keying (OOK) modulation scheme by encoding 1-bit information into the presence or absence of a single exciton, we information theoretically analyzed the capacity of the channel between them. We also investigated the pulsed excitation scheme in which the information is encoded into an excitonic ns-duration pulse to increase the reliability of the channel in Chapter 4. Lastly, with a Monte Carlo approach, we simulated the information transmission through point-to-point channel in a three dimensional aqueous medium comprising a varying concentration of relay fluorophores, and showed that information can be reliably transmitted through 200 nm distance at a rate over 10 $Mbps$ Chapter 6. However, due to the high degree of randomness, we were not able to give an analytical expression for the probability of successful transmission of information. Furthermore, in the simulations, we assumed that the fluorophores are stationary, and orientation of the fluorophores are constant during the excited state lifetime to ease the computation, therefore, we applied the classical Förster theory which is not valid for diffusing fluorophores with relatively long lifetimes.

In case the fluorophores with sufficiently long excited state lifetimes are used, a donor and acceptor pair with long intermolecular distance at the time of excitation can get into proximity during the lifetime of the donor molecule. Therefore, the probability for an excited donor to get into proximity with more ground-state acceptors during its lifetime increases. As a result of such conditions, the classical Förster theory fails to express the FRET probability for an excited state fluorophore. Fortunately, Stryer et al. derived an expression for the transfer rate of the fluorophores with long lifetimes diffusing in a three dimensional environment [75].

In this chapter, using the expressions derived in [75], [76], we investigate the performance of FRET-based communication between mobile nanonodes for two network scenarios: *i*) *FRET-based mobile molecular sensor/actor network (FRET-MSAN)*; and *ii*) *FRET-based mobile ad hoc molecular network (FRET-MAMNET)*. In FRET-MSAN, bioluminescent molecules which are special kind of fluorophores that are excited upon binding a target molecule are considered as the sensor nodes. There are also actuators in the network that can realize a specific task upon receiving an exciton. This deployment can be used for autonomous sensing and actuating tasks at the molecular level. FRET-MAMNET consists

of transmitter, relay and receiver nanonodes which are also fluorophores. The single nanotransmitter in the network receives a pulsed excitation signal from an information source and sequentially transmits the excitons to the relay nodes or directly to the nanoreceivers in a probabilistic manner.

In order to model the single message propagation in both networks, we benefit from the SIR model of epidemics [61] which is widely used in modeling mobile ad hoc networks [40]-[32]. In the SIR model, a node can be in three states: susceptible state which corresponds to the ground-state of the nanonodes in FRET-based networks; infected state which is analogous to the excited state of nanonodes; and recovered state which we adapt to our model as the ground-state that comes after the transfer of exciton, i.e., infection, to an actuator or receiver. Similar to the SIR model, we construct the Markov Chain models of both networks. We derive closed form expressions for the probability of a single message to be successfully transferred from the sensor nodes to the actuator nodes in FRET-MSAN, and for the detection time of a single message by one of the nanoreceivers in FRET-MAMNET.

The remainder of this chapter is organized as follows. In Section 7.2, we present the mathematical models for single message propagation in FRET-MSAN and FRET MAMNET. The results of the numerical analysis for performance evaluation are given in Section 7.3.

7.2 Mathematical Model of FRET-Based Mobile Molecular Nanonetworks

In this section, we model the single message propagation both in FRET-MSAN and FRET-MAMNET. We derive closed form expressions for the successful detection probability of a single message in FRET-MSAN, and for the average message detection time in FRET-MAMNET assuming the mobile network nodes, i.e., fluorophores, satisfy the rapid diffusion condition.

We exploit the model of basic epidemic disease spreading to model the information propagation in both networks. In the SIR model of epidemics, there are three possible states for a network node: *i*) suspicious state in which the node is susceptible to the illness; *ii*) infected state in which the node has the illness; and *iii*) recovered state in which the node is recovered from the illness. Similarly, in FRET-based networks, the nodes except the actors and the receivers can be in the same three states. The susceptible nodes are

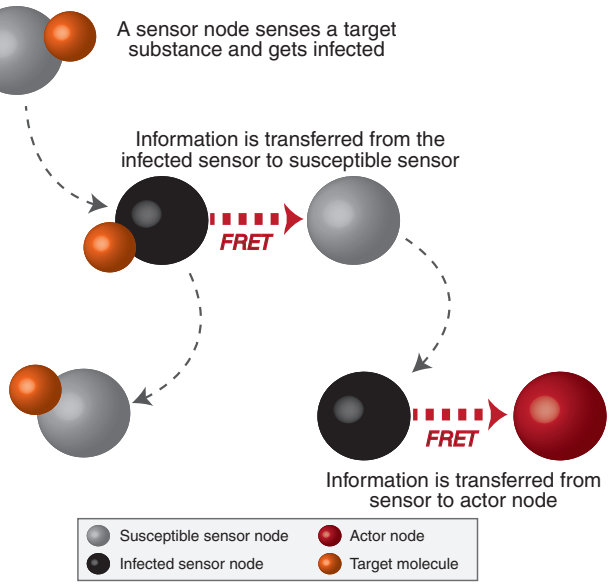

Figure 7.1: Information flow in FRET-MSAN.

the molecules that have been never excited or have transferred their exciton to one of the sensor nodes (or relay nodes in FRET-MAMNET), and become susceptible to be excited. The infected nodes are the molecules that have been excited, i.e., infected by an exciton, and cannot be re-excited until they return to the ground state. The recovered nodes are the molecules that have transferred their exciton to one of the actor nodes (or receiver nodes in FRET-MAMNET). The recovered nodes are also susceptible to the infection, however, they do not lead to any ambiguity in the model, because, we model the signal propagation until the first excitation of any actor or receiver nodes. Therefore, the model is valid until one of the network nodes are recovered.

Note that, excited fluorescent molecules can randomly return to the ground state by releasing a photon without transferring the exciton to another molecule at the natural fluorescence rate, i.e., self-relaxation rate [51]. Therefore, in our model, all of the infected nodes are assumed to randomly return to the susceptible state at this rate. Another fundamental difference between our model and the SIR model resulting from the characteristics of FRET is that an infected node gets rid of the infection and returns to the susceptible state when it transfers the infection to another node.

7.2.1 Mathematical Model of FRET-MSAN

Bioluminescent molecules define a class of fluorescent molecules which are excited upon binding a target molecule [51]. Since they do not need a remote excitation source, e.g., optical laser, they are extensively used in biotechnological research as biomolecular sensors optically indicating the presence of a certain kind of molecule [18]. For example, *aequorin*, a bioluminescent protein, reacts with calcium ions, and relaxes through releasing a photon, thus, it is extensively used to measure $Ca2+$ concentration [5].

Fluorescent molecules also find applications in photodynamic therapy (PDT) of cancer as actuators. In QD-based PDT, QDs are excited by optical energy from a remote source and then transfer its exciton to the conjugated photosensitizing agent which synthesizes a reactive singlet oxygen via energy transfer [71]. The produced singlet oxygen initiates the apoptosis of nearby cancer cells. However, the reactive singlet oxygen is also harmful for normal cells, therefore, the spatial precision of the activation of singlet oxygen is crucial.

Here, we focus on a molecular sensor and actor network, namely FRET-MSAN, composed of mobile bioluminescent sensors and fluorophore-based actors that can collect the information from the sensors and perform an appropriate action upon the environment. The investigated scenario in this section can pave the way for designing autonomous networks of nanomachines which are able to collaboratively sense the presence of tumor cells, and act precisely for the apoptosis of them. The information flow in FRET-MSAN is demonstrated in Fig. 7.1.

Adapting the SIR model of epidemic disease spreading, we model the signal propagation in FRET-MSAN starting from the generation of excitons on the sensors to the detection by an actor node. We derive a closed form expression for the probability of successful transmission of a one-bit detection message generated on bioluminescent sensors to one of the actor nodes. The model is based on the following assumptions:

- Initially N_0 number of sensors are in the infected state, i.e., excited state.
- No additional exciton is generated during the message propagation.
- The number of sensor nodes, N_s, and the number of actor nodes, N_a, are constant.
- An infected sensor node gets rid of the infection and returns to the susceptible state without transfer of infection at a rate of k_0. Note that, this is the natural fluorescence

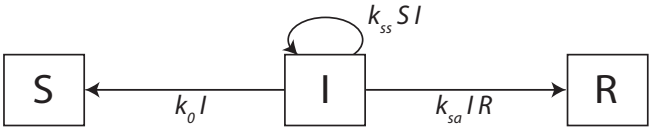

Figure 7.2: Markov chain model of FRET-MSAN.

rate of the bioluminescent fluorophores used as molecular sensors.

- An infected sensor node transfers the infection to a susceptible sensor node making it infected while returning to the susceptible state with a rate of $k_{t,ss}$.
- An infected sensor node transfers the infection to an actor, and get recovered with a rate of $k_{t,sa}$.
- The transfer of infection is pairwise, i.e., an infected nanonode can transfer its infection to only a single nanonode.

The information transfer rate from an infected sensor node to the susceptible, i.e., available, sensor nodes in the environment is given by

$$k_{t,ss} = k_{ss} N_{sc} = \frac{4\pi k_0 R_{0,ss}^6}{3V a_{ss}^{-3}} N_{sc} \tag{7.1}$$

where k_{ss} is the transfer rate between a single pair of infected and susceptible sensor nodes, N_{sc} is the number of susceptible sensor nodes, $R_{0,ss}$ is the Förster radius between two sensor nodes, and a_{ss} is the intermolecular distance of closest approach of two sensor nodes. We assume that the bioluminescent sensors are spherical with radius r_s, therefore, $a_{ss} = 2r_s$. Similarly, the rate of the information transfer from an infected sensor node to an actor node is given by

$$k_{t,sa} = k_{sa} N_a = \frac{4\pi k_0 R_{0,sa}^6}{3V a_{sa}^{-3}} N_a \tag{7.2}$$

where k_{sa} is the transfer rate between an infected sensor node and an actor node, N_a is the number of actor nodes in the environment, $R_{0,sa}$ is the Förster radius between a sensor node and an actor node, and a_{sa} is the intermolecular distance of closest approach of a sensor node with an actor node. Assuming that the actor nodes are also spherical with radius r_a, $a_{sa} = r_s + r_a$.

Based on the listed assumptions, and following a similar way with the SIR model, we construct the Markov chain model of the single message propagation as demonstrated in

Fig. 7.2. Here, $S(t)$, $I(t)$, $R(t)$ denote the number of susceptible, infected and recovered sensor nodes at time t, respectively. From the model we infer that until the first time offloading of the message, the number of infected sensor nodes is governed by the following differential equation:

$$\frac{dI}{dt} = k_{ss}S(t)I(t) - (k_0 I(t) + k_{ss}S(t)I(t)) = -k_0 I(t) \tag{7.3}$$

Assuming that N_0 number of nanosensors are initially infected, i.e., $I(0) = N_0$, (7.3) can be solved as

$$I(t) = N_0 \mathrm{e}^{-k_0 t} \tag{7.4}$$

The cumulative distribution function (CDF) of the delay between the generation of a message on the nanosensor and its transmission to an actor node can be derived from (7.4). Assuming $Pr(event\ in\ [0,t))$ is independent of $Pr(event\ in\ [t,t+\epsilon))$, we can follow the same derivation in [32], and write the differential equation for $F(t)$ as

$$\frac{dF}{dt} = k_{t,sa} I(t)\,(1 - F(t)) = k_{sa} N_a I(t)\,(1 - F(t)) \tag{7.5}$$

Assuming that an exciton is transferred with a probability of 1, when an infected sensor node and an actor node make contact, an initial condition for the differential equation (7.5) can be given by

$$F_0 = N_a N_0 \frac{4\pi\left((r_a + 2r_s)^3 - r_a^3\right)}{3V} \tag{7.6}$$

Note that, $F(0)$ is the probability that an initially infected sensor node is adherent with an actor node. Using $F(0)$, (7.6) can be solved as

$$F(t) = 1 - (1 - F_0)\mathrm{e}^{\frac{k_{sa}N_a N_0}{k_0}(\mathrm{e}^{-k_0 t} - 1)} \tag{7.7}$$

Using (7.7), the probability of successful transmission of information from bioluminescent sensors to one of the actor nodes can be given by

$$Pr(success) = \lim_{t \to +\infty} F(t) = 1 - (1 - F_0)\mathrm{e}^{-\frac{k_{sa}N_a N_0}{k_0}} \tag{7.8}$$

7.2.2 Mathematical Model of FRET-MAMNET

In FRET-MAMNET, there are three kinds of fluorophore-based nanonodes randomly dispersed in the same environment: *i*) nanotransmitter; *ii*) nanorelays; and *iii*) nanoreceivers.

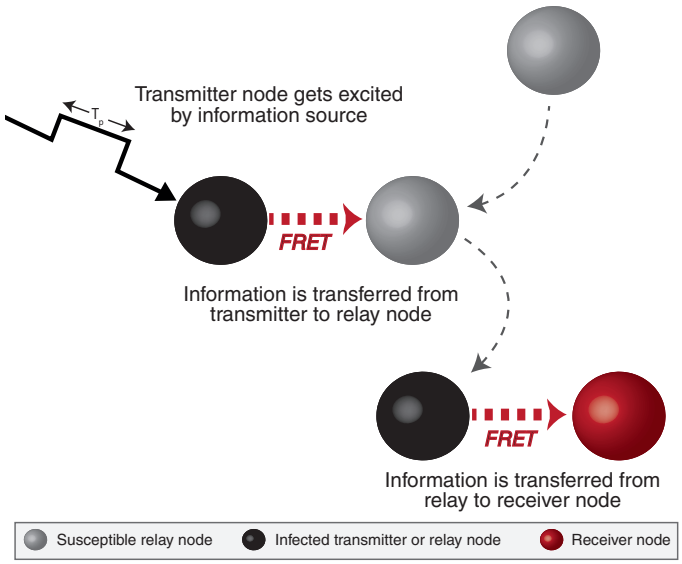

Figure 7.3: Information flow in FRET-MAMNET.

The single nanotransmitter in the network is continuously excited by an information source, e.g., a remote optical source or a nearby electrical source, with a pulse of duration T_p. The excited transmitter node generates excitons randomly during T_p. The relay nodes are not directly excited by an information source. The excitons generated on the nanotransmitter follow random hopping with sequential transfers through the relay nodes, and carry the message from the nanotransmitter to the nanoreceivers. The nanoreceivers are assumed to realize a specific task, e.g., singlet oxygen sensitization, when they receive an exciton. This configuration is similar to the scenario simulated in [47], however, here we assume that the characteristics of the network nodes satisfy the rapid-diffusion limit, therefore, we are able to derive closed form expression for the average detection time of a single message, T_d. The information flow in FRET-MAMNET is demonstrated in Fig. 7.3.

We model the single message propagation from the nanotransmitter to a nanoreceiver until an exciton is first received by an receiver node. We again benefit from the SIR model. The model is based on the following assumptions:

- Transmitter and relay nodes are of same type of fluorophores, i.e., they have the same fluorescence rate (k_0), Förster radius ($R_{0,hh}$) and molecular radius (r_h).
- There is only a single nanotransmitter that can receive excitation signal from the

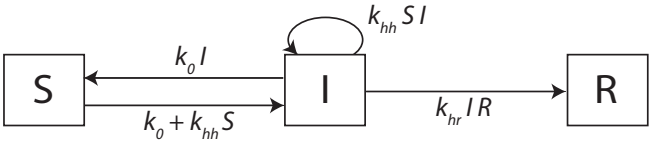

Figure 7.4: Markov chain model of FRET-MAMNET.

information source.

- An infected nanonode gets rid of the infection and returns to the susceptible state without transfer of infection at a rate of k_0.
- An infected nanonode transfers the infection to a susceptible nanonode with a rate of $k_{t,hh}$.
- An infected nanonode transfers the infection to a receiver with a rate of $k_{t,hr}$.
- During the pulse, infection is generated on the transmitter node with a rate of k_g.
- Pulse is applied until the message is detected by one of the nanoreceivers, i.e., ($T_p = T_d$).
- The total number of transmitter and relay nodes, N_h, and the number of receiver nodes, N_r, are constant.

On the nanotransmitter, when an infection is removed either by self relaxation, i.e., fluorescence, or by transfer to another node, another infection is generated immediately. Therefore, the infection generation rate on the nanotransmitter is given by

$$k_g(t) = k_0 + k_{t,hh}(t) = k_0 + k_{hh}S(t) \tag{7.9}$$

Note that, $S(t)$ is the number of susceptible nodes, i.e., nodes available for energy transfer, at time t. k_{hh} is the transfer rate between a single transmitter-relay (or relay-relay) pair, that can be expressed as in (2.8).

The Markov chain model of the single message propagation is given in Fig. 7.4. In the Markov model, the differential equation for the number of infected nanonodes in the system

at time t is expressed by

$$\begin{aligned}\frac{dI}{dt} &= k_0 + k_{hh}S(t) + k_{hh}S(t)I(t) - (k_0 I(t) + k_{hh}S(t)I(t)) \\ &= k_0 + k_{hh}\left(N - I(t)\right) - k_0 I(t) \\ &= k_0 + k_{hh}N - (k_0 + k_{hh})I(t) \end{aligned} \tag{7.10}$$

Considering only a single node, i.e., the transmitter node, is initially infected, the initial condition for (7.10) is $I(0) = 1$. The solution of (7.10) can be given by

$$I(t) = K + (1 - K)\mathrm{e}^{-(k_0 + k_{hh})t} \tag{7.11}$$

where $K = (k_0 + k_{hh}N)/(k_0 + k_{hh})$.

Following the same derivation in the first network scenario, the differential equation for the CDF of the average message detection time is expressed as in (7.5). The initial condition for the CDF, i.e., F_0 can be given as in (7.6) with $N_0 = 1$. Using the initial condition, the solution of (7.5) is given by

$$F(t) = 1 - C\mathrm{e}^{\frac{k_{hr}N_r(1-K)}{(k_0+k_{hh})\mathrm{e}^{(k_0+k_{hh})t}} - Kk_{hr}N_r t} \tag{7.12}$$

with $C = (1 - F(0))\, exp\left(k_{hr}N_r \frac{k_{hh}(N-1)}{(k_0+k_{hh})^2}\right)$.

Using (7.12), the average detection time of the message can be expressed by

$$E[T_d] = \int_0^\infty (1 - F(t))\, \mathrm{d}t \tag{7.13}$$

which can be numerically computed.

7.3 Performance Analysis of FRET-Based Mobile Molecular Nanonetworks

In this section, we numerically evaluate the performance of the two network scenario described in Section III. We use the derived expressions of successful detection probability of a single message in FRET-MSAN, and the average detection time in FRET-MAMNET with varying network and node parameters to understand the effect of each parameter on the network performance and gain insight on the feasibility of the FRET-based mobile nanonetworks.

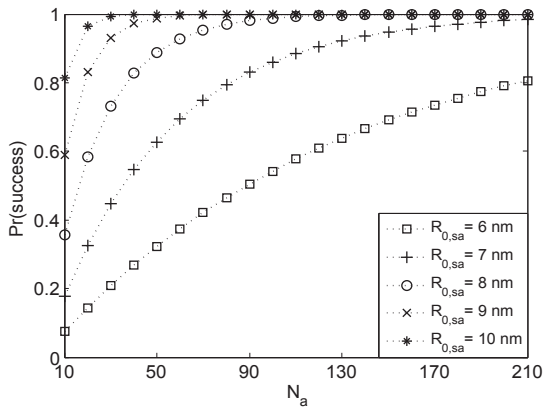

(a) $Pr(success)$ with varying N_a for different $R_{0,sa}$.

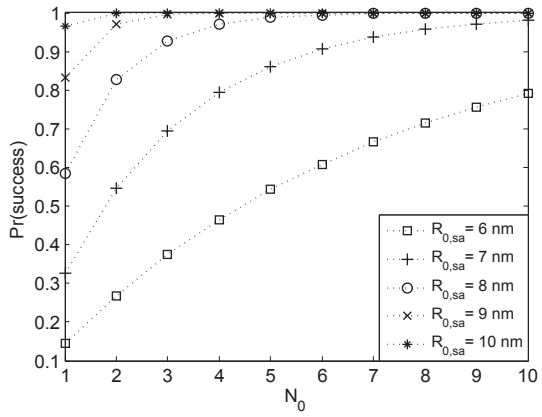

(b) $Pr(success)$ with varying N_0 for different $R_{0,sa}$.

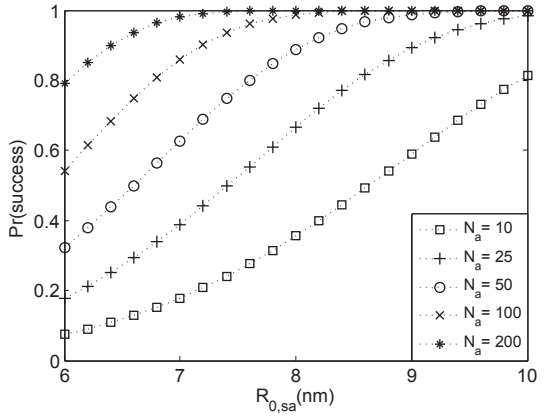

(c) $Pr(success)$ with varying $R_{0,sa}$ for different N_a.

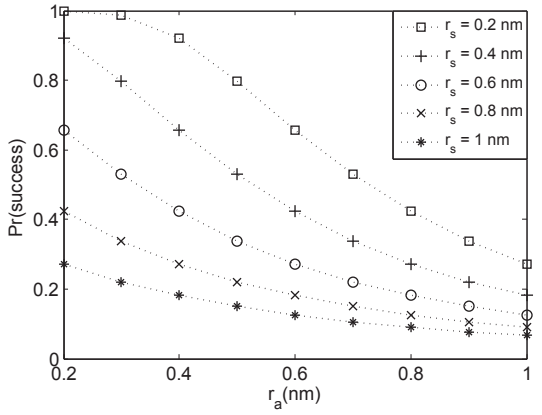

(d) $Pr(success)$ with varying r_a for different r_s.

Figure 7.5: Results of numerical analysis for detection probability of single message in FRET-MSAN.

7.3.1 Performance Analysis of FRET-MSAN

In this section, we present the numerical analysis for the reliability performance of FRET-MSAN using the closed form expression of $Pr(success)$ derived in Section III. We analyze the single-message transmission probability for varying number of nanoactors and initially infected nanosensors, varying Förster radius between nanosensors and nanoactor, and varying size of nanomachines. Note that, the number of initially susceptible nanosensors, the Förster radius of nanosensor-nanosensor pair, and the fluorescence rate of the nanonodes do not affect the detection probability. The default values of parameters used in the numerical simulations are presented in Table 7.1.

Table 7.1: Simulation Parameters

Molecular radii (r_s, r_a, r_h, r_r)	0.25 (nm)
Natural fluorescence rate of molecules (k_0)	10^6 (sec^{-1})
Volume (V)	1 (μm^3)
Förster radii ($R_{0,ss}$, $R_{0,sa}$, $R_{0,hh}$, $R_{0,hr}$)	8 (nm)
Number of initially excited sensor nodes in FRET-MSAN (N_0)	5
Total number of sensor nodes in FRET-MSAN (N_s)	100
Number of actor nodes in FRET-MSAN (N_a)	100
Total number of transmitter and relay nodes in FRET-MAMNET (N_h)	100
Number of receiver nodes in FRET-MAMNET (N_r)	100

Effect of Number of Actor Nodes

The probability of detection with varying number of nanoactors, N_a, for different values of Förster radius of nanosensor-nanoactor pair, $R_{0,sa}$, is shown in Fig. 8.4(a). We observe that the detection probability significantly increases with increasing number of actors, since the chance for an infected nanosensor to be in the communication range of an actor node at any time increases.

Effect of Number of Initially Infected Nanosensors

The effect of the number of initially infected nanosensors on the detection probability is shown in Fig. 8.4(b) with varying number of nanoreceivers. Since we assume that no other external infection occurs, and the infection is only transferred between the network nodes, the number of infected nanosensors is a decreasing function of time. Therefore, the initial number of infection is an important parameter for the detection performance. It is observed that the detection probability significantly increases even with a small increase in the number of initially infected nanosensors.

Effect of Förster Radius

In Fig. 8.4(c), Pr(success) with varying $R_{0,sa}$ for different number of receiver nodes is presented. It is shown that as $R_{0,sa}$ increases, the probability of detection is significantly enhanced. In fact, Förster radius is analogous of the communication range of a network node in traditional networks. Therefore, with a large communication range of a nanosensor, more nanoactors as acceptors become available for the energy transfer. As a result, the transfer probability of excitons on each node increases with a decrease in the removal probability of excitons by fluorescence. We also observe that for small values of $R_{0,si}$, a large number of nanoreceivers are required to successfully detect the message of nanosensors. However, by employing nanosensor-nanoactor pairs with relatively large $R_{0,sa}$, less than 50 receiver nodes will be enough for successful detection.

Effect of Size of Nanomachines

The size of nanomachines also significantly affects the successful detection probability, since the extent of the distance of closest approach has a direct effect on the energy transfer rate between nanonodes. The detection probability for varying radii of nanosensors and nanoactors is shown in Fig. 7.5(d). The selected values for radii are in the range of size of common fluorophores, e.g., fluorescent dyes. We observe that, using small-size nodes significantly increases the detection probability.

7.3.2 Performance Analysis of FRET-MAMNET

In this section, we present the results of numerical simulations to investigate the performance of FRET-MAMNET in terms of average transmission time of a single message, i.e., T_d. We evaluate the effect of varying number network nodes, varying Förster radii of different pairs, varying lifetime of the nanosensors, and varying size of nanonodes. Note that, different from FRET-MSAN, the number of nanosensors and the excited state lifetime of nanosensors have effect on the performance of FRET-MAMNET. The default values of system parameters used in the simulations are given in Table 7.1.

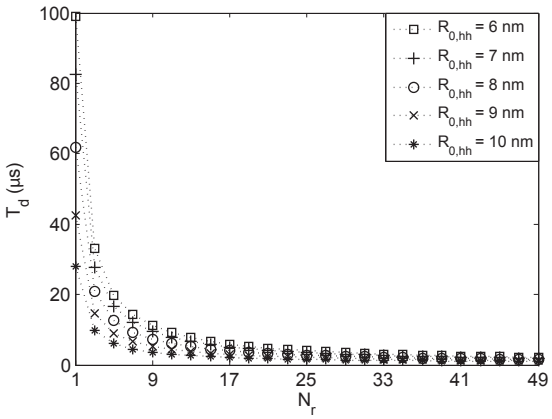

(a) T_d with varying N_r for different $R_{0,hh}$.

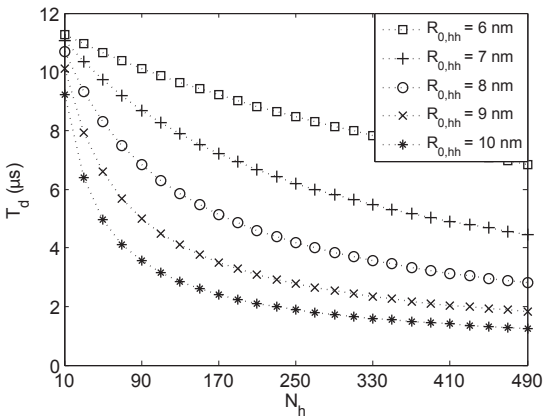

(b) T_d with varying N_h for different $R_{0,hh}$.

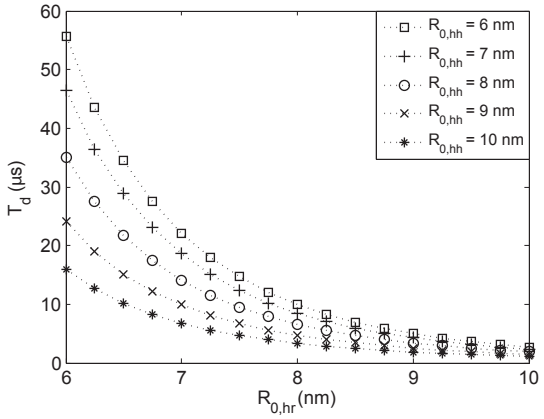

(c) T_d with varying $R_{0,hr}$ for different $R_{0,hh}$.

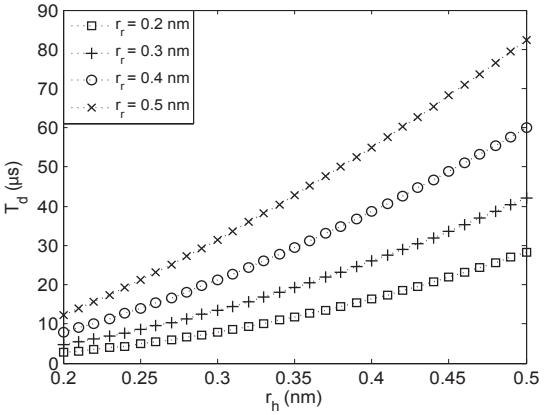

(d) T_d with varying r_h for different r_r.

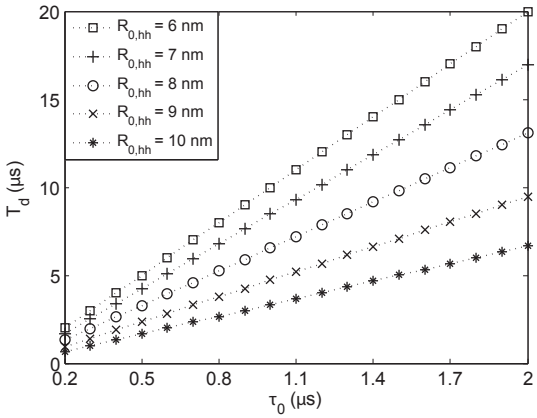

(e) T_d with varying τ_0 for different $R_{0,hh}$.

Figure 7.6: Results of numerical analysis for average detection time of single message in FRET-MAMNET.

Effect of Number of Receiver Nodes

The number of nanoreceivers significantly affects the detection time as shown in Fig 7.6(a). This is because, as there are more receiver nodes, the chance for an infected nanonode to enter the proximity of a receiver during the lifetime of its infection increases. Considering point-to-point communication channel with a single nanotransmitter-nanoreceiver pair, i.e., the case of $N_r = 1$, the detection time is over 25 μs, even when employing fluorophores with large Förster radius.

Effect of Number of Relay Nodes

Fig. 7.6(b) demonstrates the effect of total number of transmitter and relay nodes on the detection time of a single message with varying $R_{0,hh}$. Note that, there is only a single nanotransmitter, therefore, the number of relay nodes is equal to $N_h - 1$. It is clearly shown that the detection time significantly decreases with increasing number of nanorelays. Increasing the concentration of the relay nodes increases the number of susceptible nodes in the range of an infected node, thus, increases the transfer rate for each of the nanonode. Therefore, the probability of removal of excitons, i.e., infections, with fluorescence, i.e., self-relaxation, is decreased. Keeping the number of infected nanorelays high increases the probability for a receiver to encounter an infected nanonode in its range, and thus decreases the detection time.

Effect of Förster Radius

The detection time significantly decreases with increasing Förster radii of the nanotransmitter, nanorelays and the nanoreceivers as shown in Fig. 7.6(c). As the Förster radius increases, the effective communication range of a nanonode is improved. Therefore, the number of nodes available for energy transfer in the range of an infected nanonode increases. As a result, the transfer rate for a nanonode increases, as well. This causes the decrease in the detection time.

Effect of Size of Nanonodes

The effect of radii of nanonodes is shown in Fig. 7.6(d). As the radii of nanonodes decrease, the center of nanonodes can get closer, i.e., the distance of closest approach decreases.

Therefore, the maximum possible transfer rate between any two nodes increases. Overall, the total exciton transfer rate for each nanonode increases. Higher transfer rates result in lower probability for an exciton to be removed from the network. As a result, the number of excitons randomly hopping through the nanonodes at time t increase, thus, the time required for a receiver to detect an exciton decreases.

Effect of Excited State Lifetime of Nanonodes

The effect of excited state lifetime of the nanonodes, τ_0, is shown in Fig. 7.6(e) for different $R_{0,hh}$. It is shown that increasing the lifetime linearly increases the detection time. The lifetime has a significant effect on the transmitter side, such that, it directly affects the exciton generation rate. Lifetime gives a measure of average occupation time of an exciton on a nanonode. When the lifetime is short, the excitons are generated more frequently on the nanotransmitter, therefore, the number of infected nanonodes on the network at time t increases, and the time required for a receiver to encounter an infected nanonode decreases.

Chapter 8

EXPERIMENT

8.1 Introduction

Despite the considerable literature on the development of nanocommunication techniques and derivation of analytical models for nanocommunication networks, very little attention has been paid to the experimental validation of the feasibility of the proposed nanocommunication methods and the validity of the derived analytical models. In this chapter, we present the results of the first attempt to realize an FRET-based nanocommunication system. This is, at the same time, the first successful demonstration of information transmission at nanoscale.

Besides its extensive theory, FRET is also a well-experimented phenomenon. However, the empirical studies about FRET are mostly directed towards the derivation of the transfer efficiency for intermolecular distance calculations. There is no investigation in the literature about the FRET-based information transmission characteristics from the communication theoretical perspective.

For the demonstration of FRET-based nanocommunications, we implement a system that can optically send a pseudorandom binary digital information sequence to a molecular sample at a tunable rate, and, at the same time, detect and analyze the succeeding optical signal released from the sample to decode the transmitted information. Through the optical excitation of the dye sample and the optical observation of the transmitted information, this experiment is also an implementation of a macro/nano interface between a computer network in macroscale and an FRET-based nanonetwork.

We use a common pair of fluorescent dyes, Fluorescein and Rhodamine B, as the donor and acceptor samples, respectively, and prepare a bulk solution of donor and acceptor in ethanol for the FRET sample. The FRET sample consists of many donors and many acceptors randomly dispersed in the solvent. Therefore, with a laser excitation, many donors, as well as acceptors, can be simultaneously excited, and fluorescence of many acceptors can be

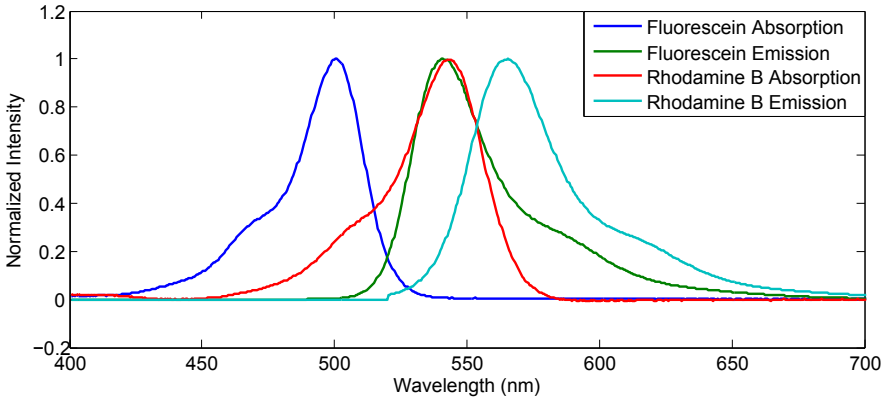

Figure 8.1: Normalized absorption and emission spectra of Fluorescein and Rhodamine B.

sensitized through FRET for a single pulse excitation. For this reason, the FRET sample represents a multi source multicast network topology from the communication theoretical perspective. Although we have not derive an analytical model for FRET-based multi source multicast networks to be validated by the results of this experiment, we demonstrate the feasibility of FRET-based nanocommunications with the experiment, and investigate its performance in terms of error rate at different information transmission rates.

In FRET experiments, there is a probability that the acceptors can be directly excited by the laser source, and the donor molecules can directly fluorescence without FRET. This undesirable contribution of donor and acceptor fluorescence in the FRET channel is named spectral bleedthrough. In this experiment, in order to remove the spectral bleedthrough resultant from the large spectral overlap between the donor and acceptor molecules, we apply the 3-cube method which is widely-used to reveal the noiseless FRET signal [80].

8.2 Methodology and Experimental Setup

In this experiment, we use a dye pair of Fluorescein and Rhodamine B which are commonly used in FRET studies due to their relatively high Förster radius and quantum yields. The emission and absorption spectra of Fluorescein and Rhodamine B in ethanol are demonstrated in Fig. 8.1. The high spectral overlap between the emission spectrum of Fluorescein and the absorption spectrum of Rhodamine B results in a Förster radius of 5.7 nm with the assumption of free rotation of molecules [43].

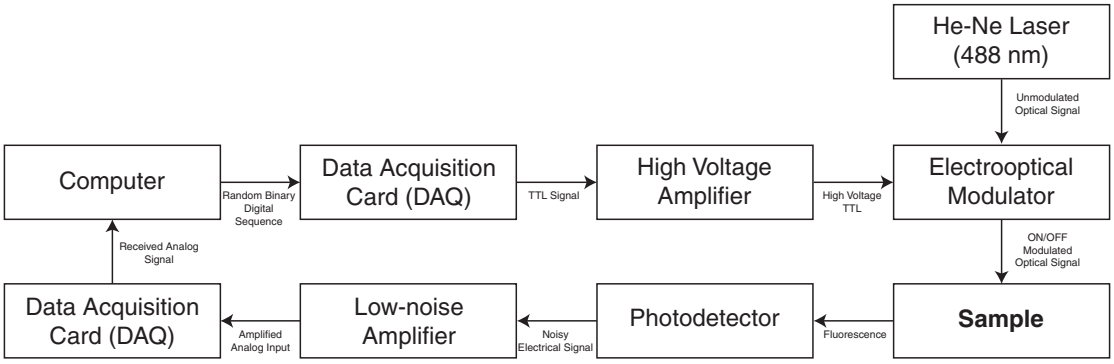

Figure 8.2: Experimental Setup.

The experimental setup which is illustrated in Fig. 8.2, consists of nine main parts. An argon-ion laser is the optical source of the system. The wavelength of the laser is 488 nm, and close to the wavelength where the absorption of Fluorescein, i.e., the donor, is at its maximum. A pseudorandom binary sequence with a length of 2^{19} bits is generated and stored in a laboratory system-design platform called LabVIEW. The sequence is converted to a 0-5 V TTL control signal by a Data Acquisition Card (DAQ) and transferred to the modulation instruments at different rates. The pseudorandom TTL signal is amplified and transmitted to the Electro-Optic Modulator (EOM) which electrically modulates the optical beam of the laser. The modulated optical signal is forwarded to the molecular sample at the microscope. The fluorescence of the signal is collected by the microscope and transferred to the optical filters. The optical filter set is composed of all-pass and band-pass optical filters which concentrate and pass the optical signals with wavelengths in the desired wavelength range. The passed optical signal is converted to the electrical signal through a photodetector, and the electrical signal is amplified by a low-noise amplifier. The recorded output of the amplifier is transmitted to the computer through the analog input of the DAQ and recorded for signal processing and decoding.

In FRET experiments, the donor-acceptor sample is exposed to a laser signal with a wavelength belonging to the absorption spectra of the donor, and the resultant FRET signal is detected through optical filters with range at the emission spectrum of the acceptor molecule. Therefore, the spectral overlap between the donor and acceptor molecules always results in contamination of resultant FRET signal by donor emission into the acceptor

channel and by the excitation of acceptor molecules by the donor excitation wavelength [25]. These contaminations are named Spectral Bleed-Through (SBT) signal into the FRET channel. Specifically, the donor's contribution in the FRET channel is termed Donor SBT (DSBT), and the acceptor's contribution is termed Acceptor SBT (ASBT). To remove the SBT and obtain the noiseless FRET signal, a post signal processing is required. In the literature, the 3-cube method is regarded as the most efficient solution for this problem. In the 3-cube method, three solutions which contains only donor (C_D), only acceptor (C_A) and the mixture of donor and acceptor (C_M) are excited by a laser with a wavelength near the maximum absorption wavelength of the donor [80]. The resultant fluorescence signals are then transmitted through two different optical pass-band filters. One of the pass-band filters passes only the signals with the wavelengths near the maximum emission wavelength of the donor (Donor Filter (DF)) and the other one passes the signals with the wavelengths close to the maximum emission wavelength of acceptor (Acceptor Filter (AF)). The transmitted signals are then detected by a photodetector and recorded for the post signal processing. The formula to calculate the pure FRET signal using the data obtained from the three cubes is as follows

$$S_{FRET} = S_{M,AF} - S_{A,AF} - S_{D,AF}\frac{I_{M,DF}}{I_{D,DF}} \tag{8.1}$$

where $S_{M,AF}$, $S_{A,AF}$ and $S_{D,AF}$ are the continuous signals received from C_M, C_A and C_D, respectively, through the acceptor filter. $I_{M,DF}$ and $I_{D,DF}$ are the fluorescence intensities of the mixture and donor samples, respectively, detected through the donor filter set.

Following the 3-cube method in our experiment, we prepare three separate solutions containing 3 mM Fluorescein in ethanol for the donor only cube (C_D), 3 mM Rhodamine B in ethanol for the acceptor only cube (C_A), and 3 mM Fluorescein and 3 mM Rhodamine B in ethanol for the mixture cube (C_M). The common pseudorandom sequence is transmitted at the rates of 50, 150 and 250 kpbs through these three samples separately for each filter, and the resultant fluorescence signals are detected by the photodetector. The amplified photodetector outputs are sampled by the DAQ at the sampling rates of 400 kHz, 1.2 MHz and 2 MHz (8 samples per bit), respectively. Note that, at the specified molar concentrations, the mean distance between the donor and acceptor molecules in the mixture cube is 6.51 nm. The band-pass filters, DF and AF, are selected according to the emission spectra of donor and acceptor samples, and their pass bands are 525/50 nm and 607/67

nm, respectively.

The fluorescence intensity of a sample is proportional to the power of the detected waveforms. The power of the detected waveforms can be calculated as the square of the Root-Mean-Sqaure (RMS) amplitudes of the waveforms. The RMS values of the waveforms for different rates are listed in Table 8.1. Using the RMS values, the efficiency of FRET is calculated as follows

$$E_{FRET} = 1 - (\frac{RMS_{M,DF}}{RMS_{D,DF}})^2 \tag{8.2}$$

Table 8.1: RMS of the Received Signals

Sample and Filter	RMS Voltage (mV)
$C_{M,AF}$	780
$C_{M,DF}$	130
$C_{D,AF}$	205
$C_{D,DF}$	715
$C_{A,AF}$	480
$C_{A,DF}$	41

Using the detected RMS voltages, we calculate the FRET efficiency as 0.96. This contradicts with the theoretical efficiency calculated as 0.31 using R_0 and the mean intermolecular distance. This enhancement of the efficiency can be attained to the diffusion of the molecules and the non-uniformity of the sample which can result in a significantly different value for the mean intermolecular distance [75], [76].

8.3 Results

In this section, based on the experimental results, we evaluate the performance of the multi source multi-cast FRET-based nanocommunications for different information transmission rates.

The performance of digital information transmission processes is best understood by observing eye diagrams, i.e., eye patterns. Eye diagrams are plotted through the several

repetitions of the received signal traces with a specified trace length. For this experiment, we plot eye diagrams for the fluorescence of the mixture sample, and the pure FRET signal derived using (8.1). To increase the resolution of the eye diagrams, the sampling rate of the observed signals is increased 32 times through lowpass interpolation in MATLAB.

The obtained eye diagrams which store 1000 traces of 4 bit-length for the observed signal S_{MIX} and the calculated signal S_{FRET} are demonstrated in Fig. 8.3 and Fig. 8.4, respectively, for different transmission rates. The results show that the signal quality significantly decreases as the transmission rate increases.

We also obtain the optimum threshold values that minimize the erroneous decoding of the signal S_{FRET} for each transmission rate. The Bit-Error-Rate (BER) is calculated according to these thresholds for the numerical performance evaluation. The optimum threshold voltages and the corresponding error rates are listed in Table 8.2. The BER for 50 kbps and 150 kbps are acceptable for a reliable communications but at the rate of 250 kbps, the error rate significantly increases and the decoding becomes very erroneous.

Table 8.2: Optimum Thresholds and Bit Error Rates

Received Signal and Transmission Rate ($kbps$)	Threshold (mV)	BER (bit^{-1})
$S_{FRET,50}$	216	1.7166×10^{-5}
$S_{FRET,150}$	202	5.7221×10^{-5}
$S_{FRET,250}$	167	3.0449×10^{-2}

As the transmission rate decreases, the length of the excitation pulses increases which also increases the probability of the donor molecules to be excited. The exponential decay of the fluorescence of the acceptors also complicates the detection at the high transmission rates. Nevertheless, the results of the experiment reveal that reliable communication is possible for relatively high rates as 150 kpbs with using FRET as the nanocommunication method.

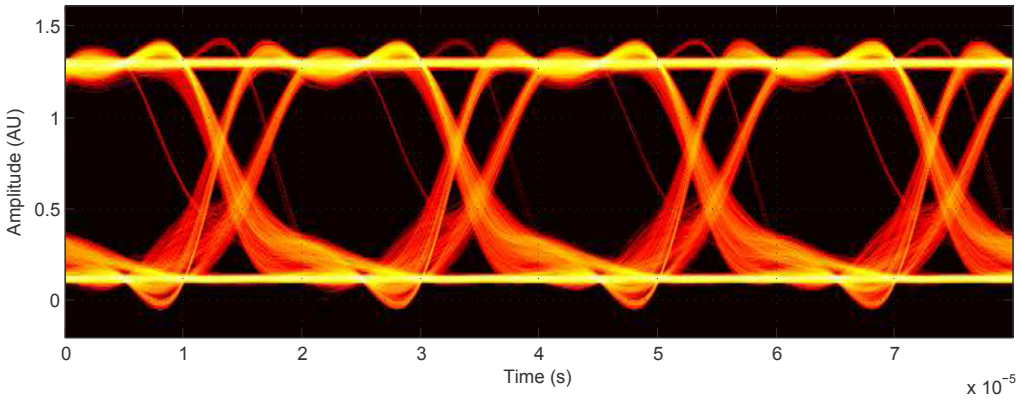

(a) Rate = 50 kbps.

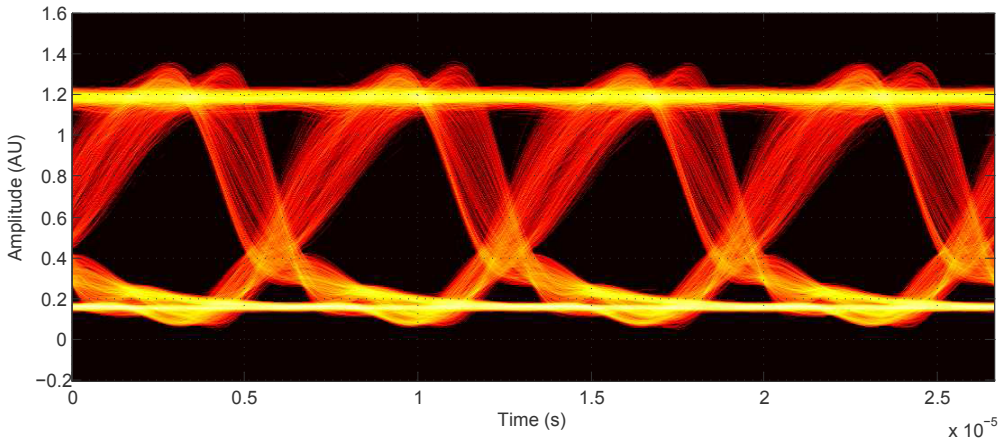

(b) Rate = 150 kbps.

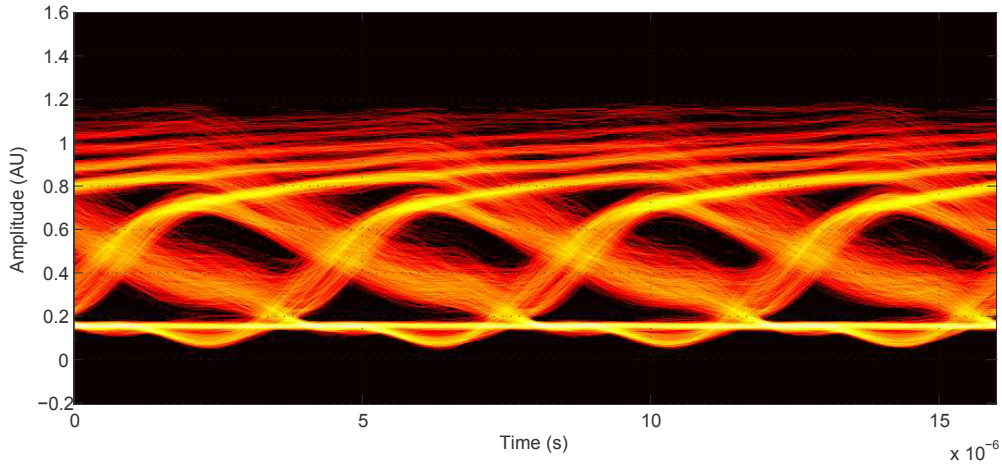

(c) Rate = 250 kbps.

Figure 8.3: Eye diagrams for the fluorescence of mixture cube (C_M) at different information transmission rates.

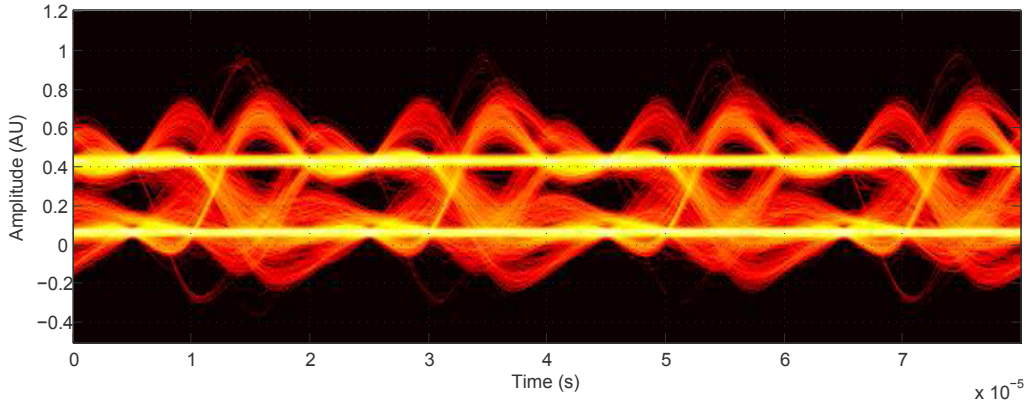

(a) Rate = 50 kbps.

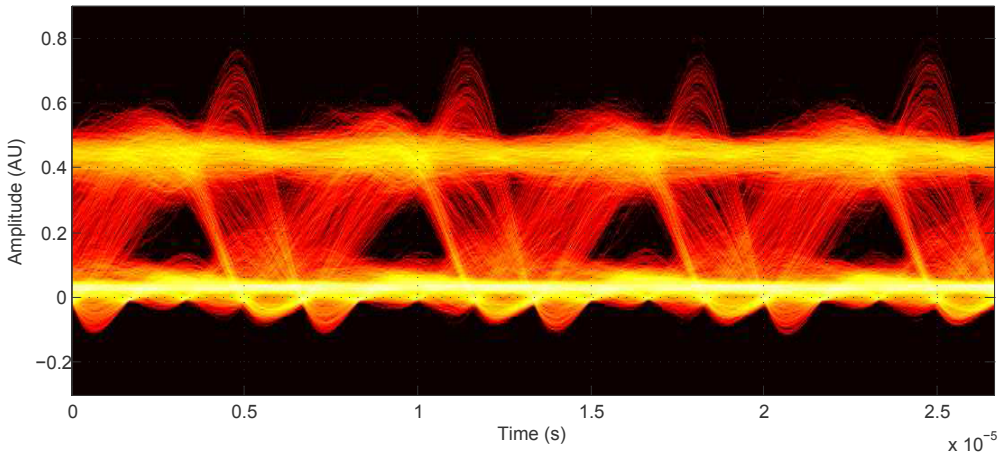

(b) Rate = 150 kbps.

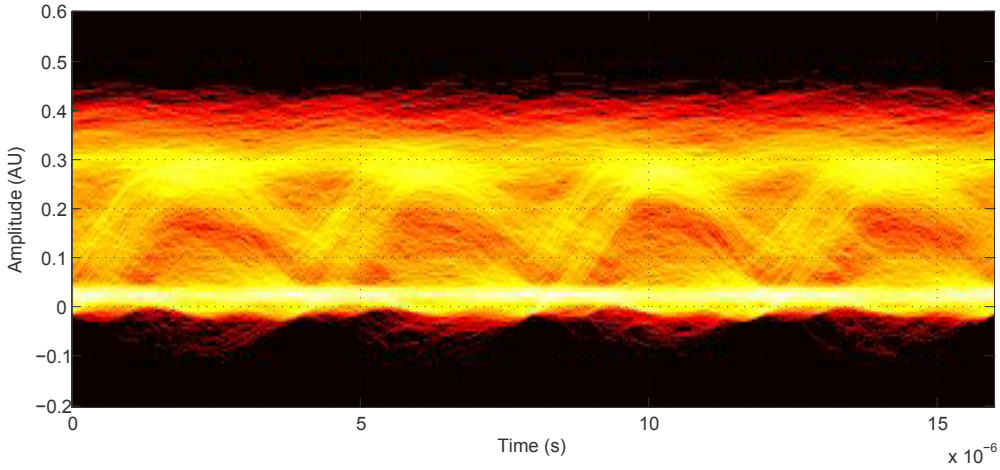

(c) Rate = 250 kbps.

Figure 8.4: Eye diagrams for the pure FRET signal at different information transmission rates.

Chapter 9

CONCLUSION AND FUTURE RESEARCH DIRECTIONS

In this thesis, we propose a nanoscale molecular communication method exploiting a well-known phenomenon FRET, for the first time in the literature. First, we investigate FRET-based point-to-point nanoscale communication channel from the information theoretical perspective employing ON/OFF Keying modulation with single-exciton transmission scheme. Later, using multiple excitons as the information carrier, we simulate the information transmission through FRET-based nanoscale point-to-point and broadcast channels and analyze their performance for varying system parameters. Furthermore, we propose electrically and chemically controllable information routing techniques for FRET-based nanonetworks. In order to extend the communication range of the FRET-based communications, we propose a long-range nanoscale communication channel based on multi-step FRET applying multi-exciton transmission scheme. Moreover, we analyze FRET-based mobile molecular nanonetworks, and derive analytical expressions to analyze the performance of FRET-based mobile molecular sensor and actor networks (FRET-MSAN) and FRET-based mobile ad hoc molecular networks (FRET-MAMNET). Lastly, we conduct an experiment in which we transmit data through a mixture of commonly used organic dyes, Fluorescein and Rhodamine B, in order to validate the feasibility of FRET-based nanoscale communication. As with the further advances in nanotechnology, we believe that FRET-based nanocommunication and nanonetworking concepts which are proposed in this thesis, will pave the way for the design of efficient and reliable nanonetworks to be used for groundbreaking applications.

In the next sections, we provide the details of the contributions and point out future issues regarding FRET-based nanoscale communications.

9.1 Contributions

In this section, we sum up the contributions of each chapter and underline the important results.

9.1.1 FRET-based Point-to-Point Nanoscale communication Channel with Single Exciton Transmission

In this chapter, we propose a novel molecular communication technique exploiting a well-known phenomenon FRET, for the first time in the literature. We define a realistic communication channel model for a single transmitter-receiver pair (point-to-point) within the scope of FRET theory. Succeeding that, the capacity of the newborn channel is formalized information-theoretically and the variation in the communication channel capacity is analyzed for different environmental and intrinsic parameters. The result of analysis reveals that the capacity of the channel can be increased significantly by appropriately choosing the parameters in accordance with each other.

Throughout the paper, we show that with the relatively low dependency on the environmental factors, high level controllability of the parameters and simplicity, FRET-based molecular communication model stands as a promising solution to high rate nanoscale communication between nanomachines. Furthermore, we show the potential of the model for long range nanonetworks by serially connecting the channels using relay nanomachines.

9.1.2 FRET-based Point-to-Point and Broadcast Nanoscale Communication Channels with Multi-exciton Transmission

In this chapter, FRET-based nanoscale communication is investigated for point-to-point and broadcast cases utilizing multiple excitons as information carrier. We information theoretically analyze the performance of the channels by simulating information transmission with realistic Monte Carlo algorithms for varying stimulation length, varying intermolecular distance and varying number of receiver nanomachines for the broadcast case. The results of the simulations demonstrate that the multi-exciton transmission brings a remarkable performance improvement by means of channel reliability and coverage area, and makes the broadcast communication realizable with notably high channel capacities over the same coverage as in the point-to-point case.

9.1.3 Information Routing in FRET-Based Nanonetworks

In this chapter, we propose electrically and chemically controllable routing methods applicable to the FRET-based nanonetworks. The electrical routing method exploits the de-

pendence of FRET probability on the spectral similarity of donor and acceptor molecules. Based on Quantum Confined Stark Effect (QCSE), the emission spectrum of semiconductor donor molecule shifts with the varying magnitude of the applied electric field which also changes the spectral overlap of the donor with absorption spectra of two different acceptors. Therefore, the communication channels are switched on and off at different times based on magnitude of the electric field. The proposed chemical routing method exploits the strong dependence of FRET probability on the intermolecular distance and the nanoscale shuttle-like movement of [2]rotaxane macrocycle between two nodes with acid/base treatment. The information is transferred through one of two channels according to the location of [2]rotaxane macrocycle on the axis between two nanoreceiver nodes. The routing schemes proposed in this chapter point out the possibility of controlling the route of the information flow in FRET-based nanonetworks by electrical and chemical stimulations.

9.1.4 Multi-Step FRET-Based Long-Range Nanoscale Communication Channel

In this chapter, we propose a novel nanoscale communication method based on multi-step FRET employing multiple excitons as the information carrier, and investigate different scenarios for immobile and mobile nanomachines considering that they communicate through the channels with ordered and disordered relay fluorophores, respectively. The results of the Monte Carlo simulations for both scenarios demonstrate that with multi-step FRET-based communication, significantly high data transmission rates are achievable over extended distances up to tens of nanometers. Parallel to the advances in molecular logic gate architectures, multi-step FRET-based communication is a promising solution for molecular computers with its high transmission rates. Moreover, we underline the practicality of the multi-step FRET-based communication for mobile applications such as nanosensor networks for health monitoring and in-body drug delivery.

9.1.5 FRET-Based Mobile Molecular Nanonetworks

In this chapter, based on our previous studies, we introduce FRET-based mobile molecular nanonetworks. We present mathematical models for FRET-based mobile molecular sensor and actor networks (FRET-MSAN) and FRET-based mobile ad hoc molecular networks (FRET-MAMNET) benefiting from the SIR models of epidemic disease spreading. We

derive closed form expressions for the single message transmission probability in FRET-MSAN, and for the average detection time of single message in FRET-MAMNET assuming that the network nodes satisfy the rapid-diffusion criterion. Using these expressions, the performance of the networks are evaluated in terms of reliability and delay with varying network and FRET-related parameters. The numerical results reveal that it is possible to achieve reliable communication at high-rates with FRET-based mobile molecular networks.

The deployment of bioluminescent sensor fluorophores and photoactive actor fluorophores makes FRET-MSAN promise autonomous applications of target detection and acting at nanoscale such as highly precise PDT applications with singlet oxygen sensitizer fluorophores as actor nodes. FRET-MAMNET provides the opportunity of remotely controlling the operation of nanonetworks by an optical information source. This optical link can be made bidirectional if the fluorescence outputs of nanoreceivers are observed by photodetectors, and therefore, it can provide a connection between nanonetworks and larger communication networks, which is currently not possible for other molecular networks proposed so far.

9.1.6 Experiment

In this chapter, we present the results of one of the first attempts to realize a nanocommunication system. We carry out an experiment in which we succesfully transmit a binary digital information through a fluorophore-based multi-source multicast nanonetwork using FRET. We investigate the communication performance of the designed system in terms of bit error rate. The experimental results prove that information can be transmitted reliably with the transmission rates up to 150 kbps which is significantly higher than the communication rates achievable with other molecular communication techniques.

This experiment is also an implementation of an interface between macro- and nanonetworks. Using a laser as the excitation source, and observing the fluorescence of the acceptors through a photodetector, we realize an interface between an FRET-based nanonetwork and an optical communication network.

9.2 Applications

In this section, we discuss some prospective applications of FRET-based nanoscale communications proposed in this thesis. We do not go into detail about their physical realizations,

but we relate our investigations as promising solutions to some open problems.

Nanomachines are expected to perform very basic tasks, such as simple logic operations, sensing, or actuating. The most important promise of a nanonetwork is to coordinate the nanomachines with different capabilities in order to perform more complex tasks and to increase the effective range of the operation combining these tiny machines deployed in relatively large area.

There is a large number of studies concerning the design of molecular machines some of which exploit the excitons to realize their functionalities [12]. For example, photoactive nanovalves and nanoimpellers that are activated with the excitation of functional fluorophores have been designed [82]. There are also several nanosensors employing fluorophores as functional unit in that the functional fluorophore becomes excited and then fluoresces when a target molecule bounds to them [56]. FRET-based communication promises a nanonetwork that combines the different functionalities of this kind of molecular machines without a need for additional complex processing or energy conversion units. Since the nanosensors output as excitons when they detect a target, and the molecular machines can actuate when they are activated by excitons, the communication between all these different nanomachines can be realized by the transfer of excitons, i.e., FRET-based communications. For example, consider a drug delivery task that needs a precise control of the location where the drugs are delivered. This need is important especially for cancer treatment, since the delivered drug might be harmful for healthy cells, and must be delivered precisely to the tumor cells. A nanonetwork composed of nanosensors that can detect the tumor cells, and nanoactuators, e.g., a combination of nanopores and nanovalves, that can release the drug molecules when it is activated by an exciton, might be a solution to this problem if the communication of the nanosensor with the nanoactuators is realized. FRET-based communication is the simplest and realizable option to connect these primitive molecular devices without additional complexity.

Another example about the cancer treatment is photodynamic therapy (PDT) that is based on the apoptosis of tumor cells by reactive singlet oxygen species. The singlet oxygen is generated when a photosensitizer agent is excited and transfers its excited energy to a nearby oxygen molecule. It has been shown that the photosensitizer agent also can be excited through FRET by designing a system with additional QD as the energy donor [71]. The

system can be considered as the actuating unit in a nanonetwork composed of FRET-based communicating nanosensors and other nanoactuators specialized in cancer treatment.

An FRET-based nano sensor network composed of many molecular sensors deployed in a large area can be employed to gain a spatial diversity increasing the detection area. The outputs of the molecular sensors can be gathered through FRET-based communication in a processing unit that might have a more complex structure as compared to the sensors. This kind of nanosensor network extends the resolution of molecular diagnostics to single-molecule level in a coordinated manner, and can find applications in the areas like water-quality control, nuclear defence [2].

In this thesis, we show that FRET-based communication provides high data transfer rates compared to other short-range communication techniques especially when we have the advantage of placing fluorophores at prescribed locations. Parallel to the advances in the molecular logic gates and memories based on photochromic fluorophores, FRET is a promising communication technique in nanoscale on-chip applications such as nanoprocessors. Furthermore, exploiting the quantum coherence behavior of the energy transfer, FRET-based communication can find applications in quantum computers.

9.3 Future Research Directions

In the last phase of this thesis study, we have successfully experimented information transmission through a solution of donor and acceptor fluorophores in ethanol. Although this experiment clearly demonstrates the realizability of FRET-based nanocommunications, the experimental results are not comparable to our theoretical findings, since we derive mathematical models at the single molecular level. Therefore, a throughout experimentation of the proposed communication channels using single molecules as the nanocommunication units to validate the mathematical models is an open issue.

Other open issues about FRET-based nanoscale communications include the development of more reliable modulation schemes, design of interfaces with other molecular communication methods, analysis of FRET-based multiple-access networks, and development of biomedical, environmental and industrial applications based on FRET-based nanoscale communications.

BIBLIOGRAPHY

[1] I. F. Akyildiz, F. Brunetti, and C. Blazquez, "Nanonetworks: A New Communication Paradigm," *Computer Networks,* vol. 52, no. 12, pp. 2260-2279, August 2008.

[2] I. F. Akyildiz and M. J. Jornet, "Electromagnetic Wireless Nanosensor Networks," *Nano Communication Networks (Elsevier),* vol. 1, no. 1, pp. 3-19, March 2010.

[3] I. F. Akyildiz, J. M. Jornet, and M. Pierobon, "Nanonetworks: A New Frontier in Communications," *Communications of the ACM,* vol. 54, no. 11, pp. 84-89, 2011.

[4] A. P. Alivisatos, "Semiconductor Clusters, Nanocrystals, and Quantum Dots", *Science,* vol. 271, no. 5251, pp. 933-937, 1996.

[5] D. G. Allen and J. R. Blinks, "Calcium Transients in Aequorin-Injected Frog Cardiac Muscle," *Nature,* vol. 273, no. 5663, pp. 509-513, 1978.

[6] P. R. Ashton, R. Ballardini, V. Balzani, I. Baxter, A. Credi, M. C. T. Fyfe, M. T. Gandolfi, M. Gomez-Lopez, M. Martinez-Diaz, A. Piersanti, N. Spencer, J. F. Stoddart, M. Venturi, A. J. P. White, and D. J. Williams, "Acid-Base Controllable Molecular Shuttles," *Journal of the American Chemical Society,* vol. 120, no. 46, pp. 11932-11942, 1998.

[7] B. Atakan and O. B. Akan, "Carbon Nanotube-Based Nanoscale Ad Hoc Networks," *IEEE Communications Magazine,* vol. 48, no. 6, pp. 129-135, June 2010.

[8] B. Atakan, O. B. Akan, and S. Balasubramaniam, "Body Area Nanonetworks with Molecular Communications in Nanomedicine," *IEEE Communications Magazine,* vol. 50, no. 1, pp. 2834, January 2012.

[9] D. Badali and C. C. Gradinaru, "The Effect of Brownian Motion of Fluorescent Probes on Measuring Nanoscale Distances by Frster Resonance Energy Transfer", *Journal of Chemical Physics,* vol. 134, no. 22, pp. 225102, 2011.

[10] J. D. Badjic, V. Balzani, A. Credi, S. Silvi, and J. F. Stoddart, "A Molecular Elevator," *Science,* vol. 303, no. 5665, pp. 1845-1849, 2004.

[11] J. D. Badjic, V. Balzani, A. Credi, J. N. Lowe, S. Silvi, and J. F. Stoddart, "A Mechanically Interlocked Bundle," *Chemistry,* vol. 10, no. 8, pp. 1926-1935, 2004.

[12] V. Balzani, A. Credi, F. M. Raymo, and J. F. Stoddart, "Artificial Molecular Machines," *Angewandte Chemie International Edition,* vol. 39, no. 19, pp. 3348-3391, 2000.

[13] K. Becker, J. M. Lupton, J. Müller, A. L. Rogach, D. V. Talapin, H. Weller, and J. Feldmann, "Electrical Control of Förster Energy Transfer," *Nature Materials,* vol. 5, pp. 777-781, 2006.

[14] C. Berney and G. Danuser, "FRET or No FRET: A Quantitative Comparison," *Biophysical Journal,* vol. 84, no. 6, pp. 3992-4010, June 2003.

[15] G. Calzaferri and K. Lutkouskaya, "Mimicking the Antenna System of Green Plants", *Photochemical and Photobiological Sciences,* vol. 7, no. 8, pp. 879-910, 2008.

[16] H. Chen, H. L. Puhl, S. V. Koushik, S. S. Vogel, and S. R. Ikeda, "Measurement of FRET Efficiency and Ratio of Donor to Acceptor Concentration in Living Cells," *Biophysical Journal,* vol. 91, no. 5, pp. 39-41, September 2006.

[17] J. Collin, C. Dietrich-Buchecker, P. Gavina, M. C. Jimenez-Molero, and J. Sauvage, "Shuttles and Muscles: Linear Molecular Machines Based on Transition Metals," *Accounts of Chemical Research,* vol. 34, no. 6, pp. 477487, 2001.

[18] C. H. Contag and M. H. Bachmann, "Advances in In Vivo Bioluminescence Imaging of Gene Expression," *Annual Review of Biomedical Engineering,* vol. 4, pp. 235-260, 2002.

[19] T. M. Cover and J. A. Thomas, *Elements of Information Theory,* New York: Wiley, 1991.

[20] R. E. Dale, J. Eisinger, and W. E. Blumberg, "The Orientational Freedom of Molecular Probes. The Orientation Factor in Intramolecular Energy Transfer," *Biophysical Journal,* vol. 26, no. 2, pp. 161-193, May 1979.

[21] V. Derycke, R. Martel, J. Appenzeller, and Ph. Avouris, "Carbon Nanotube Inter- and Intramolecular Logic Gates," *Nano Letters,* vol. 1, no. 9, pp. 453-456, 2001.

[22] W. R. Dichtel, J. M. Serin, C. Edder, J. M. J. Frechet, M. Matuszewski, L. Tan, T. Y. Ohulchanskyy, and P. N. Prasad, "Singlet Oxygen Generation via Two-photon Excited FRET," *Journal of the American Chemical Society,* vol. 126, no. 17, pp. 53805381, 2004.

[23] V. V. Didenko, "DNA Probes Using Fluorescence Resonance Energy Transfer (FRET): Designs and Applications," *Biotechniques,* vol. 31, no. 5, pp. 1106-1121, November 2001.

[24] R. C. Dunn, "Near-Field Scanning Optical Microscopy," *Chemical Reviews,* vol. 99, no. 10, pp. 2891-2928, 1999.

[25] M. Elangovana, H. Wallrabeb, Y. Chena, R. N. Dayc, M. Barrosob, and A. Periasamy, "Characterization of One- and Two-Photon Excitation Fluorescence Resonance Energy Transfer Microscopy," *Methods,* vol. 29, no. 1, pp. 58-73, January 2003.

[26] S. A. Empedocles and M. G. Bawendi, "Quantum-Confined Stark Effect in Single CdSe Nanocrystallite Quantum Dots," *Science,* vol. 278, pp. 2114-2117, 1997.

[27] R. A. Freitas, "Current Status of Nanomedicine and Medical Nanorobotics," *Journal of Computational and Theoretical Nanoscience,* vol. 2, no. 1, pp. 1-25, 2005.

[28] T. Hogg and R. A. Freitas, "Acoustic Communication for Medical Nanorobots," *Nano Communication Networks (Elsevier),* vol. 3, no. 2, pp. 83-102, 2012.

[29] T. Förster, "Zwischenmolekulare Energiewanderung und Fluoreszenz," *Annalen der Physik,* vol. 437, no. 1-2, pp. 55-75, 1948.

[30] L. P. Giné and I. F. Akyildiz, "Molecular Communication Options for Long Range Nanonetworks," *Computer Networks (Elsevier),* vol. 53, no. 16, pp. 2753-2766, November 2009.

[31] M. Gregori and I. F. Akyildiz, "A New Nanonetwork Architecture Using Flagellated Bacteria and Catalytic Nanomotors," *IEEE J. Sel. Areas Commun.,* vol. 28, no. 4, pp. 612-619, May 2010.

[32] A. Guney, B. Atakan, and O. B. Akan, "Mobile Ad Hoc Nanonetworks with Collision-Based Molecular Communication," *IEEE Transactions on Mobile Computing,* vol. 11, no. 3, pp. 353-366, 2012.

[33] Z. J. Haas and T. Small, "A New Networking Model for Biological Applications of Ad Hoc Sensor Networks," *IEEE/ACM Transactions on Networking,* vol. 14, no. 1, pp. 27-40, 2006.

[34] A. Harada, "Cyclodextrin-Based Molecular Machines," *Accounts of Chemical Research,* vol. 34, no. 6, pp. 456464, 2001.

[35] M. Heilemann, P. Tinnefeld, G. S. Mosteiro, M. G. Parajo, N. F. Hulst, and M. Sauer, "Multistep Energy Transfer in Single Molecular Photonic Wires," *Journal of the American Chemical Society,* vol. 126, no. 21, pp. 6514-6515, 2004.

[36] M. Heilemann, R. Kasper, P. Tinnefeld, and M. Sauer, "Dissecting and Reducing the Heterogeneity of Excited-State Energy Transport in DNA-Based Photonic Wires," *Journal of the American Chemical Society,* vol. 128, no. 51, pp. 1686416875, 2006.

[37] T. Heyduk, "Measuring Protein Conformational Changes by FRET/LRET," *Current Opinion in Biotechnology,* vol. 13, no. 4, pp. 292-296, August 2002.

[38] E. A. Jares-Erijman and T. M. Jovin, "FRET Imaging," *Nature Biotechnology,* vol. 21, pp. 1387-1395, 2003.

[39] C. Joo, H. Balci, Y. Ishitsuka, C. Buranachai, and T. Ha, "Advances in Single-Molecule Fluorescence Methods for Molecular Biology," *Annual Review of Biochemistry,* vol. 77, pp. 51-76, July 2008.

[40] A. Khelil, C. Becker, J. Tian, and K. Rothermel, "An Epidemic Model for Information Diffusion in MANETs," in *Proc. 5th ACM International Workshop on Modeling Analysis and Simulation of Wireless and Mobile Systems,* Atlanta, Georgia, September 2002.

[41] K. Kinosita, T. Kouyama, and A. Ikegami, "Criteria for the Rapid Diffusion Limit of Fluorescence Energy Transfer," *Journal of Chemical Physics,* vol. 86, no. 6, pp. 3273-3282, 1987.

[42] R. Korlacki, R. F. Saraf, and S. Ducharme, "Electrical Control of Photoluminescence Wavelength from Semiconductor Quantum Dots in a Ferroelectric Polymer Matrix", *Applied Physics Letters,* vol. 99, no.15, pp. 153112, 2011.

[43] A. Kurian, S. D. George, V. P. N. Nampoori, and C. P. G. Vallabhan, "Study on the Determination of Molecular Distance in Organic Dye Mixtures Using Dual Beam Thermal Lens Technique," *Spectrochimica Acta Part A,* vol. 61, no. 13-14 pp. 2799-2802, October 2005.

[44] M. Kuscu and O. B. Akan, "A Nanoscale Communication Channel with Fluorescence Resonance Energy Transfer (FRET)," *Proc. 1st IEEE Int. Workshop Molecular Nano Scale Commun./IEEE Conf. Comput. Commun. Workshops,* Shanghai, China, April 2011, pp. 425-430.

[45] M. Kuscu and O. B. Akan, "A Physical Channel Model and Analysis for Nanoscale Molecular Communications with Förster Resonance Energy Transfer (FRET)," *IEEE Transactions on Nanotechnology,* vol. 11, pp. 200-207, Jan. 2012.

[46] M. Kuscu, D. Malak, and O. B. Akan, "An Information Theoretical Analysis of Broadcast Networks and Channel Routing for FRET-Based Nanoscale Communications," in *Proc. 2nd IEEE Int. Workshop Molecular Nano Scale Commun./IEEE Conf. Commun. Workshops,* Ottawa, Canada, June 2012, pp. 6167-6171.

[47] M. Kuscu and O. B. Akan, "Multi-Step FRET-Based Long-Range Nanoscale Communication Channel," *IEEE Journal on Selected Areas in Communications,* to be published, 2013.

[48] M. Kuscu and O. B. Akan, "FRET-Based Nanoscale Point-to-Point and Broadcast Communications with Multi-Exciton Transmission and Channel Routing," submitted for publication.

[49] M. Kuscu and O. B. Akan, "FRET-Based Mobile Molecular Nanonetworks," *Proc. IEEE 12th Annual Mediterranean Ad Hoc Networking Workshop,* Ajaccio, Corsica, France, June 2013.

[50] M. Kuscu and O. B. Akan, "Nanoscale Communications Based on Förster Resonance Energy Transfer (FRET)," *Modeling, Methodologies and Tools for Molecular and Nanoscale Communications,* Edited by J. Suzuki, T. Nakano and M. J. Moore, Springer, to be published, 2014.

[51] J. R. Lakowicz, *Principles of Fluorescence Spectroscopy*, 3rd ed., Baltimore, MD: Springer-Verlag, 2006.

[52] Y. Li, H. Li, Y. Li, H. Liu, S. Wang, X. He, N. Wang, and D. Zhu, "Energy Transfer Switching in a Bistable Molecular Machine," *Organic Letters,* vol. 7, no. 22, pp. 4835-4838, 2005.

[53] S. Lloyd, "A Potentially Realizable Quantum Computer," *Science,* vol. 261, no. 5128, pp. 1569-1571, September 1993.

[54] B. J. MacLennan, "Morphogenesis as a Model for Nano Communication," *Nano Communication Networks (Elsevier),* vol. 1, no. 3, pp. 199-208, September 2010.

[55] G. McNamara, A. Gupta, J. Reynaer, T. D. Coates, and C. Boswell, "Spectral Imaging Microscopy Web Sites and Data," *Cytometry,* vol. 69A, no. 8, pp. 863-871, August 2006.

[56] I. L. Medintz, A. R. Clapp, H. Mattoussi, E. R. Goldman, B. Fisher, and J. M. Mauro, "Self-Assembled Nanoscale Biosensors Based on Quantum Dot FRET Donors," *Nature Materials,* vol. 2, pp. 630-638, 2003.

[57] J. Muller, J. M. Lupton, P. G. Lagoudakis, F. Schindler, R. Koeppe, A. L. Rogach, J. Feldmann, D. V. Talapin, and H. Weller "Wave Function Engineering in Elongated Semiconductor Nanocrystals with Heterogeneous Carrier Confinement", *Nano Letters,* vol. 5, no. 10, pp. 2044-2049, 2005.

[58] T. Nakano, T. Suda, M. Moore, R. Egashira, A. Enomoto, and K. Arima, "Molecular Communication for Nanomachines Using Intercellular Calcium Signaling," in *Proc. of the 5th IEEE Conf. on Nanotechnology,* vol. 2, pp. 478481, Nagoya, Japan, July 2005,.

[59] T. Nakano, T. Suda, T. Koujin, T. Haraguchi, and Y. Hiraoka, "Molecular Communication through Gap Junction Channels," *Transactions on Computational Systems Biology (Springer),* vol. 5410, pp. 81-99, 2008.

[60] T. Nakano and M. Moore, "Molecular Communication Paradigm Overview," *Journal of Next Generation Information Technology,* vol. 2, pp. 9-16, 2011.

[61] M. E. J. Newman, "Spread of Epidemic Disease on Networks," *Physical Review E,* vol. 66, no. 1, pp. 016128(11) , 2002.

[62] H. Onagi and J. Rebek, "Fluorescence Resonance Energy Transfer across a Mechanical Bond of a Rotaxane," *Chemical Communications,* no. 36, pp. 4604-4606, 2005.

[63] G. H. Patterson, D. W. Piston, and B. G. Barisas, "Förster Distances between Green Fluorescent Protein Pairs," *Analytical Biochemistry,* vol. 284, no. 2, pp. 438-440, September 2000.

[64] M. Pauchard, A. Devaux, and G. Calzaferri, "Dye-Loaded Zeolite L Sandwiches as Artificial Antenna Systems for Light Transport", *Chemistry,* vol. 6, no. 18, pp. 3456-3470, 2000.

[65] A. R. Pease, J. O. Jeppesen, J. F. Stoddart, Y. Luo, C. P. Collier, and J. R. Heath, "Switching Devices Based on Interlocked Molecules," *Accounts of Chemical Research,* vol. 34, no. 6, pp. 433-444, 2001.

[66] R. Pepperkok, A. Squire, S. Geley, and P. I. H. Bastiaens, "Simultaneous Detection of Multiple Green Fluorescent Proteins in Live Cells by Fluorescence Lifetime Imaging Microscopy," *Current Biology,* vol. 9, no. 5, pp. 269-274, March 1999.

[67] B. A. Pollok and R. Heim, "Using GFP in FRET-based applications," *Trends in Cell Biology,* vol. 9, no. 2, pp. 57-60, February 1999.

[68] S. Ramachandra, Z. D. Popovic, K. C. Schuermann, F. Cucinotta, G. Calzaferri, and L. De Cola, "Förster Resonance Energy Transfer in Quantum DotDye-Loaded Zeolite L Nanoassemblies", *Small,* vol. 7, no. 10, pp. 1488-1494, 2011.

[69] T. Ritz, A. Damjanovic, and K. Schulten, "The Quantum Physics of Photosynthesis," *ChemPhysChem,* vol. 3, no. 3, pp. 243-248, 2002.

[70] E. Rothenberg, M. Kazes, E. Shaviv, and U. Banin, "Electric Field Induced Switching of the Fluorescence of Single Semiconductor Quantum Rods", *Nano Letters,* vol. 5, no. 8, pp. 1581-1586, 2005.

[71] A. C. S. Samia, X. Chen, and C. Burda, "Semiconductor Quantum Dots for Photodynamic Therapy," *Journal of the American Chemical Society,* vol. 125, no. 51, pp. 1573615737, 2003.

[72] S. K. Sekatskii, M. Chergui, and G. Dietler, "Coherent Fluorescence Resonance Energy Transfer: Construction of Nonlocal Multiparticle Entangled States and Quantum Computing," *Europhysics Letters,* vol. 63, p. 21, 2003.

[73] P. T. Snee, R. C. Somers, G. Nair, J. P. Zimmer, M. G. Bawendi, and D. G. Nocera, "A Ratiometric CdSe/ZnS Nanocrystal pH Sensor," *Journal of the American Chemical Society,* vol. 128, no. 41, pp. 1332013321, 2006.

[74] L. Stryer, "Fluorescence Energy Transfer as a Spectroscopic Ruler," *Annual Review of Biochemistry,* vol. 47, pp. 819-846, 1978.

[75] D. D. Thomas, W. F. Carlsen, and L. Stryer, "Fluorescence Energy Transfer in the Rapid-Diffusion Limit," *Proceedings of the National Academy of Sciences,* vol. 75, no. 12, pp. 5746-5750, 1978.

[76] L. Stryer, "Diffusion-Enhanced Fluorescence Energy Transfer," *Annual Review of Biophysics and Bioengineering,* vol. 11, pp. 203-222, 1982.

[77] S. Vyawahare, S. Eyal, K. D. Mathews, and S. R. Quake, "Nanometer-Scale Fluorescence Resonance Optical Waveguides," *Nano Letters,* vol. 4, no. 6, pp. 1035-1039, 2004.

[78] J. Wang, J. Han, J. Yan, Y. Ma, and J. Pei, "A Mechanically Interlocked [3]rotaxane as a Light-Harvesting Antenna: Synthesis, Characterization, and Intramolecular Energy Transfer," *Chemistry,* vol. 15, no. 14, pp. 3585-3594, 2009.

[79] H. M. Watrob, C. Pan, and M. D. Barkley, "Two-Step FRET as a Structural Tool," *Journal of the American Chemical Society,* vol. 125, no. 24, pp. 7336-7343, 2003.

[80] D. C. Youvan, W. J. Coleman, C. M. Silva, J. Petersen, E. J. Bylina, and M. M. Yang, "Fluorescence Imaging Micro-Spectrophotometer (FIMS)," *Biotechnology et alia,* vol. 1, pp. 1-16, 1997.

[81] Z. Zhou, M. Yu, H. Yang, K. Huang, F. Li, T. Yi, and C. Huang, "FRET-Based Sensor for Imaging Chromium(III) in Living Cells," *Chemical Communications,* no. 29, pp. 33873389, 2008.

[82] J. Lu, E. Choi, F. Tamanoi, and J. I. Zink, "Light-Activated Nanoimpeller-Controlled Drug Release in Cancer Cells," *Small,* vol. 4, no. 4, pp. 421-426, 2008.

VITA

MURAT KUŞCU was born in Karabük, on December 13, 1988. He received the B.S. degree in Electrical and Electronics Engineering from Middle East Technical University, Ankara, Turkey in 2011. He received his M.S. degree in Electrical and Electronics Engineering under the supervision of Prof. Özgür B. Akan from Koç University, İstanbul, Turkey in 2013. His research interests include FRET-based nanoscale communications and molecular communications.